# From inert to active: biofunctionalised PEG hydrogels to guide stem cell behaviour

---

A doctoral thesis by

Aman S. Chahal


Department of Biomaterials

Institute of Clinical Dentistry

Faculty of Dentistry

University of Oslo

Norway

*Series of dissertations submitted to the*
*Faculty of Dentistry, University of Oslo*

ISBN 978-82-8327-041-9



Cover: Hanne Baadsgaard Utigard.
Print production: Reprosentralen, University of Oslo.

*“Let them think what they liked, but I didn’t mean to drown myself. I meant to swim till I sank—but that’s not the same thing”*

—Joseph Conrad

# Acknowledgements

This work was conducted at the Department of Biomaterials, Faculty of Dentistry, University of Oslo during the years 2015–2019. Financial support was provided by the Osteology Foundation and the Norwegian Research Council.

I wouldn't have been in Oslo, if it wasn't for that skype conversation with Håvard J. Haugen, who welcomed me well before I set foot into the department. You've had your door open ever since and almost never said no to a conversation with me. I truly appreciate that. Janne E. Reseland and Ståle Petter Lyngstadaas, I thank you both for the critical cell-based discussions which made me think over questions I wouldn't have otherwise considered.

Hanna, where do I begin? You knew when to let me fight against the current and when to jump in and pull me out. I would have drowned a long time ago, if it weren't for you. Despite our logician-campaigner disagreements, you've had my back all along. The conversations we've had over numerous bowls of Ramen have slowly grown into a ritual for both the body and the mind. But above all, I thank you for showing me that sometimes, the obstacle itself is the way. I still don't understand how people can not like coriander.

My time in Portugal was enriching in more ways than I expected. I thank everyone at 3B's Research group for being so welcoming and helpful during my time there. I cannot mention Portugal and not think of Manu and Carla. I will forever be thankful for your hospitality during my months in Portugal. Scientific conversations while walking Rufo will never be forgotten. You've taught me that sometimes it takes as few as five ingredients to get the most out of life. Thank you Rui for bringing entropy to our conversations, that really made us think over each step along the way.

I am extremely grateful for the support I had gotten from you, Catherine. You always thought outside the box, and that was often the way that worked best. How boring life would have been without 'crazy Fridays' with Seb, Aina, Jonas, Alejandro, Rune and Flo. No matter how much you had on your plate David, you always made time for a discussion. The office has never been the same without you and you will always have my love and respect. Anne, I couldn't have asked for a better friend. But make sure you never forget to go back to the 'T'. I feel extremely lucky to have friends like Emmi, Maja, Piotr, Marte, Johnny, Elena and Camilla. You saw me through some of the toughest times and it is truly people like you that makes Oslo feel like home. Javier and Hao– 'Hao' I wish that the both of you lived in Oslo instead. I have had some

of the best times with you both and I look forward to many more. Saad and Sana, I can't thank you both enough for the delicious food when I had no time to cook while writing this thesis. It meant a lot to me. Manu, we both took on a project from the ground up and together know what a struggle it has been at times. You've enriched this PhD in more ways than presented in this thesis. I truly couldn't ask for a better partner to ride shotgun with me on this one.

Marc, I hope you enjoyed your time in Oslo as much as I enjoyed having you here. And to Bhua, thanks for always being just a phone call away, when the rest of the world was asleep. Virji and Shar, your emotional support is what kept me going. I am yet to come across people with bigger hearts than you two. It's a long way from first year chemistry now. To my mother, I could count on you, no matter the time difference. It was your encouragement that warmed me up when Norway felt ice cold. Sanna, you've been absolutely selfless through my times of writing and you made stressful times feel like a breeze. Thank you for taking care of me and reminding me to live a little amidst all the madness. I feel very lucky to have you and Jaro in my life.

Pops, every day you would ask me if my cells were behaving– and that simple gesture meant the world to me. You haven't just supported me, but understood me too. That is what made me never feel alone while being away from home. This one is for you.

Aman S. Chahal

Oslo, September 2019

# Table of contents

# List of publications

**Paper I** **Attachment and spatial organisation of human mesenchymal stem cells on poly(ethylene glycol) hydrogels.**

A.S. Chahal, M. Schweikle, C.A. Heyward, H. Tiainen

*Journal of the Mechanical Behavior of Biomedical Materials*, 2018; 84:46-53.

**Paper II** **Osteogenic potential of poly(ethylene glycol)-amorphous calcium phosphate composites on human mesenchymal stem cells.**

A.S. Chahal*, M. Schweikle*, A. Lian, J.E Reseland, H.J Haugen, H. Tiainen

Submitted to: *Biomedical Materials*, 2019.

*Contributed equally to this work and should be considered first authors

**Paper III** **Chemotactic capacity of human platelet lysate-loaded poly(ethylene glycol) hydrogels on hMSCs.**

A. S. Chahal, M.G. Florit, R. M. A. Domingues, M.E. Gomes, H. Tiainen

Manuscript, 2019.

# List of abbreviations

| | |
|---|---|
| **α-MEM** | α-minimum essential media |
| **AA** | ascorbic acid |
| **AFM** | atomic force microscopy |
| **ACP** | amorphous calcium phosphate |
| **ALP** | alkaline phosphatase |
| **BCA** | bicinchoninic acid |
| **BGP** | β-glycerophosphates |
| **BMP** | bone morphogenetic protein |
| **BMSCs** | bone marrow derived mesenchymal stem cells |
| **CaP** | calcium phosphates |
| **CLSM** | confocal laser scanning microscopy |
| **COM** | centre of mass |
| **DAPI** | 4′,6-diamidino-2-phenylindole |
| **$d_{i,accum}$** | accumulated distance |
| **DNA** | deoxyribonucleic acid |
| **dNTP** | deoxyribonucleotide triphosphate |
| **DPSC** | dental pulp stem cell |
| **DX** | dexamethasone |
| **ECM** | extracellular matrix |
| **ELISA** | enzyme-linked immunosorbent assay |
| **FA** | focal adhesion |
| **FBS** | fetal bovine serum |
| **FGF** | fibroblast growth factor |
| **FMI** | forward migration index |
| **GAPDH** | glyceraldehyde-3-phosphate dehydrogenase |
| **G-CSF** | granulocyte-colony-stimulating factor |
| **GF** | growth factor |
| **GMSCs** | gingival mucosa stem cells |
| **GTR** | guided tissue regeneration |
| **hMSCs** | human mesenchymal stem cells |
| **HA** | hydroxyapatite |
| **IGF** | insulin growth factor |
| **IL** | interleukin |
| **LDH** | lactate dehydrogenase |
| **MMP** | matrix metalloproteinase |
| **mRNA** | messenger ribonucleic acid |
| **MSCs** | mesenchymal stem cells |
| **MTT** | 3-(4,5-dimethylthiazol-2-yl)-2,5-diphenyltetrazolium |
| **OC** | osteocalcin |
| **OCP** | octacalcium phosphate |
| **OPN** | osteopontin |
| **OSX** | osterix |
| **PBS** | phosphate buffered saline |
| **PEG** | poly(ethylene glycol) |
| **PEG-M** | poly(ethylene glycol) functionalised with maleimide |
| **PEG-V** | poly(ethylene glycol) functionalised with vinylsulfone |
| **PDGF** | platelet derived growth factor |
| **PDL** | periodontal ligament |
| **PDLSC** | periodontal ligament stem cell |
| **PL** | platelet lysate |
| **pNPP** | *p*-nitrophenylphosphate |
| **PRP** | platelet rich plasma |
| **RA** | distance to the first neighbour |
| **R'E** | expected mean distance within a randomly distributed population |
| **RGD** | arginine-glycine-aspartate |
| **RNA** | ribonucleic acid |

| | |
|---|---|
| **RTase** | reverse transcriptase |
| **RT-qPCR** | reverse transcription quantitative polymerase chain reaction |
| **Runx2** | runt-related transcription factor 2 |
| **SCAP** | stem cells from the apical papilla |
| **SDF-1α** | stromal derived factor-1α |
| **SEM** | scanning electron microscopy |
| **SOST** | sclerostin |
| **TCPS** | tissue culture polystyrene |
| **TGF-β** | transforming growth factor-β |
| **TNF-α** | tumor necrosis factor-α |
| **TSP-1** | thrombospondin-1 |
| **VEGF** | vascular endothelial growth factor |
| $\mathbf{x_{i,end}}$ | final x-coordinates |

# 1 Introduction

Periodontitis is the sixth-most prevalent disease, affecting nearly 11% of the global population [1]. While many factors contribute to the development of periodontitis, bacterial colonisation leading to biofilm formation is regarded the main culprit for its onset (Figure 1a) [2,3]. The oral cavity copes with this bacterial imbalance with an acute inflammatory response, which manifests clinically over time as chronic inflammation of the soft and hard tissues that support the tooth (Figure 1b). Though the early stages of periodontitis may not immediately be debilitating, progression results in the loss of periodontal tissues, and eventually tooth loss, when left untreated. Diagnosis related to the severity of periodontal disease typically involves clinical evaluation of periodontal pocket depth, attachment loss and radiological assessment [4]. Current strategies to manage the disease focus on a consolidated aim: to remove biofilm and control inflammation, while preserving the integrity of the oral mucosa and preventing further alveolar bone loss (Figure 1c). The most common approach for treatment involves scaling and root surface debridement [5]. However, due to the excess production of proinflammatory cytokines, the capacity for the body to reconstruct the lost tissue is limited, and requires regenerative intervention [3,6]. While bone substitutes, guided tissue regeneration (GTR) membranes and the use of enamel matrix proteins have all been developed to facilitate this regenerative process, their success has been unpredictable [7]. In this thesis, we present an injectable scaffold material that could be implemented to stimulate endogenous regeneration within the periodontal pocket (Figure 1d).

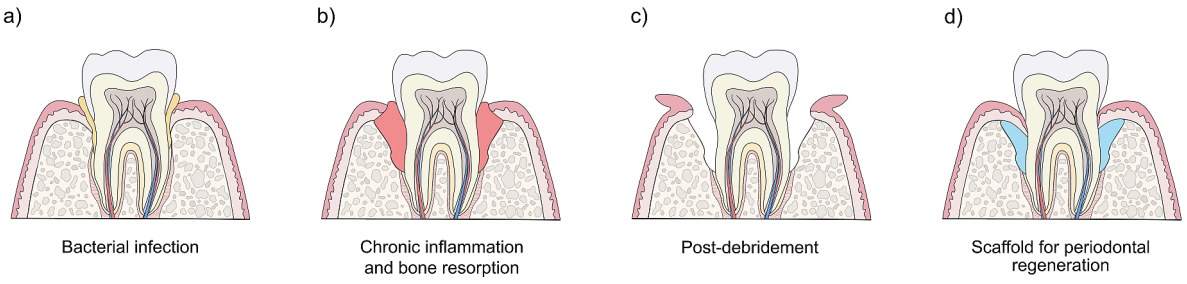


Figure 1: Periodontal disease: the problem and the proposed solution. (a) Bacterial colonisation along the lateral surface of the tooth. (b) As periodontitis manifests, inflammation occurs within the soft and hard tissue surrounding the tooth. (c) Debridement involves the removal of inflamed periodontal tissue. (d) An injectable hydrogel compliant to the geometry of the periodontal pocket (Illustration by Sanna Jacobsen. Adapted from [8])

## 1.1 Endogenous periodontal regeneration

The field of tissue engineering and regenerative medicine came about as means to restore damaged or diseased tissues and organs with structural and functional replacements [9]. Many of these solutions involve the development of biomaterials loaded with autologous cells aiming to build new tissues. However, these strategies are very limited since they rely on high numbers of cells from patients and require strict, controlled *in vitro* methods for expansion [10]. Alternatively, the body is known to be able to regenerate itself to a certain extent. Harnessing this natural capacity could side-step major hurdles involved in the translation of tissue engineered scaffolds. Hence endogenous regeneration, also referred to as autotherapy aims to utilise exogenous intervention, such as biomaterials and growth factors to prompt the body into a proregenerative state [10,11].

Since the objective of regeneration is to rebuild lost tissue within the defect, understanding the natural composition of cells and extracellular matrix (ECM) native to periodontal tissue is fundamental to the regenerative approach. An understanding of the microenvironment including the structural and functional relationships between the different cell types is a prerequisite to regeneration. The periodontium serves as a support system and as an anchoring unit to the tooth. Situated laterally around tooth root, it comprises of four anatomical structures: gingival epithelium, cementum, periodontal ligament (PDL) and alveolar bone (Figure 2) [12].

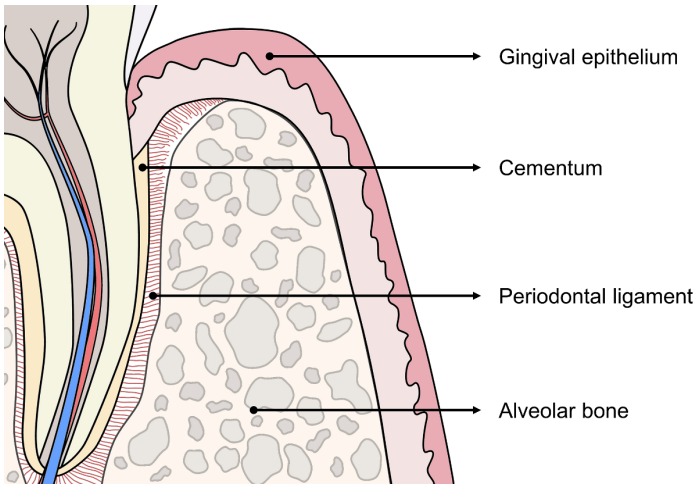


Figure 2: Structural components of the periodontium.

The gingiva surrounds and attaches to the cervical portion of the tooth on one side, and to alveolar bone on the other. The function of the gingiva is to act as a seal between the tooth and the inner layers of the epithelium to prevent fluid loss and access of external elements [12]. The

PDL is a set of collagen fibres known as the Sharpey's fibres, which are aligned horizontally and obliquely projecting from the cementum (Figure 2). They are responsible for anchoring the tooth and act as shock absorbers [13]. Unlike the PDL and gingiva, the cementum and alveolar bone are mineralised structures within the periodontium. The predominant cell types found in the gingiva and PDL are specialised gingival and PDL fibroblast cells [14,15]. On the contrary, the cellular part of the cementum mainly consists of cementoblasts, while the alveolar bone houses osteoblasts and osteocytes. The cementum is responsible for securing the attachment of PDL fibres to the root surface [16]. The fact that the periodontium consists of several different tissue types makes it a challenging tissue to regenerate. With structural margins across the periodontium, there are multiple junctions where the cells have subtle differences. For example, the gingival epithelium in the periodontium transitions from sulcular to junctional as it attaches to the cementum, each of which are known to have different morphologies [17].

Fortunately, there are certain similarities amongst the different structures within the periodontium. For example, there have been questions whether cementoblasts are essentially osteoblasts with a unique phenotype [16]. Additionally, PDL cells have been known to produce collagen and exhibit certain osteoblast-like features [18]. Even though different components of the tooth originate from different germ origins during early odontogenesis, most of the specialised cells within the periodontium arise from neural crest cells [19,20]. As illustrated in Figure 3, PDL fibroblasts are products of the mesenchymal lineage, while the gingival epithelium originates from oral epithelial cells (not shown in the Figure) [21]. Although there is some controversy regarding the origin of cementoblasts and osteoblasts of the cementum and alveolar bone, most studies do suggest they originate from the dental follicle as well [22-24].

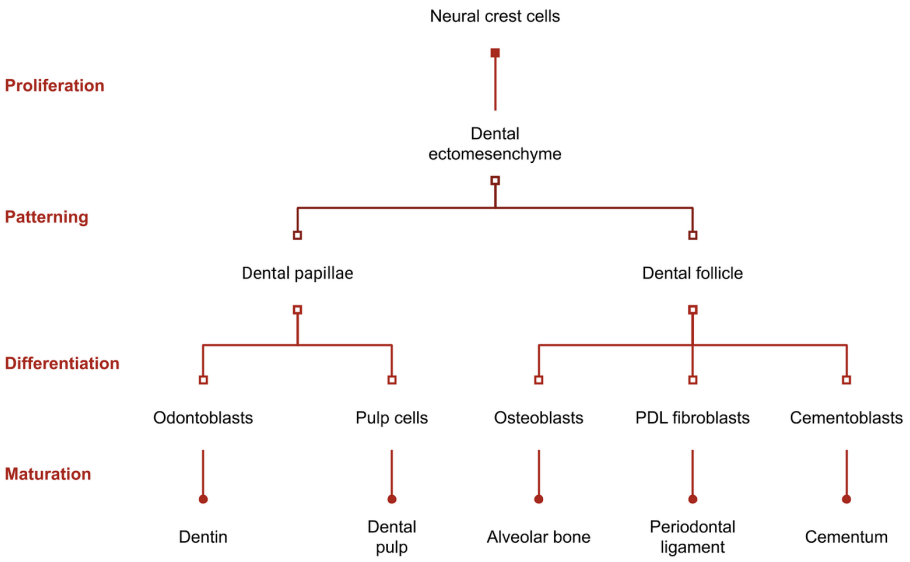


Figure 3: The origin of the main components of the peridontium. During odontogenesis, neural crest cells proliferate into the dental mesenchyme from where patterning into internal and external structures are primed. Dental follicle cells undergo further differentiation into the building blocks of specialised tissues, which mature and terminally differentiate into forming their respective structures. (Adapted from [21])

The majority of the work presented in this thesis involves *in vitro* experiments that assess cellular activity using mesenchymal stem cells. The reason for selecting mesenchymal stem cells is threefold: firstly, because periodontitis does not only result in alveolar bone loss, but also destruction of the periodontal ligament and cementum [25]. This would require unspecialised cells that have a multilineage potential to regenerate the hierarchical transitions of the periodontium. Secondly, due to the abundance and distribution of MSCs and progenitor cells within the oral cavity, it is relevant to conduct *in vitro* studies with these cells [26]. Lastly, mesenchymal stem cells have been recognised to have innate homing capabilities [27], which is pertinent when developing an acellular hydrogel that would sidestep the isolation and expansion of cells *ex vivo*. Hence, the approach involves harnessing the potential of mesenchymal stem cells to migrate, attach, colonise and differentiate into the tissues lost due to periodontitis (Figure 4).

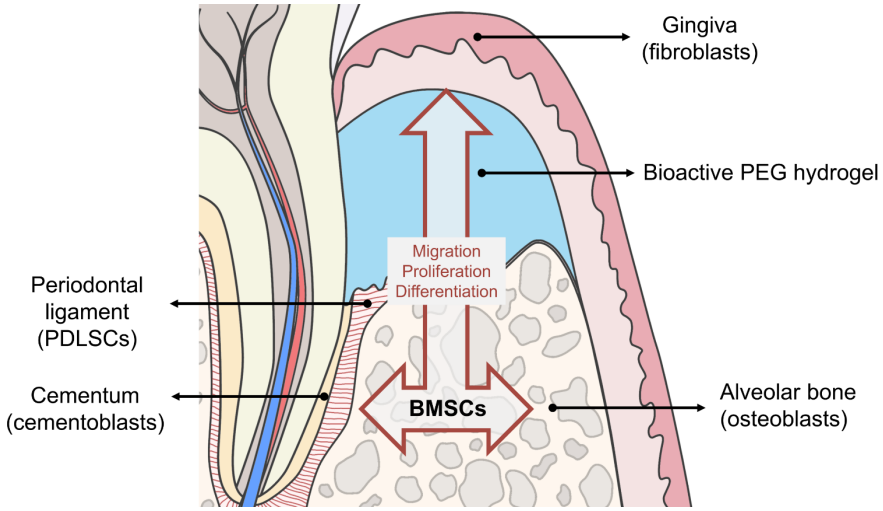


Figure 4: Mesenchymal stem cells surrounding the tooth are capable of migrating, proliferating and differentiating in to the key cell types that constitute the periodontal structures (Adapted from [19])

### *1.1.1 Stem cells in the oral cavity*

Stem cells are often characterised by their undifferentiated state and capacity to self-renew via asymmetric cell-division [28,29]. This means that they are not dedicated to becoming one specialised cell type, but instead have the ability to differentiate into a range of cell types. These cells originate very early in development as the inner cell mass within the blastocyst (also known as embryonic stem cells) [30]. As the embryo develops further, stem cells give rise to the different germ layers, followed by the generation of organ primordia. As stem cells proliferate rapidly to form organs within the foetus, dedicated niches of multipotent stem cells are deposited in each organ [31]. In cases of damage, these multipotent cells serve as the internal repair system for a dedicated set of tissues. Since many of the periodontal structures are descendants of the ecto-mesenchyme, many stores of mesenchymal stem cells are found in and around the tooth.

With their presence in many soft and hard tissues, mesenchymal stem cells (MSCs) exist in abundance throughout the body. Since they are morphologically very similar to fibroblasts, MSCs are typically identified based on their cell surface marker profiles, where they must be positive for CD73, CD105 and CD13, while being negative for haematopetic markers, CD14, CD34 and CD45 [32]. Due to stable *in vitro* expansion and the easy, but invasive access, stem cells from the bone-marrow of long bones is perhaps the most commonly tapped source for mesenchymal stem cells [33]. However, this may not be the most effective source for tissue regeneration. MSCs from the jawbone have proven to have higher proliferative and osteogenic

differentiation capacities than those present in long bones [34], which may be linked to the fact that they originate from different germ layers [35].

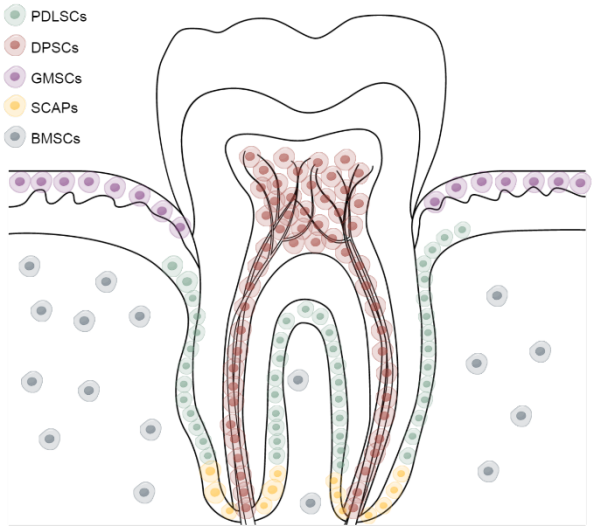


Figure 5: Stem cells within the oral cavity. PDLSCs = periodontal ligament stem cells, DPSCs = dental pulp stem cells, GMSCs = gingival mucosa stem cells, SCAPs = stem cells from the apical papilla, BMSCs = bone marrow derived mesenchymal stem cells.

Dental stem cells serve as a reservoirs dedicated to replenishing damaged structures. The different dental stem cells have dedicated names based on their location and regenerative purpose (Figure 5) [36]. However, many regenerative applications are being developed that use dental stem cells for purposes other than dental regeneration, since they have proven to have multi-differentiation potency [37-41]. For instance, periodontal ligament stem cells (PDLSCs) have been recognised for their differentiation into osteoblasts [42]. The multi-differentiation potential indicates that most dental stem cells are capable of regenerating key components of the periodontium, irrespective of their microenvironment. As the name suggests, PDLSCs likely contribute to the generation of new ligament fibres between the cementum and the alveolar bone [43]. On the contrary, dental pulp derived stem cells (DPSCs) are said to be inherent in the perivascular niche within the canal of the tooth [44]. Surrounded largely by mineralised hard tissue, these cells are not directly exposed to the periodontium. Hence, it is likely that in the case of endogenous periodontal regeneration, PDLSCs would be the first-responders in the proregenerative environment. Although, autologous porcine models and pre-clinical studies have already demonstrated the formation of PDL-cementum complexes using PDLSCs [45,46], the question still remains as to how we can harness this potential and coax these stem cells to reconstruct the damaged periodontium endogenously.

### *1.1.2 Dynamic cell-matrix reciprocity*

Building new tissue essentially means supporting cells to establish themselves in high numbers, while allowing them to form an extracellular matrix (ECM). This key component of tissue was once believe to merely serve as a "glue" to hold cells together. However, recent studies regarding cellular interaction with the ECM has changed this opinion drastically [47]. The perception that the ECM is an inert substance is no longer the case. Instead it is recognised as an interactive and dynamic backbone that regulates intricate cellular processes, while providing tissue with the morphology and homeostasis to function collectively as an organ [48]. While cells themselves build the ECM, they are also dependent on being instructed by the ECM itself. This constant dialogue and bi-directional physical and chemical relationship between the cells and the ECM has been termed as dynamic cell-matrix reciprocity (Figure 6) [49].

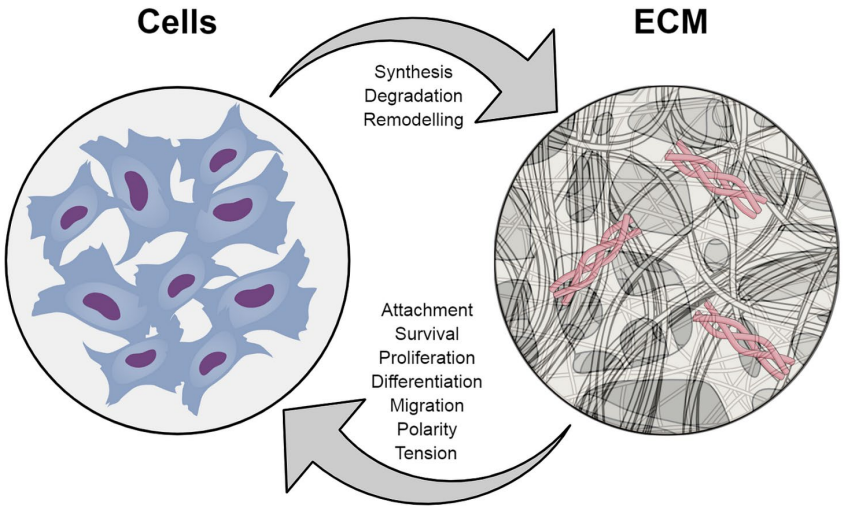


Figure 6: Dynamic reciprocity interactions between cells and the ECM. (Adapted from [50]). The cells synthesis the ECM and are capable of degrading it as part of the remodelling process. In exchange, the ECM provides the cells with attachment anchors essential to their survival and proliferation. Once cells colonise the matrix, the ECM supplies inductive cues importance to the differentiation and migration of cells across the tissue. Additionally, the cells are receptive of the mechanical tension and polarity imparted by the ECM.

The ECM typically comprises of a variety of macromolecules such as proteoglycans and collagen fibres, along with cell adhesive proteins such as fibronectin and laminin [51]. Additionally, the ECM is abundant in poly-peptide growth factors (GFs) that are distributed across the ECM, signalling cells to perform specific cell activities [52]. It is the specific localisation of these macromolecules and growth factors that allows for highly controlled interactions with cells [53]. As for the peridontium, its ECM is very rich in fibrillar collagen which gives the tissue its integrity and rigidity [47]. On a larger hierarchical level, the structure, composition and mechanical properties of these collagen fibres give the tissue its function in

supporting the tooth [54]. With both fibrous and mineralised components that make up the periodontium, the ECM across the tissue is non-uniform and particularly complex. Additionally, various diseases including periodontitis are known to alter the ECM composition within the tissue [47]. For instance, in the case of early and moderate periodontitis, the acellular cementum is damaged as opposed to the cellular cementum in severe periodontitis [21]. This further complicates the regenerative approach.

Reconstructing the damaged or absent ECM is certainly not an easy task. Since the ECM is specific to each microenvironment and undergoes constant remodelling, it is a highly ambitious endeavour. Instead, it is more feasible to create a microenvironment conducive to cell colonisation, allowing the cells themselves to model the ECM. That being said, using a material for endogenous regeneration provides the means to regulate and instruct cells via bioactive cues. This gives rise to two questions that need to be addressed: 1) what physical and chemical material features are important for periodontal regeneration, and 2) what combination of bioactive factors would coax cells into a proregenerative state? These important considerations will be discussed in the subsequent chapters.

## 1.2 Hydrogels for periodontal regeneration

### *1.2.1 Poly(ethylene glycol) hydrogels as a provisional ECM*

Naturally occurring ECM is a dynamic structure that provides structural integrity to tissue, while keenly regulating cell activity [51]. Its active participation in guiding cell behaviour has made it the basis for developing biomaterials that mimic its form and function [55]. Hydrogels are a class of materials that are structurally very similar to native ECM, in that they are typically composed of hydrophilic cross-linked networks which can resist a certain amount of tensile and compressive stress [56]. Furthermore, the molecular structure of the cross-linked mesh can be tailored to be permissive to the exchange of nutrients and the transport of macromolecules [57]. As with naturally occurring ECM, these hydrogels too can be tethered with bioactive moieties that support cell adhesion and prompt specific cell responses. As expected from a native ECM, hydrogels can also supply chemical instructive cues, while providing cells with mechanical support (Figure 7) [56]. In order to mimic specific compositions of natural ECM, a polymer backbone with predictable and controllable chemistry is essential. Star poly(ethylene glycol) (PEG) macromers have previously been used to produce hydrogels in a controllable manner, yielding many biologically desirable properties [58,59]. Star PEG arms functionalised with

reactive groups serve as tethering points for cell-adhesion motifs such as arginine-glycine-aspartate (RGD) (Figure 7). Additionally the low-protein adsorption of PEG itself enables the mesh to serve as a reservoir of growth factors with minimal undesired interactions.

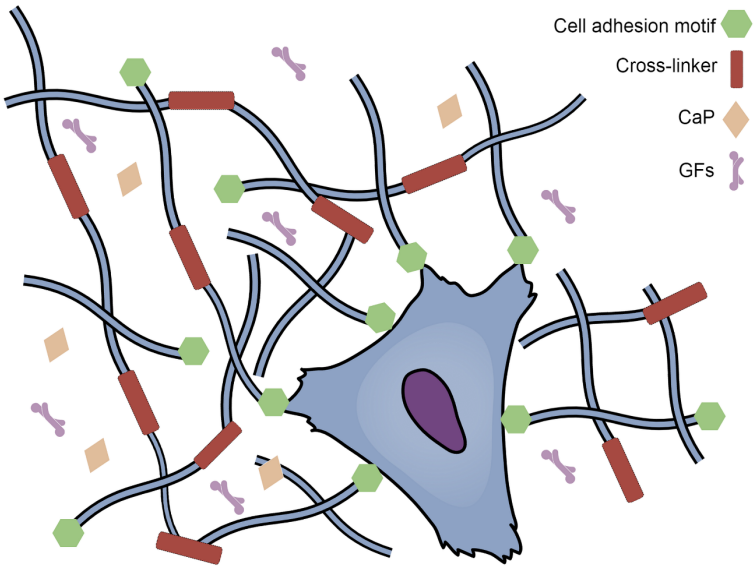


Figure 7: The cross-linked PEG hydrogel mesh acts as a provisional ECM, providing the cell with attachment sites and bioactive cues such as growth factors and minerals.

Natural ECM is under constant remodelling by the cells to meet demands of the local microenvironment. For hydrogels to perform similarly, the design would require a polymer backbone that can be degraded upon cell colonisation. As the native ECM is remodelled via cell-proteases [60], hydrogels too, can incorporate protease sensitive cross-linkers. As cells colonise the hydrogel, the polymer network would be susceptible to degradation via the release of cell-proteases such as matrix metaloproteinase (MMP) [61,62]. While such hydrogels mimic naturally occurring extracellular matrices in many aspects, nature is often a step ahead. The complex distribution, presentation and temporal release of bioactive molecules occurs in a systematic and highly regulated manner. Simultaneously, cells use and replenish extracellular stores of GFs and molecules to remodel the ECM. Hence, it is more reasonable implement a hydrogel matrix as a provisional ECM that provides the structural basis for cell-driven remodelling, rather than attempting to re-engineer a very organised and regulated network of molecules. At the same time, it would be beneficial to incorporate cell-adhesive and chemotactic cues within the hydrogel that would support cell colonisation and ultimately facilitate the remodelling process.

Considering the amount of bone loss in periodontitis is relatively small, one would expect that the body is capable of regenerating the periodontium itself. However, the body is incapable of

doing so, as the demands to treat periodontitis are highly specific. Since the tissue is in a chronic inflammatory state, innate regenerative processes are limited. At the same time, reduced alveolar bone height leads to the collapse of the junctional epithelium. This has given rise to interventions such as GTR membranes that are aimed at occluding the gingival connective tissue from the alveolar bone out of the hope to facilitate bone regeneration [63]. However, the use of an injectable material has certain advantages over the use of GTR membranes. For instance, minimal surgical intervention is required to access the defect site. Additionally, with the ability to conform to different defect geometries, an injectable material would fill the defect in a way that would provide stability to the gingival flap, but also serve as a provisional ECM, susceptible to cell infiltration. Hence an injectable hydrogel would facilitate vertical alveolar bone growth, periodontal ligament ingrowth, while also being clinically manageable.

### *1.2.2 Inducing cell migration*

Endogenous regenerative medicine is a rather nascent, yet promising field within regenerative therapy. It relies on stimulating self-healing mechanisms and harnessing the body's natural capacity to repair and regenerate diseased tissue [11]. Stem cells are in the spotlight of endogenous regeneration, since they have the innate capacity to migrate to tissues that need repair [64,65]. Stem cell migration is a highly coordinated process, involving cell-adhesion molecules, ECM components, and the stem cell niche itself [66]. Each of these molecules play a role, either in the mobilisation of stem cells or as chemokines that provide directionality to cellular migration [67]. Utilising factors that stimulate the migration of stem cells would be purposeful in endogenous regenerative applications. While the delivery and release of these factors dictate its effects [10], Table 1 summarises key factors that have been identified as chemotactic inducers for stem cell recruitment.

Table 1: Important factors identified for stem cell homing and induction of chemotaxis. Adapted from [68,69]

| **Molecules** | **References** |
|---|---|
| Platelet derived growth factor (PDGF) | [70,71] |
| CXC chemokines (especially SDF-1α) | [72-76] |
| Vascular endothelial growth factor (VEGF) | [77] |
| Tumor necrosis factor alpha (TNF-α) | [78] |
| Transforming growth factor beta (TGF-β) | [79,80] |
| Matrix metalloproteinases (MMP) | [81,82] |
| Granulocyte-colony-stimulating factor (G-CSF) | [83,84] |

Unfortunately, bolus systemic or local injections of growth factors (GFs) have low stability and undergo rapid degradation with limited half-lives *in vivo* [85-87]. Alternatively, repeated doses of these factors can have adverse systemic effects, along with unnecessary accumulation across the body [88]. Hence, direct delivery of these factors is inefficient in recruiting stem cells, since the regenerative process relies heavily on the controlled and prolonged release of these chemokines [75]. Scaffolds can serve as delivery vehicles for these molecules, providing various means of efficient loading that can be tailored as per the intended application. Bonding strategies, such as direct loading, immobilisation via ionic complexes, and particulate systems, have all been used previously. However each of these methods come with specific pros and cons [75,89-91]. Additionally, loading scaffolds with multiple recombinant factors is likely to result in better recruitment of stem cells [92]. However the safety and underlying molecular mechanisms of such approaches *in vivo* are yet to be validated.

This has prompted the use of blood derivatives such as platelet rich plasma (PRP) and platelet lysates (PL) that naturally contain many of the chemoattractants identified in Table 1 [93]. As the name suggests, PRP is a concentrate of platelets isolated from blood plasma upon multiple centrifugation steps [94]. On the other hand PL is the lysed product of PRP as a result of repeated freeze-thaw cycles or via platelet disruption using ultrasound [95]. Although both of these blood derivatives are products of platelets, PL has the upper hand over PRP in its clinical practicality and utility. Firstly, PL can be frozen and stored for use, whereas PRP needs to be used upon processing. Secondly, PL processing results in the release of growth factors that would otherwise require platelet activation in order to be released. Next, PL is void of platelet debris and does not form fibrin glue easily, which is known to trap some of the growth factors present in these blood derivatives [96]. Unlike PRP pools, growth factor concentrations from different pools of PL show insignificant variations, contributing to predictable outcomes when used to guide cell behaviour [97]. Both PL and PRP also contain cell adhesion molecules to support cell adhesion to the ECM [98].

### *1.2.3 Supporting cell adhesion*

The adherence-dependent nature of mesenchymal stem cells suggests that their survival and expansion depends on physical interactions with their environment [99]. In parallel, scaffolds and biomaterials have undergone a paradigm shift from being structural supports for damaged tissues to being actively integrated into the tissue itself. This has led to the development of

natural and synthetic approaches that facilitate cell colonisation and tissue integration as an important part of biomaterial related research [100].

As mentioned earlier, cells interact with the ECM both physically and chemically. This physical interaction occurs via transmembrane heterodimer proteins called integrins [101]. Subunits of integrin can bind to ECM molecules such as fibronectin, vitronectin and a variety of collagens [102]. However, the common denominator of these interactions is the highly specific binding of integrin with a tri-amino acid sequence, arginine-glycine-aspartate (RGD) [103]. This RGD fragment has been produced synthetically for its incorporation into biomaterials. It is not only inexpensive and highly reproducible, but also comes with many advantages over using native ECM proteins. Given the size of the small RGD fragment in comparison to whole ECM proteins, scaffolds can be functionalised with high spatial control and presentation of RGD ligands [104]. Additionally, RGD fragments are less susceptible to proteolytic degradation compared to whole proteins. While RGD is synthetically produced, it brings minimal risk of pathogen transmission and immune reactivity. Simultaneously, the synthetic production process enables the addition of flanking amino acids to the RGD sequence, allowing it to be chemically tethered to a wide range of biomaterials. *In vitro* assessments combining RGD with non-fouling materials such as PEG have high predictability for *in vivo* translation since unspecific binding is negligible [104].

RGD can facilitate more than just cell attachment. The presentation, density and isoform of RGD can influence cell morphology, migration and differentiation of cells [105-107]. The two main isoforms of RGD are cyclic and linear, mainly differ in their spatial conformation [108]. Additionally, it is believed that both isoforms differ in specificity to different integrin subunits, while cyclic RGD is known to have higher stability *in vivo* [107,109]. However to achieve tissue regeneration, RGD functionality alone would be inadequate to achieve tissue regeneration. Bioactive molecules such as growth factors and osteoinductive minerals can be added into the biomaterial matrix to guide cells to terminally differentiate and ultimately form tissue.

### *1.2.4 Driving stem cell differentiation*

The high-inflammatory conditions within the periodontal defect prevents cells such as osteoblasts, PDL cells and mesenchymal stem cells from performing their regular reparative duties [110]. Minimising inflammation alone is insufficient to drive repair, and the cells require a conducive microenvironment that promotes the regeneration of damaged tissue. Hence, the

right inductive cues are necessary to coax both residential and recruited cells into a proregenerative state that would ideally result in tissue formation. The multilineage capacity of dental stem cells implies that different external cues, would direct cells differently [111]. With numerous naturally occurring growth factors in blood derivatives, different responses from each of the cell types could be expected [93].

Blood derivatives such as PL not only contain factors that are capable of inducing cell migration, but also stimulants that drive cell differentiation [97]. The most abundant products from the α-granules of platelets are PDGF, IGF and TGF-β, which have been linked to the recruitment of progenitor cells as well as the differentiation of pre-osteoblast cells. Additionally, other important factors such as VEGF and BMP are known to be potent inducers of vascularization and bone formation [112]. BMP along with IGF and TGF-β belong to the same superfamily of proteins, which play significant roles in the differentiation of cells to form hard tissue [97,113]. BMPs are perhaps the most popular of them all, widely recognised for their potential in inducing ectotopic osteogenesis, and have received both credit and criticism for their use as a recombinant protein [114-116]. In addition to BMPs, FGF has also shown increased bone healing when used in combination with calcium phosphates in periodontal rat defects [117]. Additionally, FGF alone is capable of driving PDL cells into osteogenic phenotypes *in vitro* [118]. TGF-β, on the other hand plays a very different role when it comes to bone formation. It is known to inhibit osteoclast activity, while also stimulating osteoblastic bone formation [119]. Hence, it is a key regulator of bone homeostasis, with the capacity to recruit stem cells as well [120]. Among others, FGF, TSP-1 and TNF-α also actively contribute to the wound healing and regenerative process [121,122]. However it is the combination of these GFs that makes PL an attractive source for the induction of cell differentiation [93].

Though each GF mentioned above has been associated with differentiation when isolated, whether the same effects would be observed via blood derivatives is questionable. Nonetheless, it is clear that GFs in blood derivatives provide a nurturing microenvironment for cells, while effectively recruiting progenitor cells [97,122]. Hence, the use of osteoinductive materials in combination with blood derivatives could possibly have synergistic effects towards cell differentiation and periodontal tissue formation [97,117]. Supplying calcium phophates (CaP) would replenish the microenvironment with raw materials necessary to form mineralised tissue. CaP are known to have osteoconductive and inductive properties that have been used to promote MSC differentiation [123,124]. Hydroxyapatite (HA), tricalcium phosphates (TCP) and amorphous calcium phosphates (ACP) have all been used based on their differences in

solubility, stability, ionic release and mechanical strength [125]. Although HA is the main CaP present in naturally occurring bone, its high stability makes it less susceptible to remodelling [126]. This is important because the degradation and local ion release from soluble calcium phophates have been associated with upregulation of key osteoblastic differentiation genes [127]. Additionally, cells exposed to HA scaffolds with soluble CaP have shown increased collagen synthesis and ECM mineralisation, when compared to HA scaffolds alone [128]. This suggests that soluble CaP may be a better choice than stable HA in promoting the regeneration of mineralised tissue within the periodontal defect.

# 2 Research concept

The idea behind utilizing an injectable, synthetic and modular PEG hydrogel system was to develop a clinically viable and minimally invasive approach for periodontal regeneration, while side-stepping any hindrances related to cell therapies that involve *ex vivo* cell isolation and expansion. PEG hydrogels alone are insufficient to actively induce periodontal tissue regeneration. Therefore, PL and CaP were incorporated into the injectable system to direct cell migration and differentiation respectively. The key components and likely mechanisms that would orchestrate cellular responses within the periodontal pocket are highlighted in Figure 8.

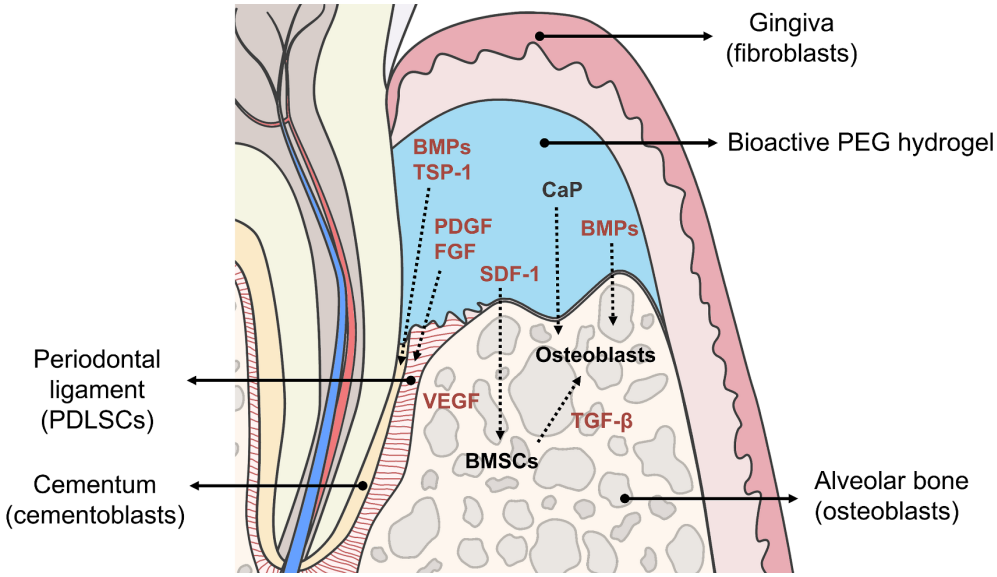


Figure 8: Conceptualisation of endogenous regeneration for periodontal defects with an injectable bioactive hydrogel scaffold.

In order to assess the individual role of each of the biofunctional components added to PEG hydrogels, *in vitro* studies were carried out separately. First, PEG was functionalised with the synthetic integrin binding peptide, RGD, enabling cells to adhere and colonise the scaffold (Paper I). Next, in order to drive differentiation towards the osteogenic lineage, there was a selection of factors to choose from that could guide the stem cells in this direction. We chose to study the osteogenic effects of ACPs within the hydrogel scaffold (Paper II), not only because calcium and phosphate are prerequisites for bone formation, but also because the addition of minerals could potentially add mechanical integrity to load bearing applications of the hydrogel under development. Finally, to circumvent the isolation and expansion of cells for clinical use, we decided to incorporate platelet lysate within the gel substrate as means of attracting cells towards the hydrogel scaffold (Paper III).

The general hypothesis of the thesis is that specific bioactive cues incorporated into the hydrogel system would enable the cells to attach, differentiate and migrate towards the hydrogel scaffold. As a result, emphasis in this thesis is placed on cellular responses when in contact or exposed to hydrogels containing bioactive molecules.

The following research questions were addressed in individual papers as part of this thesis:

**Paper I: Cell attachment studies**

- What concentration of RGD is required for hMSCs to attach on PEG hydrogels?
- How do cells organize themselves on hydrogels of varying RGD concentration and conformation of the RGD ligand?
- Does increased RGD concentration compromise the mechanical stiffness of the hydrogel matrix?

**Paper II: Cell differentiation studies**

- Do minerals in the hydrogel serve as adhesion points for hMSCs?
- Does the release of minerals pose any cytotoxic effects on hMSCs?
- Do composite hydrogels promote osteogenic differentiation of hMSCs?

**Paper III: Cell migration studies**

- Do platelet lysate loaded PEG hydrogels stimulate directional migration of hMSCs?
- Do platelet lysate loaded PEG hydrogels increase the invasiveness of hMSCs in 3D?

An experimental design was developed to investigate these research questions (Figure 9).

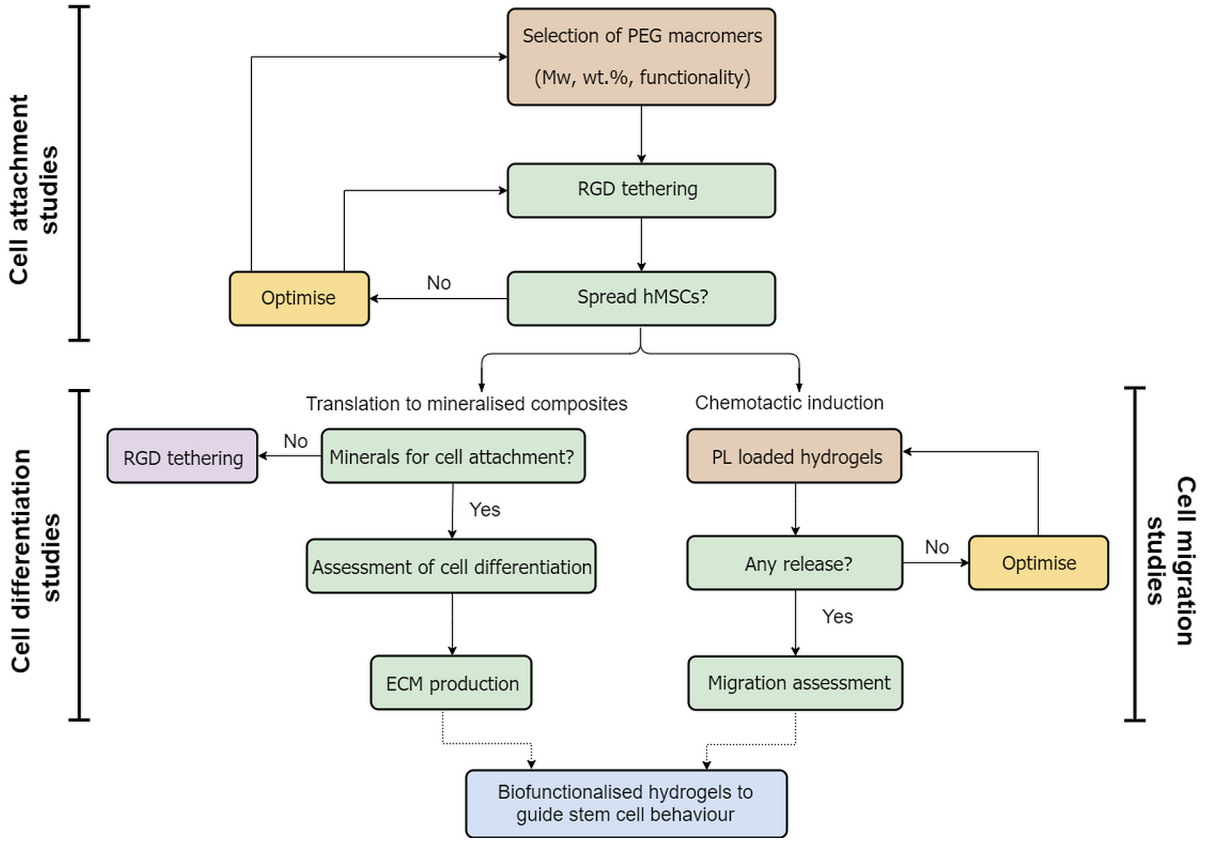


Figure 9: Summary of the experimental strategy followed in this thesis to evaluate the incorporation of cell-adhesive motifs, ACP and platelet lysate as part of the hydrogel system.

# 3 Experimental considerations

A variety of experimental and analytical techniques have been implemented in this research study, many of which are well known in the field of stem cell biology and biomaterials. This section introduces the different methods adopted to address the research questions defined in the previous chapter. However, the aim of this section is not only to justify the purpose of the techniques and state any adaptations made, but also to critically assess the advantages and shortcomings of their use, while acknowledging possible alternate approaches.

## 3.1 Hydrogel formation and biofunctionalisation

### *3.1.1 PEG hydrogels*

The hydrogel system used in the experimental work of this thesis was based on previous work conducted by Lutolf and Hubbell [57,129]. In this system, four or eight armed PEG macromers containing either maleimide (M) or vinylsulfone (V) reactive groups are dissolved in buffer and cross-linked via MMP-sensitive peptides (Figure 10). A covalently linked hydrophilic network is formed as reactive groups on the PEG macromers participate in a "click" thiol-Michael addition reaction with *bis*-cysteine from the MMP-sensitive cross-linking peptide. As PEG macromers cross-link, the bulk of the material undergoes a sol-gel transition. This changes the properties of the system from a viscous to an elastic nature. Hydrogels were formed into discs by pipetting a droplet between two hydrophobic glass slides with a silicon spacer in between. This resulted in a disc with uniform surface, while the silicon spacers prevented the hydrogel from drying out during the gelation process. The main reason we adopted PEG based hydrogels was due to the modular "click" chemistry that enables biofunctionalisation with both, ease and efficiency [130]. Additionally, cross-linking via Michael-addition reactions between thiols and –enes can occur under physiological conditions, without the need for any free radicals, making it a well-suited reaction for biological applications [131-133].

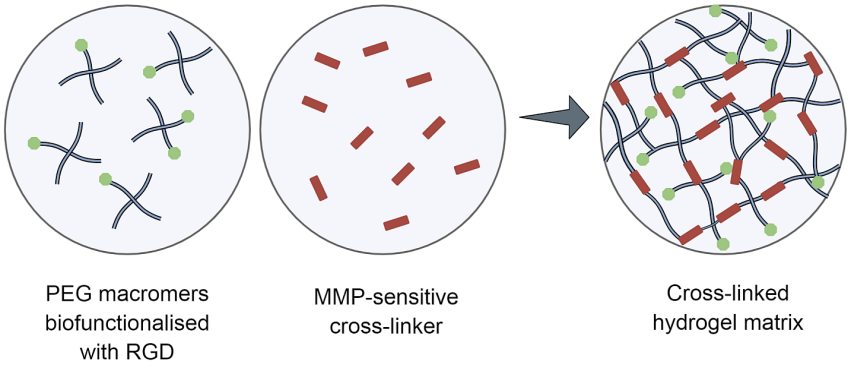


Figure 10: Schematic illustrating macromers biofunctionalised with RGD and cross-linked with an MMP-sensitive peptide to form a hydrogel network.

While both maleimide and vinylsulfone reactive groups are capable of participating in hydrogel formation, they do so under very different pH conditions. PEG-M hydrogels form under acidic conditions (pH 3.0 – 4.0), while PEG-V hydrogels form under basic conditions (pH 7.0 – 8.0) [134]. Although PEG-M hydrogels are known to have relatively high reaction efficiency with fast gelation kinetics, the acidic conditions are a prerequisite for this to occur [133]. Nonetheless, the low pH requirement comes with certain benefits and drawbacks. Since PEG-M is more tolerant to the acidic conditions, it is better suited as an injectable material into the acidic environment of a wound site. However, these acidic conditions can be unfavourable for cell encapsulation or seeding for *in vitro* studies. Hence, PEG-M hydrogels underwent a swelling step in cell culture media, prior to cell seeding for *in vitro* experiments (Papers I and II). This enabled an exchange of low-pH buffer post-gelation with cell culture media, making the scaffold compliant to cell culture. There are various other methods to make PEG-M gels more attractive for cell culture such as lowering the buffer concentration, increasing the thiol reactivity or by using more electronegative end-linking peptides [135]. Though our approach may not support cell encapsulation, it is a straightforward solution to seed cells onto the scaffold (in 2D) without compromising the gelation kinetics or mechanical properties of the hydrogel. Alternatively, PEG-V has extensively been used for *in vitro* and *in vivo* studies in the past [136-138], since hydrogels can be formed under physiological pH, allowing for cell encapsulation (Paper III). The high pH reactivity of vinylsulfone enabled us to form hydrogels by simply dissolving the polymer in cell media or platelet lysate solution while maintaining effective cross-linking of the PEG backbone. However, the PEG-V gels have previously been shown to have slower gelation kinetics and lower mechanical properties in comparison to PEG-M gels [134].

PEG-M was pursued as a more attractive system in terms of creating composite hydrogels containing ACP minerals (Paper II). The formation of CaP minerals precipitates the phosphate ions from the buffer, reducing the pH of the gel suspension as the buffer capacity of the buffer is diminished. However, high pH conditions are desirable for mineral formation. While the high pH conditions required for PEG-V hydrogels may appear useful here, the consequences due to the drop in pH with mineral formation is a lot more pronounced in the PEG-V system. This results in much slower gelation kinetics, which dismisses its clinical applicability altogether [134]. On the other hand, by increasing the pH of the buffer used in the PEG-M system, we were able to strike a balance between the two competing reactions of gelation and mineral formation resulting in hydrogels with reliable gelation kinetics and mechanical properties [139]. Additionally, the superior mechanical properties of PEG-M hydrogels could be particularly beneficial when incorporating biofunctional cues into the system.

### *3.1.2 RGD tethering*

In order to accommodate cell adhesion, whole proteins or peptide sequences need to be incorporated within the PEG network [107]. Given the reputed use of RGD in support of cell adhesion [140,141], we decided to incorporate these synthetic cell adhesive peptide into our hydrogel system. RGD peptides are typically available as two isoforms: linear (linRGD) and cyclic (cycRGD). Though there is evidence that the $\alpha_v\beta_3$ domain of integrin binds to cycRGD with increased affinity and specificity, it is significantly more expensive to produce [142,143]. At the same time, the linear isoform has shown specificity to the $\alpha_5\beta_1$ subunit, capable of affecting downstream mechanisms within the cell [107]. While both isoforms of RGD are used, there is no general consensus regarding the ideal concentration needed to enable cell attachment onto PEG hydrogels [144]. Hence, our selection criteria for the required RGD concentration was rather straightforward. We decided to incorporate RGD at low concentrations, slowly working our way up towards concentrations that have been more typically used in PEG hydrogels [141,145].

As RGD is introduced to the polymer solution prior to cross-linking, a fraction of the PEG reactive groups react with RGD via a cysteine linkage. One obvious drawback of this is that fewer reactive sites are available for end-linking [132]. This would likely result in an overall decrease in the mechanical properties of the hydrogel due to the formation of fewer elastically effective chains. Considering that PEG-M gels have demonstrated superior mechanical properties and less network imperfections compared to PEG-V gels [134], we opted to tether

RGD on PEG-M hydrogels in order to minimise any mechanical compromise imposed by the presence of RGD. Nonetheless, there are other controlled manners in which the mechanical properties of the hydrogels can be retained. Either increasing the number of arms per PEG macromer or increasing the polymer content within the hydrogel, would counter any mechanical compromises due to RGD tethering. In the experimental work presented in this thesis, PEG macromers with different polymer properties were implemented (Figure 11).

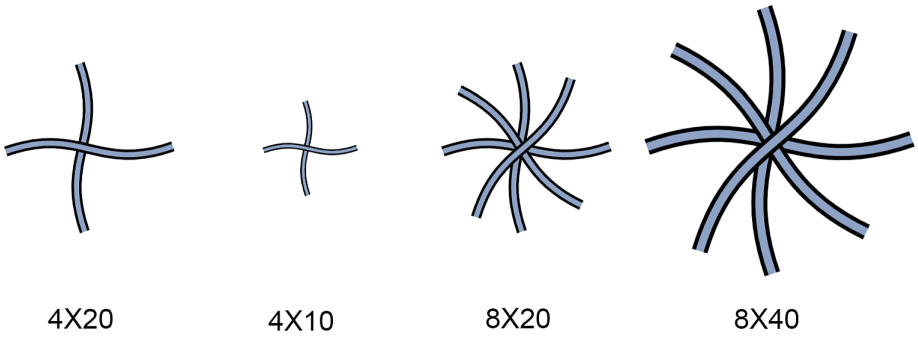


Figure 11: Schematic of 4- and 8-arm PEG macromers with varying molecular weights used to produce hydrogels, From left to right: 4-arm 20 kDa (4X20), 4-arm 10 KDa (4X10), 8-arm 20 kDa (8X20) and 8-arm 40 kDa (8X40). 'X' represents the reactive group, maleimide (M) or vinyl-sulfone (V).

However, alterations in polymer properties can have consequences associated with it. With more number of arms or increased arm lengths, RGD can be distributed very differently throughout the hydrogel. As a result, the manner in which these peptides are presented to the cells can yield different cell attachment and morphological characteristics. RGD clustering and lateral spacing between adjacent RGD peptides is known affect cell spreading, focal adhesion dynamics and cytoskeletal organisation [106,146,147]. Hence, it is important to consider whether the presentation of RGD ligands would be altered by changing the number of functional arms and the molecular weight of the macromers. There are few approaches to validate the presentation of these ligands. This would require super-resolution fluorescence microscopy, where antibodies specific to the integrin associating itself with the RGD could be labelled, allowing a visualization for the presence of RGD. However, this would only highlight the RGD peptides participating in integrin binding. Alternatively, synthesizing fluorescently labelled RGD peptide conjugates have been utilised to stain peptide interactions with specific domains of integrin [148,149]. However, the latter would likely be limited by spatial resolution, given that mesh sizes within our hydrogel system are within the order of few nanometres.

### *3.1.3 Incorporation of calcium phosphate*

ACP has been identified in matrix vesicles in hard tissues such as the enamel [150]. The formation of HA is preceded by amorphous or octa calcium phosphates (OCP) [151,152] in aqueous solution, the role of ACP as a precursor to hydroxyapatite in biological tissue is debated [153,154]. Nonetheless, the biological activity and stability of CaP is highly dependent on the solubility of CaP minerals [155]. While the solubility of CaP is highly dependent on the pH of the environment [156], the high solubility of ACP makes it more readily available to cells in comparison to minerals with lower solubility [157]. This feature of ACP serves as the basis for incorporating CaP with high solubility into hydrogels to serve as a building block for a mineralised ECM.

Considering that the polymer was dissolved in a phosphate buffer, the addition of calcium to the system would directly promote the formation of CaP minerals. By including calcium within our cross-linking solution, a simultaneous reaction of mineral precipitation and cross-linking was established. This enables the formation of well-dispersed mineral phase throughout the hydrogel. Additionally, considering that mineral phase transformation occurs rapidly in alkaline solutions, strategies that would prolong the solubility of ACP and prevent mineral transformation were applied. This involved stabilizing ACP either via ionic substitution [158,159] with ions such as $Zn^{2+}$ or via surface adsorption [160] using organic molecules such as citrate. Finally, careful selection of the reactive group for the PEG macromers was a governing factor regarding the pH of the reaction, as previously discussed. The pH of the reaction was particularly important here since it would not only determine the gelation kinetics, but also the precipitation of CaP itself. With a mechanically superior PEG-M hydrogel, the presence of minerals would further reinforce its high physical properties while soluble CaP would direct cell behaviour (Paper II).

### *3.1.4 Platelet lysate loading*

The chemotactic potential of PL loaded PEG hydrogels was studied in Paper III. In order for these hydrogels to elicit a response, it is necessary that the bioactive molecules are released and made available to the cells. Hence, we selected polymer parameters that would likely facilitate the release of proteins from the PL loaded hydrogels. As a result, PEG-V hydrogels with low polymer content (5 wt. %) and with longer polymer arms (8-arm, 40kDa) were chosen to form GF and protein permissive networks. Additionally, it is important to consider that proteins in the PL could possibly interfere with the formation of elastically effective chains. Hence, as a

precautionary measure, 8-arm PEG macromers were selected to minimise adverse consequences on the mechanical properties of the hydrogel. However, this was not the only reason for our selection. Since invasion studies involved the encapsulation of hMSC spheroids within the hydrogels, larger mesh sizes would promote the delivery of nutrients to the spheroid, while also minimally constricting cellular outgrowth. Vinylsulfone reactivity was a deliberate choice despite its previously mentioned inferior mechanical features [134]. Gelation at physiological pH readily supported the encapsulation of spheroids, without additional buffering required. Additionally, this enabled the dissolution of PEG macromers directly in PL concentrates.

## 3.2 Material characterisation

### *3.2.1 Network architecture*

Swelling ratio measurements represent an indirect measure of the network architecture within the hydrogel construct. The mechanical properties of the hydrogel depend on two factors: the cross-linking density and the equilibrium volumetric swelling ratio [161]. The cross-linking density depends on the properties of the polymer itself, such as wt.%, functionality and number of arms. These factors ultimately dictates the degree to which a hydrogel would swell. As a result, a hydrogel in the swollen state will exhibit higher equilibrium liquid content, larger mesh sizes (ξ) and inferior mechanical properties compared to its unswollen counterpart (Figure 12a). Nonetheless, an increase in the cross-linking density and polymer content restricts swelling by the presence of a larger number of elastically effective chains [162] (Figure 12b).

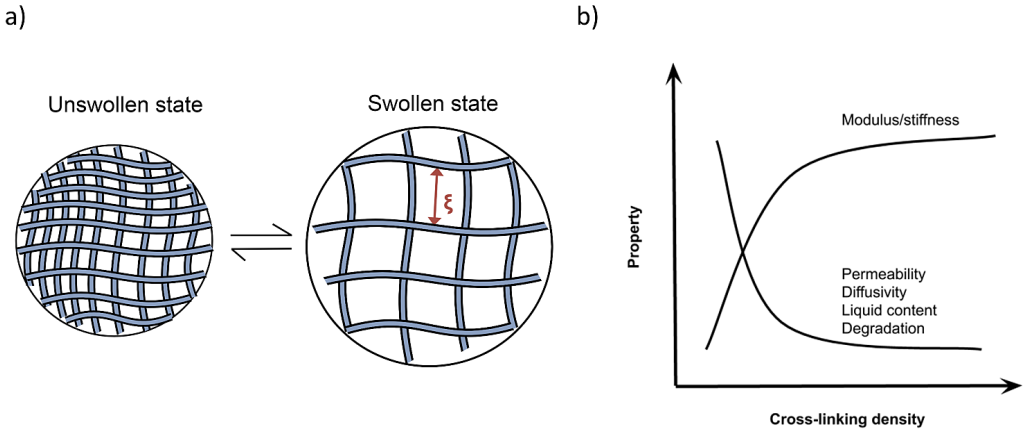


Figure 12: (a) Illustration highlighting changes in mesh sizes (ξ) as a result of hydrogel swelling upon achieving higher equilibrium liquid content. (b) Changes in hydrogel properties as a function of cross-linking density. Adapted from [162].

Swelling ratio represents the volumetric increase of the hydrogel due to liquid uptake after gelation. It is calculated based on measuring the dry weight of a sample immediately after gelation and reweighing the sample at different time points after being placed in a liquid for swelling. The volume measurements were obtained using a density determination kit, where volume of the hydrogels were assessed using a liquid of known density ($\rho_0$) as an auxiliary liquid. The weight of the hydrogels was first measured in air ($W_{air}$), followed by a weight measurement in the auxiliary liquid ($W_{liq}$). In our experiments, either PBS or cell media were used for both swelling as well as the auxillary liquid for measurements. The volume of the gel before ($V_r$) and after swelling ($V_s$) was measured using the following equation:

$$V = \alpha \frac{W_{air} - W_{liq}}{\rho_0 - \rho_L}$$

where α is a balance correction factor, taking into account the air buoyancy and $\rho_L$ is the air density. Swelling ratio was determined as the ratio between $V_s$ and $V_r$.

This method was adopted in all three manuscripts because the information extracted from this data set is particularly interesting when studying hydrogel systems. In Paper I swelling ratio measurements were used as a measure of RGD density upon swelling. Although polymers may be functionalised with the same concentration of RGD peptides prior to gelation, the degree to which the hydrogel swells determines the density at which RGD is presented to the cells. Additionally, swelling ratio measurements were used to complement AFM nanoindentation results to verify differences in liquid uptake when comparing soft and stiff hydrogels. In Paper II and Paper III, swelling ratio was implemented as a means of assessing whether the presence of minerals or PL interfered with the network formation of the hydrogels. Although swelling ratio data provides insight into the bulk network architecture of the hydrogel, it does not provide specific information regarding mechanical properties such as elasticity and stiffness of the hydrogel.

### *3.2.2 Mechanical properties of the hydrogel*

With evidence correlating cell behaviour and morphology to the stiffness of the substrate [163,164], methods that are able to assess physical properties of the substrate with high-resolution are crucial. Nanoindentation provides highly local physical information within the order of few micrometres, making it an indispensable tool to determine stiffness as it would be perceived by cells [165,166]. Acquiring this information was important in Paper I for two main

reasons. Firstly, it highlighted the extent to which doubling the number of arms per macromer added to the stiffness of the hydrogel surface. Secondly, it provided crucial information regarding any compromises in stiffness upon RGD incorporation.

Atomic force microscope (AFM) nanoindentation was used to characterise the surface stiffness of the hydrogels (Figure 13). A cantilever equipped with a colloidal probe was used to approach the surface of the hydrogel (A). As contact was established (B), load was applied onto the hydrogel surface (C) that resulted in the deflection of the cantilever (D), altering the z-position as it indented the hydrogel surface. As the cantilever retracted to its original z-position (D), negative deflection was observed caused by the adhesion forces between the cantilever and the surface of the hydrogel. The extent of cantilever deflection was recorded by reflecting a laser beam off the back of the cantilever and onto a position-sensitive photodiode. Together, this data was plotted as a deflection versus z-position curve as illustrated in Figure 13. This deflection versus z-position can be converted into a force versus indentation curve by considering the vertical displacement of the probe along with the deflection of the cantilever. In order to deduce the stiffness of the sample from force-indentation curves, the Hertz model was implemented, since this best fits spherical probes as used in our study [166].

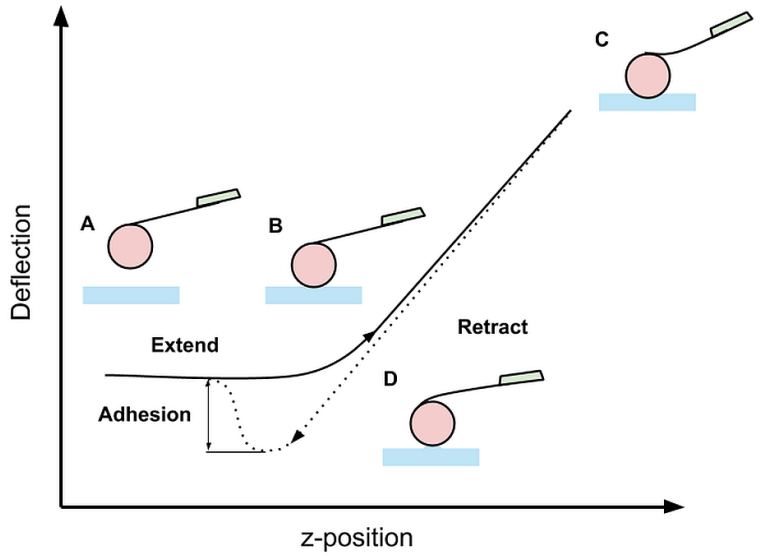


Figure 13: Schematic illustrating the process of nanoindentation resulting in a deflection versus z-position curve.

In Paper I, force-maps were recorded by individually probing areas of the gel surface in a raster fashion. This can be advantageous, since individual measurements collectively provides high spatial resolution [166]. Additionally, this method facilitates the detection of any variations in stiffness from one area to another across the hydrogel. As a result, multiple indentation curves

were obtained to determine the mean Young's moduli of the hydrogel. Nonetheless, there are certain considerations that need to be taken into account when conducting nanoindentation on compliant materials such as hydrogels. For instance, it is often difficult to determine the contact point in soft materials since a decrease in Young's moduli results in shallower force plots [167]. However, there are various fine-tuning measures and models in place to overcome this. As implemented in our study, the Hertz model is particularly well suited when using colloidal probes [166,168]. Additionally, it is important to consider the radius of the colloidal probe when correlating hydrogel stiffness values to forces sensed by cells. Taking into consideration that focal adhesion dimensions typically range from 0.25 to 10 microns [169], 2 micron colloidal probes were used in our indentation experiments.

One limitation with assessing the mechanical properties of the hydrogel with AFM is that it only considers the surface properties and neglects any variations that may occur within the substrate. For composite hydrogels, the inhomogeneous precipitation of minerals would prevent nanoindentation from yielding reliable results. This is simply because of the high spatial specificity of the probe itself. Probing the surface of composite hydrogels could result in indenting minerals instead of the PEG networks. Hence, evaluating the bulk of the material would be a better representation of the hydrogel's physical properties. Since AFM would not provide this information, dynamic mechanical testing via rheometry was conducted instead.

The most common rheological technique implemented on hydrogels is small-amplitude oscillatory shear rheometry [170]. This dynamic mechanical testing method imposes a deformation onto the hydrogel using a small strain amplitude applied via an oscillating plate. As a small amount of stress or strain is imposed on the hydrogel a stress response is measured as a function of time [171]. The response of the hydrogel determines whether its behaviour is elastic with a high storage modulus (G') or viscous with a high loss modulus (G''). Additionally, the performance of the hydrogel within a linear viscoelastic regime determines its overall storage or loss moduli. The linear viscoelastic regime was determined by applying either a fixed shear force onto the hydrogel or by rotating the oscillating plate at a fixed frequency. It is in the linear viscoelastic regime that the hydrogel's structure is at equilibrium resulting in a linear relationship between the applied forces and the resulting stress or strain. Minerals were incorporated into PEG hydrogels (Paper II) not only for their biological purpose, but also to add mechanical strength to the construct. We were particularly interested in evaluating the extent to which these minerals added to the bulk mechanical properties of the composite hydrogels compared to non-mineralised counterparts. While dynamic mechanical

testing directly evaluates the capacity of hydrogels to withstand deformation, it also sheds light upon bulk network architecture. This is because hydrogels with high storage moduli have more elastically effective chains. Hence, rheology provides complementary indirect information to swelling ratio measurements validating any inhomogeneity in bulk network architecture.

### *3.2.3 Release studies*

While network architecture determines the storage moduli and the degree of swelling, it also dictates the release of the growth factors and proteins from the hydrogels. Migration and differentiation studies in Paper II and Paper III rely on the release of factors that drive differentiation and cell migration. In order to correlate any effects of these bioactive factors, the extent to which these are released from the hydrogel is essential. In Paper II, atomic absorption spectroscopy (AAS) was implemented to determine the amount of calcium and zinc present within the media over time. This method relies on the presence of free ions in their gaseous state (upon atomisation) and is based on the absorption of light to determine their concentration [172]. Although AAS is a sensitive and reliable method, it is limited to only detecting metallic ions.

In Paper III, BCA (bicinchoninic Acid) protein assay was implemented to measure total protein release from PL loaded hydrogels. A release profile of proteins is important in order to attribute any chemotactic effects to the contents of PL itself. Under alkaline conditions, proteins are capable of reducing $Cu^{2+}$ to $Cu^{1+}$ in a reaction known as the biuret reaction [173]. BCA forms a highly specific and stable complex with $Cu^{1+}$, which results in a colour change that can be measured by spectroscopy [174]. This assay is well known for its sensitivity, with minimal interferences from salts present in buffers such as PBS. However, one shortcoming of this method is that no information regarding the type of protein is revealed. Instead the total protein content in the surrounding liquid is obtained. However, alternate methods can segregate protein by size such as western blot, or by specificity, using an enzyme-linked immunosorbent assay (ELISA) or Luminex assay. However, BCA analysis is considerably more cost effective, faster and less tedious to perform. Nonetheless, since BCA is not specific and sensitive enough to detect low concentrations of a single protein, SDF-1α release was measured via ELISA instead.

The “sandwich” ELISA was selected for its high sensitivity and specificity that would enable detection of SDF-1α concentrations as low as 80 pg/mL. In this method, wells have been pre-coated with an SDF-1α specific capture antibody in the supplied microplate. This interaction is amplified upon binding with a biotin conjugated detection antibody. A substrate enables the

detection of this via a colour change from blue to yellow, once the reaction is stopped. The hydrogels were loaded with 250 ng/mL of SDF-1α and placed in PBS, to measure the amount of SDF-1α that had been released from the construct over time. However, negligible amounts of SDF-1α was detected at all time points, despite the high sensitivity of ELISA. If all the SDF-1α present were to be released from the hydrogel into the PBS, we would expect approximately 16 ng/mL to be detected, which is well above the detection limit of the assay. Instead, no SDF-1α was detected. As a control, having accounted for the volume of the gel as well as the volume of PBS around the gel, we diluted the SDF-1α without it being loaded in the hydrogel. This revealed whether the hydrogel was retaining the SDF-1α without any release at the selected time points.

### 3.3 *In vitro* experiments

It is imperative for any biomaterial being developed to undergo *in vitro* testing in terms of biocompatibility, cytotoxicity and ultimately, for its intended application. Though i*n vitro* testing has faced criticism for inadequately representing *in vivo* scenarios, it is still the foremost step towards validating biomaterials and their efficacy. The simplicity of *in vitro* testing coupled with the right biochemical assays provide insight into cellular activities with reproducibility. Additionally, ethical requirements for cell-based experiments are minimal in comparison to *in vivo* studies. Although clinical translation is the ultimate goal, we first need to understand the cell-material interactions in a controlled and simplified environment and eventually test whether our results can be reproduced in a complex *in vivo* setting.

All *in vitro* experiments conducted as part of this thesis used primary cells instead of immortalised cell lines. Though primary cells are more expensive and less robust in comparison to cell lines, they are considered a more superior model of *in vivo* cell behaviour. That being said, it is important to acknowledge that a weakness related to cell experiments in this thesis is that all papers have utilised cells from a single donor only. Bone-marrow derived mesenchymal stem cells were used in Paper I and II, while experiments for Paper III were performed with adipose derived mesenchymal stem cells. This was purely due to convenience of cell availability. However, it is necessary to be aware that experimental observations between adipose and bone marrow derived stem cells could differ in spite of them sharing many biological characteristics [175]. Additionally, evidence suggests that passages beyond 8 may prompt rapid ageing [176], affect cell morphology and the proliferative capacity of hMSCs *in*

*vitro* [177]. Hence, stem cells were kept at a maximum confluency of 70% and had undergone no more than 6 passages in preparation for experiments.

### *3.3.1 Experimental design*

*In vitro* experiments were carefully designed to best address the research questions related to each study. Four key designs adopted as illustrated in Figure 14. A direct seeding method involved cells seeded directly on hydrogel disks, where contact between the hydrogel and the cells was essential to study cell attachment behaviours. Since we were also interested in studying the effects of the soluble factors from the composite gels in Paper II, a non-contact exposure setup was established in which the cells were seeded on the TCPS, while hydrogel discs were placed in porous well inserts above. In Paper III, two different setups were used. The use of µ- slides enabled us to document cell movement via live video microscopy (Figure 14d), while cell spheroids were encapsulated into hydrogel disks in order to assess the 3D penetrability of the cells within the hydrogel matrix.

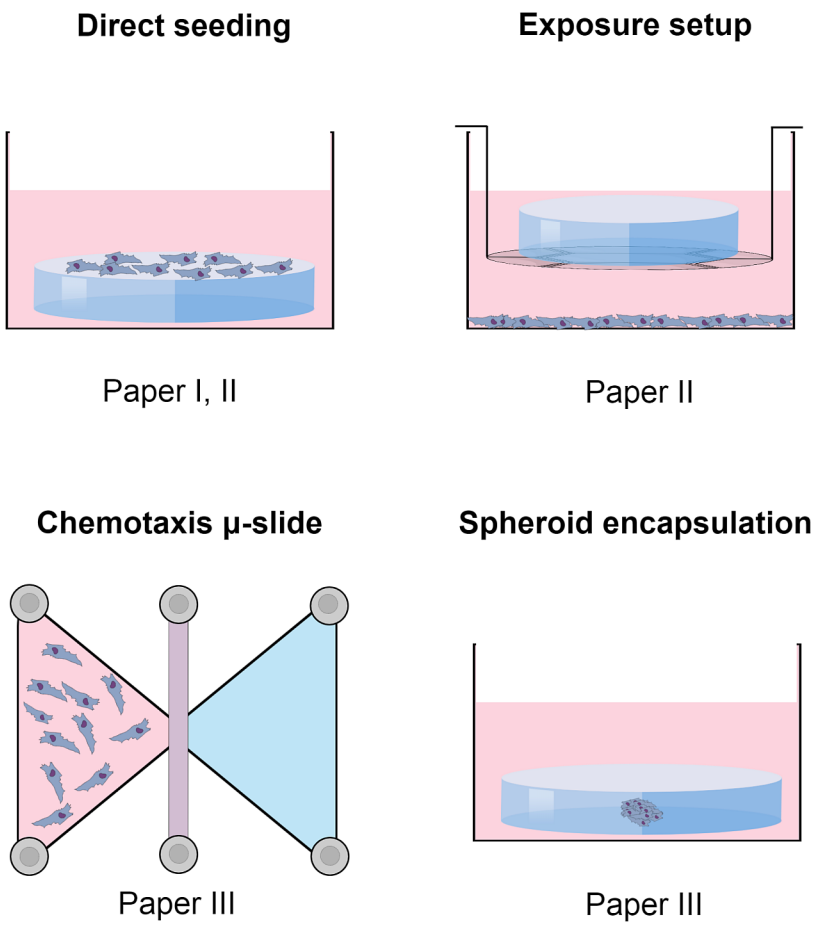


Figure 14: An illustration of the four different *in vitro* setups used in this thesis.

In Paper I, part of the study involved counting the number of attached cells within a fixed area across the gel surface. This required precise seeding such that cells are only exposed to the gel surface and not to the tissue culture plastic (TCPS). The most straightforward approach to achieve this would be to have a layer of gel at the bottom of the plate with cells seeded on top of the gel. However, gels pipetted directly into well plates had the tendency to swell against the lateral walls of the well, leaving the centre of the well void of the gel. Ultimately, the approach that worked best involved direct seeding of cells as a concentrated droplet onto the surface of a hydrogel disk hydrogel. In order to optimise this, the wettability of the swollen hydrogel surface was first measured via contact angle measurements. This allowed to maximise the volume in which cells were seeded onto the hydrogel surface without drying of the hydrogel or collapse of the droplet itself. The use of hydrogel disks placed in well plates allowed for easy fixation and immunolabelling, while the disks could be removed from the well for confocal microscopy. This was important since the confocal microscope available was upright, with objectives that would otherwise limit the proximity to the sample. The direct seeding method was utilised for assessing cell attachment (Paper I and II) and extracellular matrix formation (Paper II). Additionally, the exposure setup was designed for quantitative differentiation assays. Though seeding cells directly on to the scaffold for short periods of times (upto 7 days) worked well, the cells they would peel off the hydrogel surface shortly after they had formed multilayers. Instead, seeding cells on the TCPS allowed for better control of cell numbers and favoured multilayer formation. This was important not only because substantial cells are required in order to drive differentiation, but also because variability in cell numbers could result in unreliable results from protein quantification.

Paper III involved the use of an established μ-slide setup [178]. This best suited the study since it had three separate interconnected chambers, blocked by plugs. This was important in order to separate the cells from the gel, while allowing a concentration gradient to form. The centre chamber was left empty in order to accommodate for swelling of the hydrogel upon liquid uptake. The experiment began once the slide was placed under a microscope with an incubation chamber and the plugs were removed to enable diffusion across the chambers. Hydrogels were loaded either with PL, SDF-1α (positive control) or αMEM (negative control, without FBS) to study chemotactic potential of the released proteins and growth factors. Cells were cultured with FBS free media, in order to omit any opposing stimuli.

One aspect where our setup requires validation involves the establishment of a gradient in order to induce migration. In the case of PL loaded hydrogels, it would be impossible to accurately

visualise the presence of a gradient considering the different molecular weights of the proteins and growth factors. Additionally, accounting for the protein-protein interactions that likely occur in the PL mixture only makes it more problematic to validate the presence of a gradient. On the other hand, it would be possible to visualise the gradient of SDF-1α by loading the gel with fluorescent labelled dextran of a similar molecular weight as SDF-1α [179]. Though this approach would not account for the chemical interactions between SDF-1α and the hydrogel, it provides information on the physical aspects related to the release of the chemokine.

Paper III also dealt with the invasiveness of cells encapsulated within the hydrogel. For this, cell spheroids were generated by seeding stem cells in non-adherent round bottomed wells for 24 h. Immediately after the polymer was mixed with the end-linker solution, it was pipetted in and out of round bottomed well, such that the spheroid would be embedded into the gel mixture and formed into a disc (Figure 14). Due to the size and compactness of the spheroid, the viability of cells at the core of the spheroid may be a concern with regard to sufficient nutrient transport to this region. However, previous studies that utilise a similar approach assure that almost 90% of the hMSCs maintain their viability at 3 days in culture [180]. Phase contrast microscopy along with confocal microscopy was implemented in order to qualitatively assess the penetrability of cells into the hydrogel matrix.

### *3.3.2 Cell attachment and organisation*

In order to assess the behavioural characteristics of cell attachment and organization confocal laser scanning microscopy (CLSM) was the main technique used for image acquisition. Confocal microscopy offers multiple advantages over conventional optical microscopy. Firstly, confocal imaging techniques enables blocking light from regions other than that in focus. This allows for control over the depth of field across the specimen while collecting a series of optical sections across the z-plane with high resolution and minimal background [181]. This proved particularly useful in Paper I where cell clusters existed as 3D objects and often required a collection of z-stacks to visualise each cell belonging to the cluster. Additionally, CLSM enables fluorescent imaging of cellular structures upon immunolabelling with specific fluorophores and antibodies.

An important consideration when visualizing structures within the cell is the selection of primary and secondary antibodies for immunolabelling. In Paper I and II anti-human vinculin primary antibodies were selected to label part of the focal adhesion (FA) complex. In addition, phallodin and 4′,6-diamidino-2-phenylindole (DAPI) was used to label the cytoskeleton and

the nucleus respectively. Vinculin was selected primarily based on its role within the focal adhesion complex. It has been widely recognised as one of the main mechanosensory components within the force-transduction layer of the FA [182,183]. As shown in Figure 15, vinculin is an adaptor protein that acts as a molecular clutch between the transduction of mechanical input received by talin and the imposed force on the contractility of actin filaments [184,185]. Since we alter the mechanical stiffness of the hydrogels in Paper I via changes in polymer selection and in Paper II with the presence of minerals, the manner in which cells perceive these changes can be highlighted by vinculin localization. On the other hand, phalloidin and DAPI were selected based on their high specificity for their respective target structures and their reliability in cellular imaging [186,187]. Phalloidin enabled visualisation of cellular morphology adopted by the cells seeded on hydrogels with varying characteristics, while DAPI was used label the nucleus.

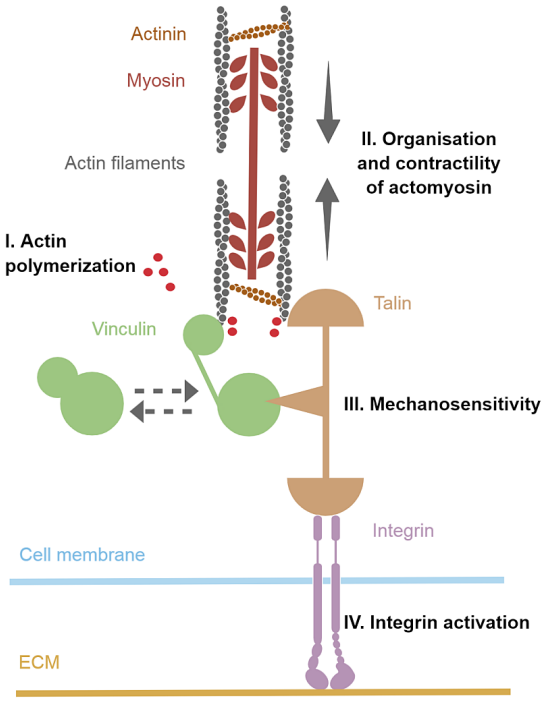


Figure 15: Illustration of vinculin as part of a molecular clutch system in the mechanotransduction process between force sensation and transmission.

Imaging of the cells provided a qualitative overview of attachment and organization. However, further quantitative analysis of these images highlighted subtle differences among the groups. In Paper I, the attachment and organizational behaviours of cells were analysed in depth. This included assessing the number of cells that had attached per unit surface area of the gel, the percentage of hydrogel surface area covered by cells and spatial relationships between the cells.

However, we also employed a technique often used in the ecological evaluation of populations, known as nearest neighbour analysis developed by Clark and Evans [188] which has also previously been employed in the field of cell biology [189]. A parameter known as the R-value, which represents the spatial uniformity and distribution within a population, is generated from the images. The R-value is calculated as a ratio between the distance to the first neighbour for each nucleus (RA) and the expected mean distance within a randomly distributed population (R'E) [188]. This value serves as an index of aggregation and can indicate whether the members of the population are clustered (R = 0), randomly distributed (R = 1), square distribution (R = 2) or have a hexagonal distribution (R = 2.15) as illustrated in Figure 16. Hence, lower R-values closer to zero represent an aggregation of cells, while values closer to 1 represent cells distributed at random. In order to extract this data from the confocal images, there are various steps involved in the process.

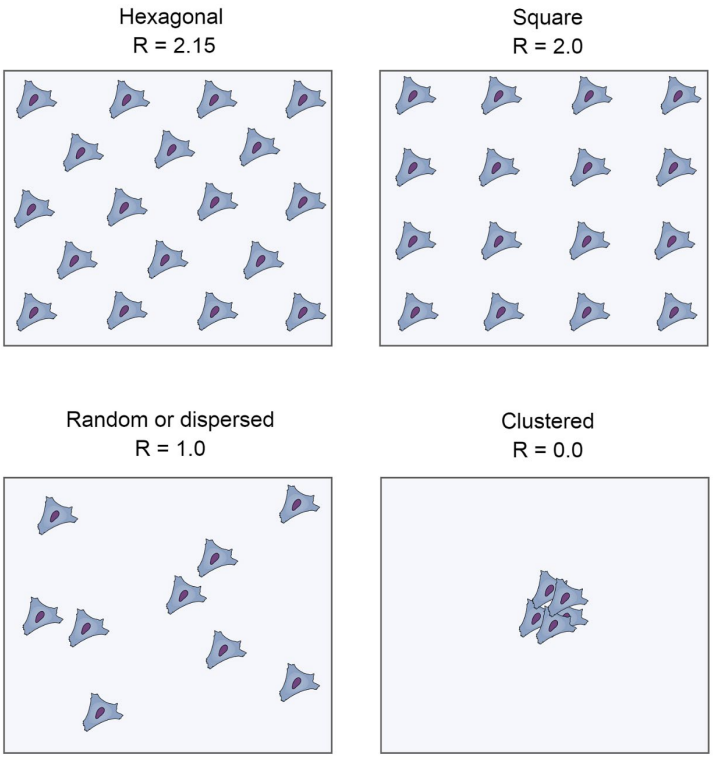


Figure 16: Interpretation of R-values based on cell distribution across a set field of view.

Cell Profiler Software was used to process the images and extract R-values from cell distributions in a given field of view. Images from DAPI channels were smoothed and segmented to recognise individual nuclei as primary objects using a size filter and intensity thresholding. Distances from each individual object to its nearest neighbour object were determined (RA) within an expanded radius of 20 pixels (corresponding to the average nuclear

diameter). The number of objects within the expanded radius (neighbours) was also counted. Subsequently a more strongly smoothed image was generated followed by segmentation for object recognition. These objects were compared to the original primary object nuclei and designated as parent/child to define cell clusters compared to individual cells. The segmentation and cluster assignment was visually cross-checked based on individual colour assignments to each object.

### *3.3.3 Assessment of cell viability and cytotoxicity*

Lactate dehydrogenase enzyme (LDH) leakage was measured as a marker of membrane damage. In healthy cells, this enzyme is typically held within the cytoplasm, however, upon damage of the phospholipid bilayer, it is released into the cell culture media. LDH in the cell media is measured via a coupled enzymatic reaction that converts tetrazolium salt to formazan resulting in a red colour that can be measured by absorbance [190]. Positive and negative controls were included in order to obtain results relative to maximum and minimum amounts of LDH released from the cells. The positive control involved the addition of Triton X-100 to cells seeded on TCPS enabling maximum membrane lysis. On the other hand, the negative control simply involved cells seeded on TCPS representing cells with intact membranes. The assessment of cytotoxicity in the LDH assay is limited to the damage to the membrane. Hence, it is important to consider the membrane permeability of the compound under investigation. While LDH provides information regarding cell death, it does not provide information regarding adverse effects that did not result in cell death.

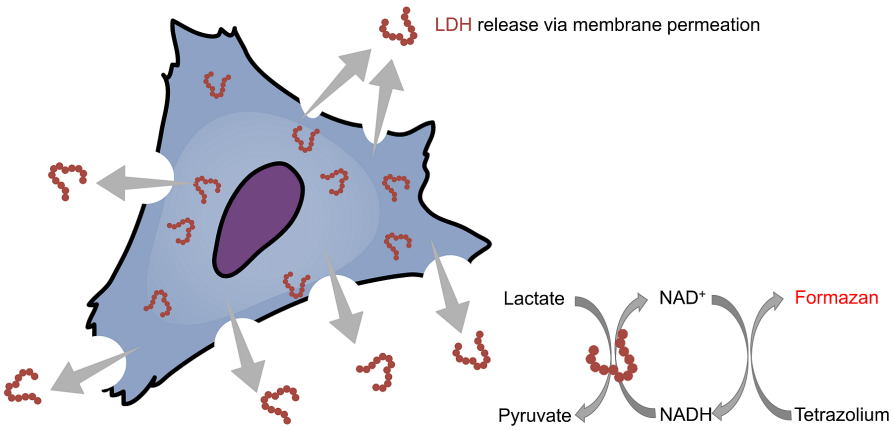


Figure 17: LDH is released upon perforation of the cell membrane. Detection involves the conversion of lactate to pyruvate

Hence, in contrast to cytotoxicity, cell viability was assessed to provide parallel information regarding the health of the cells. An alamar blue assay was used as an indicator of cell viability via the reduction capacity of the cell's metabolic status. This assay involves the reduction of resazurin, a cell permeable blue colour dye to a fluorescent pink colour upon the acceptance of an electron [191] . This internal reduction environment is typically supplied by mitochondrial reductases participating in the energy metabolism within the cell. As a result, increased reduction of resazurin to resofurin correlates to increased cellular metabolic activity, which is measured either via spectrophotometric fluorescence or absorbance [192]. The alamar blue assay has multiple advantages over frequently used tetrazolium salts in other cell viability assays such as the MTT assay. Resazurin is not only water soluble, but also non-toxic, which allows for the assessment of cell viability without it being lethal to the cells. One important consideration when utilising alamar blue is related to the incubation time of the dye. This can range from 1 to 4 hours depending on the cell density [190]. However, if alamar blue is measured at different time points through the course of an experiment, it is important to maintain the same incubation time for accurate results. Additionally, alamar blue is most sensitive when cell densities among test groups are similar. Both LDH and alamar blue were conducted in Paper II, to ensure that the presence of minerals did not have any toxic effect to the cells and to confirm that cell viability was not affected.

### *3.3.4 Cell differentiation analysis*

Once no adverse effects of the minerals was assured via LDH and alamar blue assays, *in vitro* studies in Paper II were focused on assessing the extent of osteogenic differentiation in the presence of ACP. We implemented an array of testing methods to quantify differentiation on the protein as well as the gene levels. Proteins and genes of interest were selected such that the early and late differentiation stages were considered (Figure 18). Bead-based multiplex assays (xMAP by Luminex) were used to quantify protein and cytokine products after cells were exposed to composite hydrogels. The system is based on antibody-antigen interactions and is based on the principle of sandwich ELISA assays, however this approach allows for the analysis of multiple analytes simultaneously [193]. The beads used in the assay have signature spectral properties and are coated with several specific capture antibodies that bind to target proteins. As a result of this binding, an analyte-specific biotinylated antibody is incubated following a streptavidin-reporter conjugate, similar to that mentioned in ELISA. The main difference here is that the beads are analysed via the Luminex 100/200™ instrument which reveals spectral

properties of the beads along with the reporter fluorescence, together assessing the concentrations of multiple analytes [194]. Though this assay can be expensive for the analysis of single analytes, it is more cost-effective and time saving compared to ELISA assays when analysing multiple analytes simultaneously. The main advantage of using such an assay is that it requires only small quantities of cell media and provides results with high accuracy and specificity. This allows for tracing the proteins from each replicate over the course of time without the need for separate samples for different time points. Furthermore, in contrast to ELISA assays, this method is capable of analysing multiple protein products simultaneously [195]. In Paper II, osteoprotegerin (OPG), osteopontin (OPN), osteocalcin (OC) and sclerostin (SOST) were the osteogenic proteins selected for analysis, along with the cytokines interleukin-6 (IL-6) and tumor necrosis factor (TNF-α). Though this assay is limited to protein and cytokine analytes, there are various other methods that were used to provide more insight into the differentiation process.

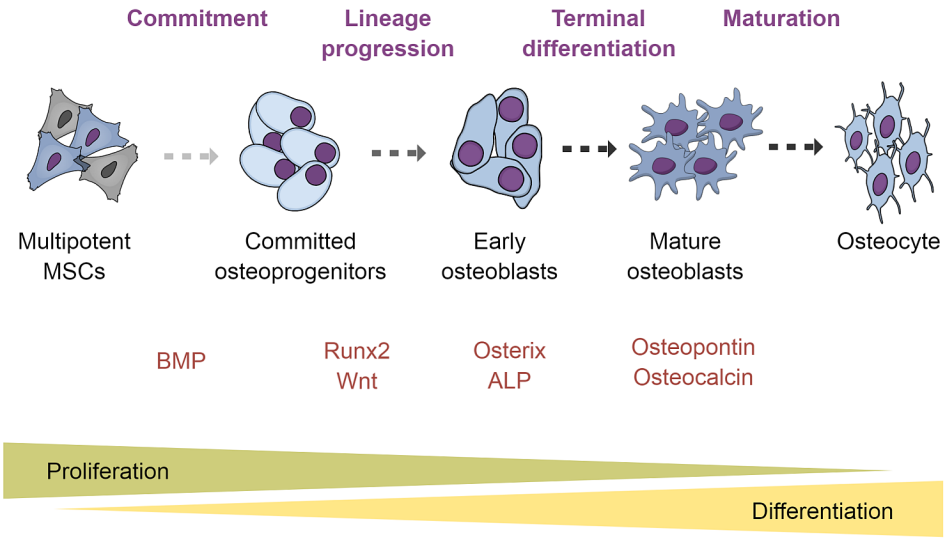


Figure 18: The main protein and genes involved in the different stages of MSC differentiation MSCs towards the osteogenic lineage (adapted from [196]).

Proteins are generated as a product of genetic translation. Hence, we chose to assess the fold changes in osteogenic gene expression via quantitative reverse transcription polymerase chain reactions (RT-qPCR). Analysis of gene expression is a multi-step process and relies on multiple factors such as the isolation efficiency of RNA, the production of cDNA from mRNA and the use of an optimised PCR thermocycle. The production of cDNA relies heavily on isolating high quality RNA. Total RNA in Paper II was isolated using TRIzol®. This method requires homogenization of samples and separates RNA and proteins on the basis of phase separation

[197]. The main drawback of this method is the use of toxic and corrosive chemicals such as phenol and chloroform. Alternative, less toxic methods involve either spin-columns or the use of magnetic beads, which are known to produce higher yields, but are significantly more expensive [198]. However, the magnetic beads contain poly-thymidine nucleotides covalently attached to the beads that bind to the poly-adenosine tails of mRNA. This added specificity to mRNA could result in less contaminants such as proteoglycans, DNA, lipids and proteins when compared to the TRIzol® method used in our study [199]. Once RNA is isolated from the cells, the next step involves first strand cDNA synthesis. This requires primer sets, deoxyribonucleotide triphosphates (dNTPs) and an enzyme such as reverse transcriptase (RTase) to form a double stranded product (Figure 19). While primers attach to the forward and reverse ends of the single strands, RTase drives the polymerization of a new complementary strand to be formed using the dNTPs as building blocks. In order for the reaction to take place, specific temperatures that facilitate the double strand separation, annealing of the primers, first strand synthesis and amplification are required [200]. This requires the use of a thermocycler that changes temperature as per the phase of the PCR process. Human primer sets were selected with an average size of 20 bp that bind separate exons and have melting temperatures of 60˚C, important factors that can affect the outcome of the PCR reaction [201]. The genes under investigation were runt-related transcription factor 2 (*RUNX2*), osteopontin (*OP)*, osteocalcin (*OC*) and osterix (*OSX*). These specific genes were selected to detect transitions at each step of the differentiation process (Figure 18). Glyceraldehyde-3-phosphate dehydrogenase (*GAPDH*) was chosen as the housekeeping gene, due to its high stability and constitutive expression [202]. The housekeeping gene within the PCR process served as a control while being the baseline for normalization of the genes under investigation [203].

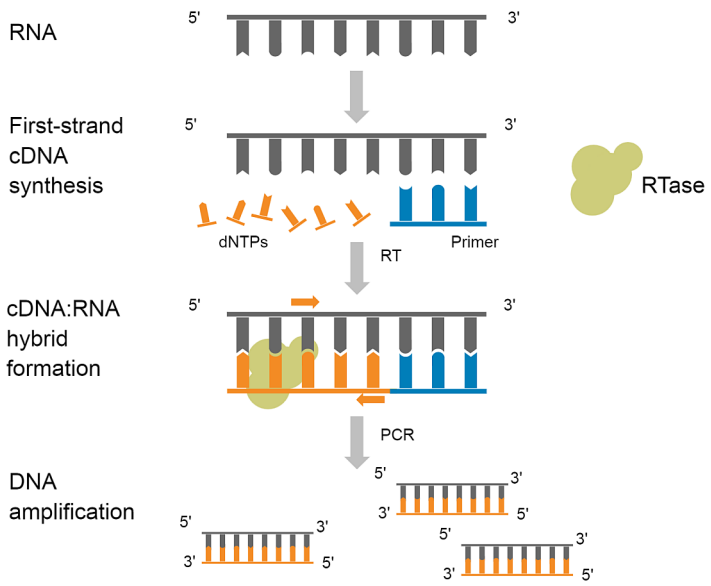


Figure 19: Molecular process of RT-qPCR. RNA is extracted and isolated from the cells in order to synthesise cDNA. The synthesis of cDNA requires dNTPs and primer sets in order to form a cDNA:RNA hybrid using RTase to drive the reaction. The PCR reaction results in amplification of the DNA used to determine the fold changes in gene expression.

Apart from osteogenic protein production and gene expression, alkaline phosphatase (ALP) activity was assessed upon hMSC exposure to composite hydrogels (Paper II). ALP is a membrane bound enzyme that is considered a product of early osteogenic differentiation [204]. Hence, the activity of this enzyme was measured at 7 and 14 days using a *p*-nitrophenylphosphate (pNPP) based spectrophotometric assay. The activity of ALP is assessed based on its catalytic capacity to convert pNPP from a colourless to a yellow compound under alkaline conditions (Figure 20) [205]. One limitation of this assay is that cells need to be lysed in order to measure membrane bound ALP, demanding separate setups for each time point. Cells were lysed via repeated freeze-thaw cycles at -80˚C, which has previously been tested to efficiently yield the highest enzyme activities [205]. Additionally, the assay was conducted on the day of harvesting the cells, minimizing any storage-related loss of enzymatic function.

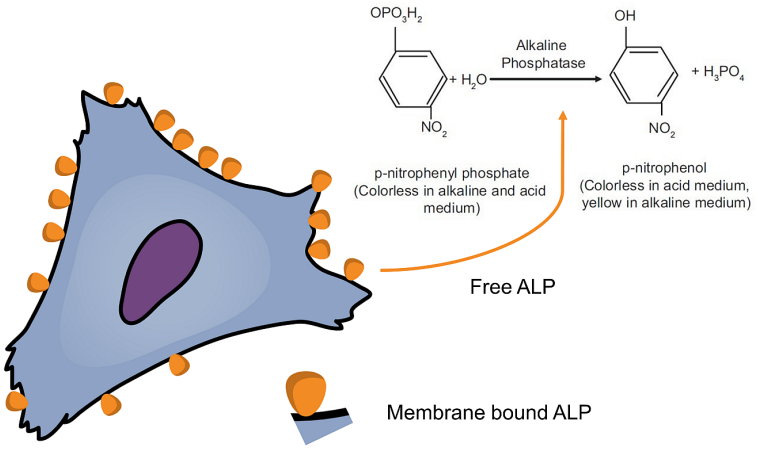


Figure 20: ALP catalysed conversion of *p*-nitrophenyl phosphate to *p*-nitrophenol under alkaline conditions resulting in a yellow colour product that absorbs light at 405 nm (adapted from [206]).

### *3.3.5 Minerals within the ECM*

In order to assess the extracellular mineral deposits by the cells in Paper II, alizarin red staining was used to visualise and quantify calcium within the cell layer 21 days after exposure to composite hydrogels. One obvious consideration in this setup was to have a control without cells present at the bottom of the well. This allowed us to distinguish calcium released from the composite hydrogels that precipitates in the medium versus calcium entrapped within cell matrix. Upon staining and removal of excess alizarin red, light microscopy was used for image acquisition. Additionally, alizarin red can easily be recovered from the stained samples in order to quantify the amount of chelated calcium. This involved the use of cetyl-pyridinium chloride, followed by absorbance detection at 562 nm.

Alternatively, von Kossa staining would also stain mineralised nodules using silver nitrate [207]. However, unlike alizarin red that forms a chelate with calcium cations, it lacks specificity to calcium cations and binds to a variety of calcium salts instead [208]. Other stains for calcium include xylenol orange, and calcein blue. The advantage of these stains is that cells can be left live in culture, allowing for real-time visualization of mineral formation [208]. Both xylenol orange and calcein blue chelate calcium in a similar fashion as alizarin red, however as fluorochromes, they require fluorescent microscopy for assessment.

Mineral entrapment within the extracellular matrix was also qualitatively assessed via scanning electron microscopy (SEM) in Paper II. In this case, cells were seeded for 21 days directly on to the scaffolds to contrast differences observed via the exposure setup used for alizarin red staining. SEM provided high resolution images that showed mineral nodules at much higher

magnifications compared to the conventional light microscopy used in alizarin red imaging. Additionally, SEM provided spatial resolution regarding the location of minerals along with structural details regarding the cell-laden composite. In the acquired images, cell morphologies were poorly preserved, and it was particularly difficult to distinguish between the ECM and the cells themselves. This is likely due to the unavoidable solvent replacement and dehydration of the sample in order to scan the sample in a vacuum, which may have ultimately compromised the integrity of the cells. Unfortunately, alternative dehydration methods such as freeze drying would likely not improve this outcome [209]. However, the use of cryo- or environmental-SEM may circumvent dehydration related issues since it can be performed under low vacuum conditions [210]. Together with optical microscopy images of the alizarin red stain and the SEM images, we can nonetheless obtain data regarding mineral deposition on both the macro and sub-micron scale. Although CLSM could be used to visualise mineral deposition in the ECM, SEM provides images with higher contrast capable of distinguishing surface landmarks easily [211]. Additionally, fluorescence CLSM could be employed to identify locations of specific cellular and ECM structures, however this would require multiple fluorophores to do so. On the other hand, SEM samples require only a single metallic coating such as gold or platinum, while providing structural information at a higher contrast and resolution than CLSM.

### *3.3.6 Cell migration analysis*

The Boyden chamber assay is one of the first and most established chemotaxis *in vitro* assays to assess induced cell migration [212-214]. It involves seeding cells on porous membranes above media containing chemotactic agents [215]. With the presence of a chemotactic gradient via the porous membrane, cells can migrate into the bottom chamber. At the end of the experiment, the migrated cells can be counted in the bottom chamber to assess the migration capacity of the cells [215]. Not only is this an end-point assay, but also has limitations associated with the setup itself and the data that can be extracted from it. Concentration gradients in this assay are steep, while migration related parameters, such as cell trajectories, distances and velocities cannot be assessed [178]. Hence, an alternate migration assay was employed in Paper III in order obtain a comprehensive assessment of cell migration.

Cells were exposed to hydrogels loaded with chemotactic factors in a μ-slide setup (Figure 21) [178]. Considering the size and format of these slides, the assay requires only small volumes of hydrogels, while fitting securely on any conventional slide stage that supports live imaging. As with most chemotaxis assays, the principle of this setup relies on the establishment of a

concentration gradient. However compared to the Boyden assay, the chambers in the µ-slide setup are known to have long-term linear gradients, which are well suited for slow migrating mammalian cells [178]. Additionally, compared to the Boyden assay, all chambers within this setup were in one z-plane, which made monitoring real-time cell migration fast and easy. This setup consisted of three interconnected chambers (C1, C2 and C3) adjacent to each other, as illustrated in Figure 21. Cells were seeded in the leftmost chamber (C1), while hydrogels were loaded in the rightmost chamber (C3). The central chamber (C2) was left empty to accommodate for hydrogel swelling, while allowing a gradient to form. As media comes in contact with the hydrogel, proteins and GFs diffuse out of the loaded hydrogel, to create a gradient of the chemotactic molecules available to the cells.

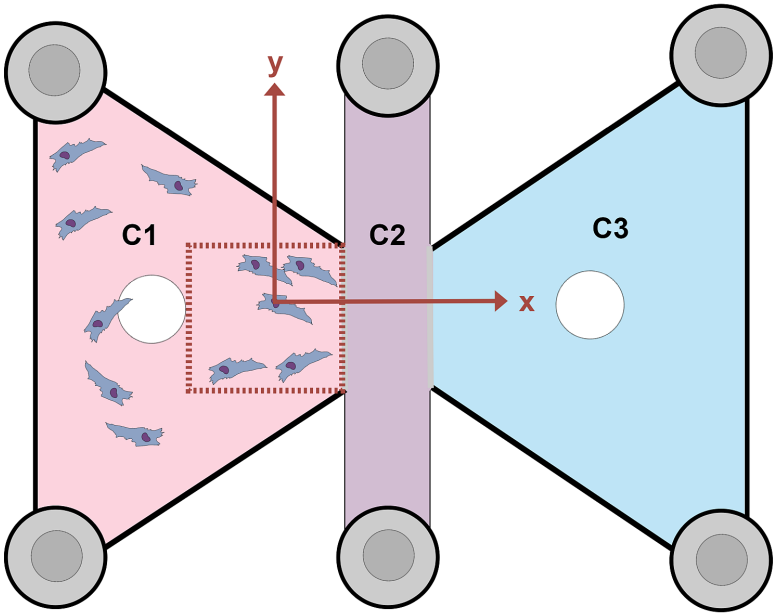


Figure 21: Schematic illustrating the µ-slide setup used for chemotaxis studies in Paper III. The µ-slide consists of three chambers (C1, C2 and C3). Cells were loaded in C1, while hydrogels were loaded in C3. C2 was left empty to establish a gradient and to accommodate for swelling of the hydrogel. The red dashed box highlights the field of view (approximately 8.3 $mm^2$) from which cells were randomly selected for migration analysis. Parameters such as forward migration index (FMI) was assessed along the x-axis in order to assess chemotactic induced migration in the direction of the hydrogel.

Images were acquired over a 50 h time period via live time-lapse microscopy, with images taken at 10 minute intervals. Cells were randomly selected from within the red dashed rectangle outlined in Figure 21. This area was selected since it was in close proximity to the corresponding chamber containing the loaded hydrogel and cells in this area would likely be most susceptible to chemotactic induced migration. The extraction of data from the images revealed information pertaining to migratory parameters, such as distances covered, velocity and directness. Additionally, the displacement of the centre of mass (COM) along with the

forward migration index (FMI) was evaluated. COM indicates the spatial average difference between the initial position and the final position of all the cells, thus representing an average displacement of the population [178]. Furthermore, FMI provides directional information regarding the efficiency of the cell to move towards its end-point. This is a very reliable parameter for chemotactic induced migration and has been implemented in very early chemotaxis studies [216,217]. Considering that the cells were placed in a chamber adjacent to the chemoattractant loaded hydrogel, we were particularly interested in the FMI along the x-axis (Figure 21). This was calculated using the following equation:

$$FMI^{\perp} = \frac{1}{n}\sum_{i=1}^{n}\frac{x_{i,end}}{d_{i,accum}}$$

where $x_{i,end}$ is the final x coordinate of the cell path, and $d_{i,accum}$ is the accumulated distance by the cell.

Directionality adopted by the cells is best represented via rose plots, highlighting the precise angles between the initial and final points of cell migration. For all rose data plots, the Rayleigh test was performed to confirm whether the distribution of cells was heterogeneous, indicating that cells being analysed were biased towards one particular direction [218]. Cells having homogenous distributions were considered to have migrated randomly, while cells heterogeneously distributed were considered to have migrated with directionality [219].

In this study, cells were tracked manually by selecting the position of a cell through approximately 300 frames per cell. The main reason we opted to track cells using a Manual tracking Image J plugin [220] was not only because it was recommended by producers of the μ-slide, but also because data obtained from this plugin is optimised to fit a custom software that generates trajectories and migratory results efficiently. Although manual tracking may increase the chance of human based errors, it is easy to use and works well if the sample size is not too large. Conversely, if high number of cells are to be tracked, manual tracking may end up being a tedious approach. While alternate automated cell tracking plugins such as MTrack2 for Image J could likely end up being more accurate and time saving where hundreds of cells need to be tracked, they require rigorous optimised thresholding and segmentation in order to recognise the cells [221]. Commercially available automated tracking software such as MotoCell [222], Imaris and Volocity could prove beneficial for larger sample sizes, with nearly half the image processing times of open-source software [221]. However, these software are

best suited to fluorescently labelled cells and require expensive licences to use. Additionally, automated tracking requires images to be taken at small time intervals, such that cells do not migrate large distances over time. Hence, automated tracking would not only require more images, but also demands higher computing power to extract the data. Furthermore, these commercial software are notoriously known to identify high percentages of non-existent cells from phase contrast images [221]. Another important consideration when tracking cells is the fact that cells divide over the period of live-cell tracking. In Paper III, one of the two daughter cells were selected at random to continue the manual track of that from the original cell. While detecting daughter cells is problematic even for automated cell tracking software, there is the possibility of identifying specific optical flow patterns as cells enter mitosis, which could be registered as a landmark for the software to segment and identify each daughter cell as a new object [223]. Nonetheless, this urges advanced bioinformatics tools to provide user friendly platforms that account for such issues, while being available as open-source software.

# 4 Summary of key findings

PEG hydrogels were functionalised with RGD, amorphous calcium phosphate and platelet lysate in three separate setups. In addition to validating hydrogel biocompatibility and cell viability, biological responses of hMSCs were assessed in terms of cell attachment, differentiation and organization as outlined below.

## 4.1 Cell attachment and organisation (Papers I and II)

In paper I, PEG hydrogels were functionalised with varying concentrations of linear and cyclic RGD, in search of the optimum concentration and isoform to enable hMSC spreading. We observed no prominent differences among the two isoforms, however, concentration of RGD along with the stiffness of the hydrogel dictated the morphology of the cells. Cells seeded on 8M20 hydrogels functionalised with cycRGD concentrations ≥ 0.5 mM supported cell spreading. However, hMSCs seeded on the softer 4M20 and 4M10 hydrogels exhibited round morphologies and led to the formation of cell clusters. We also showed that increased RGD tethering did not have a significant effect on hydrogel stiffness, irrespective of the number of functional arms on the macromer. In Paper II, cells seeded on composite hydrogels required additional RGD functionalisation to support cell spreading, suggesting that the presence of minerals alone was insufficient for cell attachment.

Interestingly, in the case of both non-mineralised (Paper I) and composite hydrogels (Paper II), localization of vinculin to the periphery of the cell bodies was not prominent, indicating the lack of mature focal adhesions.

## 4.2 Cell differentiation (Paper II)

The effect of composite hydrogels containing CaP on the differentiation of hMSCs was assessed both qualitatively and quantitatively. Higher quantities of alizarin red stain was observed when cells were exposed to composite hydrogels versus non-mineralised controls. Additionally, SEM imaging confirmed the presence of mineral nodules when cells were seeded onto the surface of the hydrogel. These results suggested that minerals were incorporated within the ECM produced by the cells. However, ALP release, protein secretome and gene expression data did not provide conclusive evidence that composite hydrogels direct hMSCs towards the osteogenic lineage.

### 4.3 Cell migration (Paper III)

Proteins released from platelet lysate loaded PEG hydrogels induced directional migration of hMSC towards the hydrogel scaffold. Analysis of migration parameters highlight that cells migrated faster and further in the presence of PL-PEG hydrogels. In contrast, end point coordinates from cell trajectories showed that cells exposed to control setups ended up homogenously distributed. Finally, cell spheroids encapsulated within PL-PEG hydrogels exhibited outward sprouting, which eventually led to the collapse of the spheroid and colonisation of the hydrogel matrix.

# 5 General discussion

It has been argued within biomaterial science that there is no such thing as a bioinert or biocompatible material [224,225]. This argument may have a lot to do with the semantics of each word, but also stresses the need for context when they are used. On one hand it is argued that developing a completely bioinert material is impossible [225]. On the other, the compatibility and inertness of implantable biomaterials depends on the biological host and location of implantation, as much as it depends on the composition of the material itself [224]. Rather than debating the semantics of inertness, we will define the word in context of this thesis. 'Inert' is used here as a relative term to describe PEG hydrogels that lack biofunctionality, thus preventing cells from interacting with the scaffold. On the contrary, the word 'active' implies that the PEG hydrogels have been functionalised with bioactive molecules, in order to elicit a 'desired' cellular response.

## 5.1 Interpreting cell responses

2D *in vitro* studies have recently received criticism in comparison 3D cell studies [226,227]. It is true that 3D cell culture provide a more realistic biochemical and biomechanical environment, representing natural tissue physiology [228]. However, 2D cell studies are still a viable approach for understanding fundamental cell behaviour translatable to *in vivo* outcomes [229]. The lack of robust 3D culture substrates prevents transferability of knowledge from one study to another. While Matrigel is considered the gold standard for 3D cell culture, it contains ECM proteins derived from mice [230]. Additionally, its reliability is questionable due to batch-to-batch variation [231], while also prompting the cautious interpretation of cellular activity when using such matrices [232]. On the other hand, cell studies are not only easier to conduct with the standardised use of tissue culture plastic, but also become relatable and reproducible across different biological disciplines. This is especially beneficial when developing studies from the ground up that require several rounds of optimisation and validation. For instance, while we seeded cells on the surface of the hydrogels, in no scenario did we see the localisation of vinculin to the periphery of the cell bodies. However, rather than questioning the antibody and the immunolabelling process, we simply seeded the cells onto glass and verified that our observation was specific to our substrate. There is no doubt that both 2D and 3D setups have their own advantages and disadvantages, however, it is important to implement each of them in perspective of the research question.

### *5.1.1 Cell attachment*

In the case of endogenous regeneration, both 2D and 3D cell experiments are important. As biofunctional PEG hydrogel is injected within the defect, GFs diffuse out over time inducing the migration of the cells. Before cells can invade the provisional matrix provided by PEG hydrogel, cells first come in contact with the hydrogel surface to begin colonisation. Hence 2D *in vitro* experiments would help understand the requirements to enable cell attachment and proliferation on the surface. Only once sufficient cells colonise the surface and cleave the MMP-sensitive cross-linker, will they make their way into the 3D construct. Factors such as stiffness, topography and distribution of cell adhesion ligands of a biomaterial are known to control cell behaviour in 2D [146,233,234]. While stiffness alone is capable of dictating cell morphology [235], we found that for inert materials such as PEG, this was not the case. A combination of hydrogel stiffness of more than ~ 15 kPa and RGD concentration of more than 0.05 mM were key to enabling cell attachment on the PEG hydrogels (Paper I). Despite the added stiffness provided by CaP minerals, these hydrogels did not support cell attachment without RGD functionalisation (Paper II). This further emphasises the dependence of integrin on the RGD ligand for successful attachment on PEG hydrogels. One may question the distribution of the RGD ligands between soft 4M20 and stiff 8M20 hydrogels. However, calculations based on the swelling ratios confirmed that RGD distribution was well above the limit to support cell spreading [106,236,237], despite the increased swelling in the softer gels. Interestingly, we observed cells with spread morphologies also on the non-mineralised 8M40 hydrogels functionalised with RGD in Paper II. It is unlikely that this spreading was a result of stiffness, since storage moduli for these gels (~2 kPa) were comparable to those of the soft 4M20 gels used in Paper I [134]. However, the 8M40 and 4M20 hydrogels differ in terms of wt. % and the number of arms, which would likely result in different RGD distributions. While the density of RGD presentation via star macromers is known to alter the morphology of cells [238], studies that control each polymer parameter are required to pinpoint the contributing factors causing these differences in RGD presentation.

However, cells did not require RGD to colonise the hydrogel surface in the presence of PL (Paper III). This implies that naturally occurring ECM proteins within the lysate were sufficient for cell attachment in 2D. Although seeding cells directly onto the hydrogel surface revealed the basic requirements for cell adhesion, it had its limitations. Cells cultured on hydrogels for upto 7 days formed multilayers with no evident penetration into the hydrogel (Paper III). Cells certainly proliferate on the hydrogel, but do not penetrate the hydrogel within 30 days of culture

(Appendix 1). This is likely not due to PEG chemistry, but instead a consequence of the abrupt change in material stiffness at the gel-liquid interface [239]. One way to overcome this pronounced stiffness shift at the interface, is by creating density gradients across the hydrogel, which would provide a gradual stiffness increase to the cells [240]. Though this approach has proven to increase cell infiltration significantly, the ways in which this can be translated to the clinic are yet to be investigated.

### *5.1.2 Making sense of migration*

Although cells seeded in direct contact with the hydrogel did not penetrate below the surface, cells did migrate towards the hydrogel when loaded with PL (Paper III). PL contains GFs with different sizes. For example, PDGF is approximately 30 kDa [241], whereas CXC chemokines such as SDF-1α are approximately 8-14 kDa [242]. It is likely that smaller growth factors are released from the hydrogel initially, while other larger proteins are either being entrapped within the hydrogel matrix or diffusing over time. Since more than 50% of the total protein had released from the PL loaded hydrogels, it would be advantageous to characterise the types of proteins that were released. Knowing which proteins released from the hydrogel would provide valuable information regarding the driving force for the chemotactic effects associated with PL. PDGF has previously been recognised as a chemotactic inducer, and considering its abundance in PL [243,244], it is highly possible that it is the driving force in our system as well. While SDF-1α is a potent inducer of mesenchymal stem cell migration [179], it is not recognised as an abundant growth factor in PL [244]. No SDF-1α was detected upon measuring the amounts of SDF-α in the PL concentrates, implying that it is likely not a contributing factor to the observed chemotaxis in our study.

We also produced hydrogels containing recombinant SDF-1α alone and evaluated the release of SDF-1α from these hydrogels via ELISA. Results indicated that SDF-1α release from the hydrogel was not detected at any time points. As a control, having accounted for the volume of the gel as well as the volume of PBS around the gel, we diluted the SDF-1α without being loaded in the hydrogel. This revealed that there was no flaw in the method per se, but instead suggested that SDF-1α was being either physically or chemically entrapped within the gel network. While forward migration index results showed directional migration of cells towards hydrogels loaded with PL, this was not the case for SDF-1α and control hydrogels. This was due to no release of SDF-1α and the absence of chemotactic factors in the media. By no means

does our study dismiss the fact that SDF-1α is capable of directing stem cell migration, but instead shows that its effects were undetected due to its retention in the hydrogel matrix.

Due to the high proliferative and cell-adhesive capacity of PL [245], cell spheroids were encapsulated within the hydrogels for 7 days to assess whether the presence of PL promoted cell invasion and facilitated the colonisation of the matrix. It was apparent that cell spheroids established outgrowths from day 1 when encapsulated in PL hydrogels, which was not observed in the other two gel groups. This may be attributed to the abundance and accessibility of ECM proteins naturally present within PL, in comparison to smaller and likely less accessible RGD fragments in the other hydrogels. Over the course of seven days, the spheroid in the PL hydrogel disintegrated completely, with cells populating the hydrogel. The collapse of the spheroid may not directly be a consequence of the cell conducive environment provided by PL, but instead, due to the fact that the presence of proteins resulted in fewer elastically effective chains. With fewer polymer networks around the spheroid, it is likely that the matrix imposed less constraint onto the spheroid, allowing its expansion. However, this can only be confirmed once the mechanical properties of these hydrogels are determined. Nonetheless, these observations are in accordance with previous studies that use MMP-sensitive cross-linkers, and illustrate the capacity for the hydrogel to be degraded and remodelled into natural ECM by cells [129].

Our choice in selecting 8V40 (5 wt. %) polymers in Paper III likely facilitated the release of proteins, since longer arms would results in larger mesh sizes and promote the diffusivity of the proteins. VS-PEG gels are known to have network imperfections innately [134], however the presence of PL results in even fewer elastically effective chains. This implies that the presence of proteins resulted in fewer elastically effective chains. However, this increased liquid uptake represents increased diffusivity and permeability of the hydrogel, which drives the release of proteins from the hydrogel, inducing cell migration. Conversely, in the larger scheme of regeneration rather than just migration, it may be beneficial to have a slow releasing system with a constant supply of bioactive molecules. One way to control this would be to use a higher polymer content or shorter arm lengths that would physically entrap proteins more effectively. Certain studies have combined multiple systems to result in initial burst releases of GFs along with slower and prolonged release, which has resulted in higher regenerative capacities [246,247]. Another approach would be to combine PL gels with CaP, wherein many of the proteins would likely be adsorbed to the CaP. This would likely retard the release of proteins, while decreasing the solubility of CaP itself.

### *5.1.3 On the differentiation of stem cells*

Once cells have been recruited to the defect site, they require specific cues that assign them their regenerative duties. These signals serve as lineage determinants, coaxing cells to reprogram into specific cell types [248]. Successful commitment results in tissue specific gene and protein profiles, while changes manifest in the ECM as well [249]. In Paper II, hydrogel-ACP composites were introduced to hMSCs in order to create a conducive environment for osteogenic differentiation. Cell differentiation was assessed comprehensively via gene expression analysis, protein production and calcium deposition.

Calcium and zinc release profiles for hydrogels containing each of these elements revealed initial burst releases of each element, which eventually plateaued to a sustained release after 5 days in culture medium. Interestingly, the calcium concentrations after 5 days was lower in cell culture media containing mineralised hydrogels rather than the non-mineralised hydrogels. This implies precipitation of the released calcium over time. Additionally, qualitative analysis via light microscopy and SEM imaging, confirmed that CaP minerals had been incorporated within the ECM when the cells were exposed to the mineralised composite hydrogels. While alizarin red staining confirmed the precipitation of calcium also in the absence of cells, significantly increased calcium deposition was observed within the ECM of the cells. This additionally confirmed that precipitated calcium was indeed entrapped within the ECM. Nevertheless, the question still remained as to whether the cells themselves produced osteogenic proteins and had the genetic machinery activated for lineage specification.

Osteogenic protein production was measured from the cell culture media. However, no differences were observed among cells exposed to either composite or non-mineralised hydrogels. In addition, ALP results indicated no significant differences among cells exposed to the different hydrogel groups. Gene expression analysis further validated these observations and confirmed that ACP did not have an effect on the differentiation of hMSCs towards the osteogenic lineage. However, protein levels and gene expression were generally higher for cells in the presence of non-mineralised hydrogels compared to the composite groups. The difference in cell numbers is an important consideration when questioning higher protein and gene expressions in the non-mineralised groups. Higher cell numbers would result in higher amounts of proteins secreted into the media, which can be perceived as false positives. Although making sure that the same number of cells were seeded initially can prevent discrepancies in cell numbers, it does not account for changes in cell densities that occur during the experiment. On the other hand, for gene expression analysis, the $2^{-\Delta\Delta CT}$ method normalises genes of interest to

a housekeeping gene that is constitutively expressed in cells [250]. This accounts for differences in the number of cells, mRNA quality and RT efficiency among different groups in the gene expression analysis [251]. Nonetheless, when protein production and gene expression do not converge in explaining experimental outcomes, it is important to consider indirect factors that may be causing these differences. While cells exposed to non-mineralised hydrogels formed multilayers across the bottom of the well plate, cells exposed to composite hydrogels showed patches where there were no cells. These differences in cell numbers in combination with protein and gene expression data are often necessary to explain the overall outcome of the experiments.

Additionally, it is possible that the differentiation effects of ACP were masked in the presence of osteogenic media. However if this was the case, all three groups would likely have similar differentiation profiles. Previous studies have cultured hMSCs on scaffolds in media with and without osteogenic supplements to attribute differentiation effects to the scaffold itself [252,253]. Perhaps a similar approach would isolate the differentiation effects of CaP in our study. However, the use of supplements for differentiation does not go unwarranted. The process of osteogenic differentiation is not triggered by a single event that results in mineralisation, but instead involves the coordination of numerous regulatory mechanisms over a period of time [254]. Osteogenic media typically contains three supplements: ascorbic acid (AA), dexamethaosone (DX) and β-glycerophosphate (BGP), each of which support cell differentiation in different ways [254]. AA is known to increase collagen-1 secretion into the ECM [255], while DX induces *Runx2* expression [256] and BGP provides a source of phosphate for mineralisation [254]. While there have been a few controversial discussions regarding the use of dexamethasone induced differentiation [257,258], it has been used *in vitro* as an osteogenic supplement since as early as 1985 [259,260].

We did not see striking evidence suggesting that ACP drives the differentiation of stem cells. However we did observe incorporation of minerals within the ECM. Previous studies that compared the osteogenic induction of ACP and hydroxyapatite (HA) nanoparticles have reported increased osteogenic differentiation using HA [261]. This suggests that the differentiation capacity of CaP is likely dependent on its crystallinity and solubility and implies that ACP may not be the most inductive source for differentiation. Nonetheless, with the high solubility of ACP, cells are supplied with the building blocks necessary to form mineralised tissue.

## 5.2 In perspective of periodontal regeneration

Endogenous regeneration relies on cell homing to harness the body's innate ability to regenerate lost tissue. This involves the use of growth factors within a scaffold that attracts cells and acts as an ECM template for the cells to colonise and remodel [10]. In this thesis we dissect the important aspects of endogenous regeneration and validate the use of bioactive hydrogels to guide stem cell attachment, differentiation and migration *in vitro*. Although we present results in favour of endogenous regeneration, there are various concerns specific to the periodontal defect that cannot be ignored.

The current idea behind periodontal regeneration involves creating a 'chamber' between the soft and hard tissue to support vertical bone regeneration, while preventing the gingiva from collapsing due to reduced bone height [262]. Our results show that composite hydrogels are mechanically superior to those without minerals, making them a viable solution where structural rigidity is of importance. Additionally, it is desirable to have MSCs and osteoblasts colonise the scaffold, while it is equally important to prevent infiltration of gingival fibroblasts [263]. We show that without incorporation of RGD or PL, cells are unable to attach and colonise the hydrogel. Hence, it would be purposeful to consider a dual compartmentalised gelation procedure [264], where hydrogels containing cell-adhesive motifs are placed in contact with the alveolar bone, while an inert gel is placed on the top on this, in contact with the gingiva. This would likely promote regeneration of the PDL, cementum and alveolar bone, while occluding the gingiva. Previous studies have implemented similar compartmentalised bi-layered systems demonstrating their potential *in vitro* as well as in animal models [265-267]. For instance, PL membranes were used with injectable CaP cements and implanted into periodontal defects in rats [265]. This resulted in connective tissue reattachment and alveolar bone growth, while impeding epithelial downgrowth. Another study reported the same in canine models [266]. However, both these studies incorporated cells derived from the animals and presented them back into the defect to augment the regenerative process. While the *ex vivo* isolation of cells defeats the purpose of endogenous regeneration, whether a compartmentalised cell-free scaffold can achieve similar results is yet to be determined.

Although we address the osteogenic differentiation of MSCs in Paper II, harnessing the multilineage capacity of MSCs towards cementoblasts and periodontal ligament cells must not be disregarded, in order to restore the function of the periodontium. The most promising study yet involving endogenous regeneration utilised SDF-1α loaded collagen scaffolds to recruit MSCs in a rat periodontal bone defect model [268]. While SDF-1α promotes bone regeneration

and angiogenesis, it is also capable of reducing inflammatory responses. Although this study highlights SDF-1α as a molecule of interest for periodontal regeneration, they do not mention anything regarding its potential to guide stem cells towards the formation of the cementum or periodontal ligaments. This suggests the use of growth factors in addition to SDF-1α to guide stem cells towards lineages other than bone. The use of blood derivatives such as platelet-rich fibrin has already shown evidence in regenerating the cementum-PDL complex in dogs [269].

Although the PEG-V hydrogels utilised in our studies can be formed under physiological pH, proteins from PL in these hydrogels were found to interfere with the formation of elastically effective chains. This would not only result in mechanically inferior hydrogels, but also raises concern for further unpredictable interferences *in vivo*. While we prove that these gels are capable of attracting stem cells *in vitro*, whether a similar effect would be observed *in vivo* is yet to be determined. Although cells do not infiltrate the hydrogel when seeded directly on the surface, the outgrowth and collapse of cell spheroids highlight the potential for cells to remodel the 3D matrix. Whether cells are able to invade the gel *in vivo* dictates the success of the intervention. Nonetheless, Lutolf and colleagues have utilised a similar hydrogel system in critical size rat calvarian defects and show successful infiltration and bone healing [129]. This implies that limitations identified *in vitro* do not necessarily amount to the same outcome *in vivo*.

# 6 Concluding remarks

In this thesis, we present injectable scaffolds with bioactive features desirable for endogenous periodontal regeneration. We demonstrate the importance of cell-adhesion motifs along with hydrogel stiffness as dictating factors in guiding cell morphology, attachment and organisation. While ACP was intended to guide stem cells towards the osteogenic lineage, we did not observe its influence in this regard. Instead, minerals were incorporated into the ECM when cells were exposed to the composite scaffolds as well as when seeded directly onto the hydrogel surface. However, minerals alone were incapable of supporting cell adhesion without RGD functionality. On the contrary, cell-adhesive proteins within PL were sufficient for cell attachment, while demonstrating chemotactic effects in attracting stem cells. These findings demonstrate the bioactive capacity of functionalised hydrogels in aspects of cell attachment, migration and differentiation independently. However, we need to combine these bioactive components into one system that would guide cells through the entire regenerative process.

While SDF-1α was retained within the hydrogel, future work regarding alternate loading methods could harness its chemotactic potential in our system. Although PL was selected as the main candidate to attract stem cells, given the myriad of growth factors it contains, it would likely also have the capacity to guide stem cell differentiation. While stem cells would migrate towards the defect site and differentiate with the guidance of PL, CaP would provide cells with the raw materials to build mineralised tissue. However, combining the two components would require rigorous optimisation, both to ensure the CaP remains highly soluble, and to prevent PL from interfering with the gelation process. At the same time, the real-time degradation of the hydrogel must be considered to ensure it behaves as a temporary ECM substitute, while effectively releasing the different bioactive molecules at different stages of the regenerative process. Future work to ensure the controlled release of GFs could include the use of thrombin and calcium to contain PL within an engineered blood clot.

For endogenous regeneration to be effective, chronic inflammation within the defect cannot be ignored [10]. Strategies to effectively control inflammation must be a prerequisite to any regenerative intervention. There is evidence that blood derivatives have the potential to limit inflammation by recruiting monocytes *in vitro* [270].Additionally, clinical studies have demonstrated local anti-inflammatory effects of blood derivatives within the periodontal pocket [271]. While *in vitro* studies were conducted using mesenchymal stem cells in this thesis, it would be interesting to assess whether other dental stem cells would perform similarly. This

would provide a more localised viewpoint into which cells respond best to our bioactive system. Nonetheless, despite the reproducibility and refinement that *in vitro* studies provide, ultimately only *in vivo* studies would validate our system of its true regenerative capacity.

# References


[1] Kassebaum NJ, Bernabé E, Dahiya M, Bhandari B, Murray CJL, Marcenes W. Global burden of severe periodontitis in 1990-2010: a systematic review and meta-regression. Journal of Dental Research, 2014, 93, 1045-1053.

[2] Darveau RP. Periodontitis: a polymicrobial disruption of host homeostasis. Nature Reviews Microbiology, 2010, 8, 481-490.

[3] Page RC, Kornman KS. The pathogenesis of human periodontitis: an introduction. Periodontology 2000, 1997, 14, 9-11.

[4] Preshaw PM. Detection and diagnosis of periodontal conditions amenable to prevention. BMC Oral Health, 2015, doi: 10.1186/1472-6831-15-S1-S5.

[5] Drisko CL. Periodontal debridement: still the treatment of choice. Journal of Evidence Based Dental Practice, 2014, 14, 33-41.

[6] Preshaw PM. Host response modulation in periodontics. Periodontology 2000, 2008, 48, 92-110.

[7] Esposito M, Grusovin MG, Papanikolaou N, Coulthard P, Worthington HV. Enamel matrix derivative (Emdogain) for periodontal tissue regeneration in intrabony defects. A Cochrane systematic review. International Journal of Oral Implantology, 2009, 2, 247-266.

[8] Schweikle M. Characterisation of mineralised synthetic hydrogel scaffolds for bone repair [Doctoral thesis]: University of Oslo; 2019.

[9] Atala A, Kasper FK, Mikos AG. Engineering complex tissues. Science Translational Medicine, 2012, 4, 160rv12.

[10] Lumelsky N, O'Hayre M, Chander P, Shum L, Somerman MJ. Autotherapies: enhancing endogenous healing and regeneration. Trends in Molecular Medicine, 2018, 24, 919-930.

[11] Wu R-X, Xu X-Y, Wang J, He X-T, Sun H-H, Chen F-M. Biomaterials for endogenous regenerative medicine: coaxing stem cell homing and beyond. Applied Materials Today, 2018, 11, 144-165.

[12] Hughes FJ. Periodontium and periodontal disease. In: Vishwakarma A, Sharpe P, Shi S, Ramalingam M, editors. Stem Cell Biology and Tissue Engineering in Dental Sciences. Boston: Academic Press; 2015. p 433-444.

[13] Reiter AM. Dental and oral diseases. In: Little SE, editor. The Cat. Saint Louis: W.B. Saunders; 2012. p 329-370.

[14] Gulabivala K, Ng YL. Tooth organogenesis, morphology and physiology. In: Gulabivala K, Ng Y-L, editors. Endodontics (Fourth Edition): Mosby; 2014. p 2-32.

[15] Bartold PM, Walsh LJ, Sampath NA. Molecular and cell biology of the gingiva. Periodontology 2000, 2000, 24, 28-55.

[16] Bosshardt DD. Are cementoblasts a subpopulation of osteoblasts or a unique phenotype? Journal of Dental Research, 2005, 84, 390-406.

[17] Jiang Q, Yu Y, Ruan H, Luo Y, Guo X. Morphological and functional characteristics of human gingival junctional epithelium. BMC Oral Health, 2014, doi: 10.1186/1472-6831-14-30.

[18] Jönsson D, Nebel D, Bratthall G, Nilsson B-O. The human periodontal ligament cell: a fibroblast-like cell acting as an immune cell. Journal of Periodontal Research, 2011, 46, 153-157.

[19] Murakami S. Emerging regenerative approaches for periodontal regeneration: the future perspective of cytokine therapy and stem cell therapy. 2017; Singapore. Springer Singapore. p 135-145.

[20] Krivanek J, Adameyko I, Fried K. Heterogeneity and developmental connections between cell types inhabiting teeth. Frontiers in Physiology, 2017, doi: 10.3389/fphys.2017.00376.

[21] MacNeil RL, Somerman MJ. Development and regeneration of the periodontium: parallels and contrasts. Periodontology 2000, 1999, 19, 8-20.

[22] Yao S, Pan F, Prpic V, Wise GE. Differentiation of stem cells in the dental follicle. Journal of Dental Research, 2008, 87, 767-771.

[23] Diekwisch TG. The developmental biology of cementum. International Journal of Developmental Biology, 2001, 45, 695-706.

[24] Bosshardt DD, Schroeder HE. Cementogenesis reviewed: a comparison between human premolars and rodent molars. The Anatomical Record, 1996, 245, 267-292.

[25] Narayanan AS, Bartold PM. Biochemistry of periodontal connective tissues and their regeneration: a current perspective. Connective Tissue Research, 1996, 34, 191-201.

[26] Sharpe PT. Dental mesenchymal stem cells. Development, 2016, 143, 2273-2280.

[27] Zachar L, Bačenková D, Rosocha J. Activation, homing, and role of the mesenchymal stem cells in the inflammatory environment. Journal of Inflammation Research, 2016, 9, 231-240.

[28] Watt FM, Hogan, M. BL. Out of Eden: stem cells and their niches. Science, 2000, 287, 1427-1430.

[29] Knoblich JA. Mechanisms of asymmetric stem cell division. Cell, 2008, 132, 583-597.

[30] Zakrzewski W, Dobrzyński M, Szymonowicz M, Rybak Z. Stem cells: past, present, and future. Stem Cell Research & Therapy, 2019, 10.
[31] Mokry J, Pisal R. The basic principles of stem cells. In: Vishwakarma A, Sharpe P, Shi S, Ramalingam M, editors. Stem Cell Biology and Tissue Engineering in Dental Sciences. Boston: Academic Press; 2015. p 237-248.
[32] Dominici M, Le Blanc K, Mueller I, Slaper-Cortenbach I, Marini F, Krause D, Deans R, Keating A, Prockop D, Horwitz E. Minimal criteria for defining multipotent mesenchymal stromal cells. The international society for cellular therapy position statement. Cytotherapy, 2006, 8, 315-317.
[33] Le Blanc K, Pittenger MF. Mesenchymal stem cells: progress toward promise. Cytotherapy, 2005, 7, 36-45.
[34] Akintoye SO, Lam T, Shi S, Brahim J, Collins MT, Robey PG. Skeletal site-specific characterization of orofacial and iliac crest human bone marrow stromal cells in same individuals. Bone, 2006, 38, 758-768.
[35] Chai Y, Jiang X, Ito Y, Bringas P, Han J, Rowitch DH, Soriano P, McMahon AP, Sucov HM. Fate of the mammalian cranial neural crest during tooth and mandibular morphogenesis. Development, 2000, 127, 1671-1679.
[36] Yang B, Qiu Y, Zhou N, Ouyang H, Ding J, Cheng B, Sun J. Application of stem cells in oral disease therapy: progresses and perspectives. Frontiers in Physiology, 2017, doi: 10.3389/fphys.2017.00197.
[37] Gronthos S, Mankani M, Brahim J, Robey PG, Shi S. Postnatal human dental pulp stem cells (DPSCs) in vitro and in vivo. Proceedings of the National Academy of Sciences, 2000, 97, 13625-13630.
[38] Gronthos S, Brahim J, Li W, Fisher LW, Cherman N, Boyde A, DenBesten P, Robey PG, Shi S. Stem cell properties of human dental pulp stem cells. Journal of Dental Research, 2002, 81, 531-535.
[39] Yamada Y, Nakamura S, Ito K, Sugito T, Yoshimi R, Nagasaka T, Ueda M. A feasibility of useful cell-based therapy by bone regeneration with deciduous tooth stem cells, dental pulp stem cells, or bone-marrow-derived mesenchymal stem cells for clinical study using tissue engineering technology. Tissue Engineering Part A, 2010, 16, 1891-1900.
[40] Martínez-Sarrà E, Montori S, Gil-Recio C, Núñez-Toldrà R, Costamagna D, Rotini A, Atari M, Luttun A, Sampaolesi M. Human dental pulp pluripotent-like stem cells promote wound healing and muscle regeneration. Stem Cell Research & Therapy, 2017, doi: 10.1186/s13287-017-0621-3, 175.
[41] Marei MK, El Backly RM. Dental mesenchymal stem cell-based translational regenerative dentistry: from artificial to biological replacement. Frontiers in Bioengineering and Biotechnology, 2018, doi: 10.3389/fbioe.2018.00049.
[42] Nagatomo K, Komaki M, Sekiya I, Sakaguchi Y, Noguchi K, Oda S, Muneta T, Ishikawa I. Stem cell properties of human periodontal ligament cells. Journal of Periodontal Research, 2006, 41, 303-310.
[43] Meyer JR. The regenerative potential of the periodontal ligament. The Journal of Prosthetic Dentistry, 1986, 55, 260-265.
[44] Oh M, Nör JE. The perivascular niche and self-renewal of stem cells. Frontiers in Physiology, 2015, 6, 367-367.
[45] Seo B-M, Miura M, Gronthos S, Mark Bartold P, Batouli S, Brahim J, Young M, Gehron Robey P, Wang CY, Shi S. Investigation of multipotent postnatal stem cells from human periodontal ligament. The Lancet, 2004, 364, 149-155.
[46] Liu Y, Zheng Y, Ding G, Fang D, Zhang C, Bartold PM, Gronthos S, Shi S, Wang S. Periodontal ligament stem cell-mediated treatment for periodontitis in miniature swine. Stem Cells, 2008, 26, 1065-1073.
[47] Mariotti A. The extracellular matrix of the periodontium: dynamic and interactive tissues. Periodontology 2000, 1993, 3, 39-63.
[48] Vu TH. Don't mess with the matrix. Nature Genetics, 2001, 28, 202-203.
[49] Bissell MJ, Hall HG, Parry G. How does the extracellular matrix direct gene expression? Journal of Theoretical Biology, 1982, 99, 31-68.
[50] Schultz GS, Davidson JM, Kirsner RS, Bornstein P, Herman IM. Dynamic reciprocity in the wound microenvironment. Wound Repair and Regeneration, 2011, 19, 134-148.
[51] Aumailley M, Gayraud B. Structure and biological activity of the extracellular matrix. Journal of Molecular Medicine, 1998, 76, 253-265.
[52] Cross M, Dexter TM. Growth factors in development, transformation, and tumorigenesis. Cell, 1991, 64, 271-280.
[53] M. K. Fibronectin and other cell interactive glycoproteins. Cell Biology of Extracellular Matrix: Second Edition: Springer US; 2013. p 111-146.
[54] Ho SP, Marshall SJ, Ryder MI, Marshall GW. The tooth attachment mechanism defined by structure, chemical composition and mechanical properties of collagen fibers in the periodontium. Biomaterials, 2007, 28, 5238-5245.
[55] Hubbell JA. Bioactive biomaterials. Current Opinion in Biotechnology, 1999, 10, 123-129.

[56] Lutolf MP, Hubbell JA. Synthetic biomaterials as instructive extracellular microenvironments for morphogenesis in tissue engineering. Nature Biotechnology, 2005, 23, 47-55.
[57] Lutolf MP, Hubbell JA. Synthesis and physicochemical characterization of end-linked poly(ethylene glycol)-co-peptide hydrogels formed by Michael-type addition. Biomacromolecules, 2003, 4, 713-722.
[58] Lee KY, Mooney DJ. Hydrogels for tissue engineering. Chemical Reviews, 2001, 101, 1869-1880.
[59] Zalipsky S, Harris JM. Introduction to chemistry and biological applications of poly(ethylene glycol). Poly(ethylene glycol): American Chemical Society; 1997. p 1-13.
[60] Birkedal-Hansen H. Proteolytic remodeling of extracellular matrix. Current Opinion in Cell Biology, 1995, 7, 728-735.
[61] Lutolf MP, Raeber GP, Zisch AH, Tirelli N, Hubbell JA. Cell-responsive synthetic hydrogels. Advanced Materials, 2003, 15, 888-892.
[62] West JL, Hubbell JA. Polymeric biomaterials with degradation sites for proteases involved in cell migration. Macromolecules, 1999, 32, 241-244.
[63] Sculean A, Chapple ILC, Giannobile WV. Wound models for periodontal and bone regeneration: the role of biologic research. Periodontology 2000, 2015, 68, 7-20.
[64] Chen F-M, Wu L-A, Zhang M, Zhang R, Sun H-H. Homing of endogenous stem/progenitor cells for in situ tissue regeneration: promises, strategies, and translational perspectives. Biomaterials, 2011, 32, 3189-3209.
[65] Cornelissen AS, Maijenburg MW, Nolte MA, Voermans C. Organ-specific migration of mesenchymal stromal cells: who, when, where and why? Immunology Letters, 2015, 168, 159-69.
[66] Chute JP. Stem cell homing. Current Opinion in Hematology, 2006, 13, 399-406.
[67] Lapidot T, Petit I. Current understanding of stem cell mobilization: the roles of chemokines, proteolytic enzymes, adhesion molecules, cytokines, and stromal cells. Expreimental Hematology, 2002, 30, 973-81.
[68] Kholodenko IV, Konieva AA, Kholodenko RV, Yarygin KN. Molecular mechanisms of migration and homing of intravenously transplanted mesenchymal stem cells. Journal of Regenerative Medicine and Tissue Engineering, 2013, 2, 4.
[69] Ko IK, Lee SJ, Atala A, Yoo JJ. In situ tissue regeneration through host stem cell recruitment. Experimental & Molecular Medicine, 2013, 45, e57.
[70] Phipps MC, Xu Y, Bellis SL. Delivery of platelet-derived growth factor as a chemotactic factor for mesenchymal stem cells by bone-mimetic electrospun scaffolds. PLoS ONE, 2012, 7, e40831.
[71] Ozaki Y, Nishimura M, Sekiya K, Suehiro F, Kanawa M, Nikawa H, Hamada T, Kato Y. Comprehensive analysis of chemotactic factors for bone marrow mesenchymal stem cells. Stem Cells and Development, 2007, 16, 119-129.
[72] Ringe J, Strassburg S, Neumann K, Endres M, Notter M, Burmester G-R, Kaps C, Sittinger M. Towards in situ tissue repair: human mesenchymal stem cells express chemokine receptors CXCR1, CXCR2 and CCR2, and migrate upon stimulation with CXCL8 but not CCL2. Journal of Cellular Biochemistry, 2007, 101, 135-146.
[73] Dillenburg-Pilla P, Patel V, Mikelis CM, Zárate-Bladés CR, Doçi CL, Amornphimoltham P, Wang Z, Martin D, Leelahavanichkul K, Dorsam RT and others. SDF-1/CXCL12 induces directional cell migration and spontaneous metastasis via a CXCR4/Gαi/mTORC1 axis. The FASEB Journal, 2015, 29, 1056-1068.
[74] Chen Q, Zheng C, Li Y, Bian S, Pan H, Zhao X, Lu WW. Bone targeted delivery of SDF-1 via alendronate functionalized nanoparticles in guiding stem cell migration. ACS Applied Materials & Interfaces, 2018, 10, 23700-23710.
[75] Zhao W, Jin K, Li J, Qiu X, Li S. Delivery of stromal cell-derived factor 1α for in situ tissue regeneration. Journal of Biological Engineering, 2017, doi: 10.1186/s13036-017-0058-3.
[76] Kucia M, Jankowski K, Reca R, Wysoczynski M, Bandura L, Allendorf DJ, Zhang J, Ratajczak J, Ratajczak MZ. CXCR4–SDF-1 signalling, locomotion, chemotaxis and adhesion. Journal of Molecular Histology, 2004, 35, 233-245.
[77] Fiedler J, Leucht F, Waltenberger J, Dehio C, Brenner RE. VEGF-A and PlGF-1 stimulate chemotactic migration of human mesenchymal progenitor cells. Biochemical and Biophysical Research Communications, 2005, 334, 561-568.
[78] Shi L, Fu S, Fahim S, Pan S, Lina H, Mu X, Niu Y. TNF-alpha stimulation increases dental pulp stem cell migration in vitro through integrin alpha-6 subunit upregulation. Archives of Oral Biology, 2017, 75, 48-54.
[79] Dubon MJ, Yu J, Choi S, Park K-S. Transforming growth factor β induces bone marrow mesenchymal stem cell migration via noncanonical signals and N-cadherin. Journal of Cellular Physiology, 2018, 233, 201-213.
[80] Fu X, Han B, Cai S, Lei Y, Sun T, Sheng Z. Migration of bone marrow-derived mesenchymal stem cells induced by tumor necrosis factor-α and its possible role in wound healing. Wound Repair and Regeneration, 2009, 17, 185-191.

[81] Klein G, Schmal O, Aicher WK. Matrix metalloproteinases in stem cell mobilization. Matrix Biology, 2015, 44-46, 175-183.
[82] Ho IAW, Chan KYW, Ng W-H, Guo CM, Hui KM, Cheang P, Lam PYP. Matrix metalloproteinase 1 is necessary for the migration of human bone marrow-derived mesenchymal stem cells toward human glioma. Stem Cells, 2009, 27, 1366-1375.
[83] Liang Y, Jensen TW, Roy EJ, Cha C, DeVolder RJ, Kohman RE, Zhang BZ, Textor KB, Rund LA, Schook LB and others. Tuning the non-equilibrium state of a drug-encapsulated poly(ethylene glycol) hydrogel for stem and progenitor cell mobilization. Biomaterials, 2011, 32, 2004-2012.
[84] Petit I, Szyper-Kravitz M, Nagler A, Lahav M, Peled A, Habler L, Ponomaryov T, Taichman RS, Arenzana-Seisdedos F, Fujii N and others. G-CSF induces stem cell mobilization by decreasing bone marrow SDF-1 and up-regulating CXCR4. Nature Immunology, 2002, 3, 687-694.
[85] Bowen-Pope D, Malpass T, Foster D, Ross R. Platelet-derived growth factor in vivo: levels, activity, and rate of clearance. Blood, 1984, 64, 458-469.
[86] Yamakawa S, Hayashida K. Advances in surgical applications of growth factors for wound healing. Burns & Trauma, 2019, doi: 10.1186/s41038-019-0148-1.
[87] Anitua E, Sánchez M, Orive G, Andia I. Delivering growth factors for therapeutics. Trends in Pharmacological Sciences, 2008, 29, 37-41.
[88] Zhang S, Uludag H. Nanoparticulate systems for growth factor delivery. Pharmaceutical Research, 2009, 26, 1561-1580.
[89] Purcell BP, Elser JA, Mu A, Margulies KB, Burdick JA. Synergistic effects of SDF-1α chemokine and hyaluronic acid release from degradable hydrogels on directing bone marrow derived cell homing to the myocardium. Biomaterials, 2012, 33, 7849-7857.
[90] Lee K-W, Johnson NR, Gao J, Wang Y. Human progenitor cell recruitment via SDF-1α coacervate-laden PGS vascular grafts. Biomaterials, 2013, 34, 9877-9885.
[91] Zamani M, Prabhakaran MP, Thian ES, Ramakrishna S. Controlled delivery of stromal derived factor-1α from poly lactic-co-glycolic acid core–shell particles to recruit mesenchymal stem cells for cardiac regeneration. Journal of Colloid and Interface Science, 2015, 451, 144-152.
[92] Baek SJ, Kang SK, Ra JC. In vitro migration capacity of human adipose tissue-derived mesenchymal stem cells reflects their expression of receptors for chemokines and growth factors. Experimental & Molecular Medicine, 2011, doi: 10.3858/emm.2011.43.10.069.
[93] Mendes BB, Gómez-Florit M, Babo PS, Domingues RM, Reis RL, Gomes ME. Blood derivatives awaken in regenerative medicine strategies to modulate wound healing. Advanced Drug Delivery Reviews, 2018, 129, 376-393.
[94] Marx RE. Platelet-rich plasma (PRP): what is PRP and what is not PRP? Implant Dentistry, 2001, 10, 225-228.
[95] Fortunato TM, Beltrami C, Emanueli C, De Bank PA, Pula G. Platelet lysate gel and endothelial progenitors stimulate microvascular network formation in vitro: tissue engineering implications. Scientific Reports, 2016, 6, 25326.
[96] Araki J, Jona M, Eto H, Aoi N, Kato H, Suga H, Doi K, Yatomi Y, Yoshimura K. Optimized preparation method of platelet-concentrated plasma and noncoagulating platelet-derived factor concentrates: Maximization of platelet concentration and removal of fibrinogen. Tissue Engineering Part C: Methods, 2012, 18, 176-185.
[97] Babo PS, Reis RL, Gomes ME. Periodontal tissue engineering: current strategies and the role of platelet rich hemoderivatives. Journal of Materials Chemistry B, 2017, 5, 3617-3628.
[98] Maynard DM, Heijnen HFG, Horne MK, White JG, Gahl WA. Proteomic analysis of platelet α-granules using mass spectrometry. Journal of Thrombosis and Haemostasis, 2007, 5, 1945-1955.
[99] Colter DC, Class R, DiGirolamo CM, Prockop DJ. Rapid expansion of recycling stem cells in cultures of plastic-adherent cells from human bone marrow. Proceedings of the National Academy of Sciences, 2000, 97, 3213-3218.
[100] Rahmany MB, Van Dyke M. Biomimetic approaches to modulate cellular adhesion in biomaterials: a review. Acta Biomaterialia, 2013, 9, 5431-5437.
[101] Hynes RO. Integrins: bidirectional, allosteric signaling machines. Cell, 2002, 110, 673-687.
[102] Alberts B, Johnson A, Lewis J, Raff M, Roberts K, Walter P. Cell junctions and the extracellular matrix. Molecular Biology of the Cell 6th Edition; 2002. p 1035-1090.
[103] Arnaout MA, Mahalingam B, Xiong J-P. Integrin structure, allostery, and bidirectional signaling. Annual Review of Cell and Developmental Biology, 2005, 21, 381-410.
[104] Bellis SL. Advantages of RGD peptides for directing cell association with biomaterials. Biomaterials, 2011, 32, 4205-4210.
[105] Wang X, Yan C, Ye K, He Y, Li Z, Ding J. Effect of RGD nanospacing on differentiation of stem cells. Biomaterials, 2013, 34, 2865-2874.

[106] Frith JE, Mills RJ, Cooper-White JJ. Lateral spacing of adhesion peptides influences human mesenchymal stem cell behaviour. Journal of Cell Science, 2012, 125, 317-27.
[107] Hersel U, Dahmen C, Kessler H. RGD modified polymers: biomaterials for stimulated cell adhesion and beyond. Biomaterials, 2003, 24, 4385-4415.
[108] Verrier S, Pallu S, Bareille R, Jonczyk A, Meyer J, Dard M, Amédée J. Function of linear and cyclic RGD-containing peptides in osteoprogenitor cells adhesion process. Biomaterials, 2002, 23, 585-596.
[109] Kantlehner M, Schaffner P, Finsinger D, Meyer J, Jonczyk A, Diefenbach B, Nies B, Holzemann G, Goodman SL, Kessler H. Surface coating with cyclic RGD peptides stimulates osteoblast adhesion and proliferation as well as bone formation. ChemBioChem, 2000, 1, 107-114.
[110] Liu A-Q, Hu C-H, Jin F, Zhang L-S, Xuan K. Contributions of bioactive molecules in stem cell-based periodontal regeneration. International Journal of Molecular Sciences, 2018, 19, 1016.
[111] Peng L, Ye L, Zhou Xd. Mesenchymal stem cells and tooth engineering. International Journal Of Oral Science, 2009, doi: 10.4248/ijos.08032.
[112] Kempen DHR, Lu L, Heijink A, Hefferan TE, Creemers LB, Maran A, Yaszemski MJ, Dhert WJA. Effect of local sequential VEGF and BMP-2 delivery on ectopic and orthotopic bone regeneration. Biomaterials, 2009, 30, 2816-2825.
[113] Ducy P, Karsenty G. The family of bone morphogenetic proteins. Kidney International, 2000, 57, 2207-2214.
[114] James AW, LaChaud G, Shen J, Asatrian G, Nguyen V, Zhang X, Ting K, Soo C. A review of the clinical side effects of bone morphogenetic protein-2. Tissue Engineering Part B, Reviews, 2016, 22, 284-297.
[115] Uwagie-Ero E, O.C. kene R, Chilaka F. Bone morphogenetic proteins an update and review. Tropical Journal of Natural Product Reseach, 2017, 1, 1-11.
[116] Sipe JB, Zhang J, Waits C, Skikne B, Garimella R, Anderson HC. Localization of bone morphogenetic proteins (BMPs)-2, -4, and -6 within megakaryocytes and platelets. Bone, 2004, 35, 1316-1322.
[117] Oortgiesen DAW, Walboomers XF, Bronckers ALJJ, Meijer GJ, Jansen JA. Periodontal regeneration using an injectable bone cement combined with BMP-2 or FGF-2. Journal of Tissue Engineering and Regenerative Medicine, 2014, 8, 202-209.
[118] An S, Huang X, Gao Y, Ling J, Huang Y, Xiao Y. FGF-2 induces the proliferation of human periodontal ligament cells and modulates their osteoblastic phenotype by affecting Runx2 expression in the presence and absence of osteogenic inducers. International Journal of Molecular Medicine, 2015, 36, 705-711.
[119] GR M. The Effects of TGF-β on Bone. Ciba Foundation Symposium 157 - Clinical Applications of TGF-β, doi: 10.1002/9780470514061.ch9. p 137-151.
[120] Xu X, Zheng L, Yuan Q, Zhen G, Crane JL, Zhou X, Cao X. Transforming growth factor-β in stem cells and tissue homeostasis. Bone Research, 2018, doi: 10.1038/s41413-017-0005-4.
[121] Amable PR, Carias RBV, Teixeira MVT, da Cruz Pacheco Í, Corrêa do Amaral RJF, Granjeiro JM, Borojevic R. Platelet-rich plasma preparation for regenerative medicine: optimization and quantification of cytokines and growth factors. Stem Cell Research & Therapy, 2013, doi: 10.1186/scrt218.
[122] Crespo-Diaz R, Behfar A, Butler GW, Padley DJ, Sarr MG, Bartunek J, Dietz AB, Terzic A. Platelet lysate consisting of a natural repair proteome supports human mesenchymal stem cell proliferation and chromosomal stability. Cell Transplantation, 2011, 20, 797-811.
[123] Shih Y-RV, Hwang Y, Phadke A, Kang H, Hwang NS, Caro EJ, Nguyen S, Siu M, Theodorakis EA, Gianneschi NC and others. Calcium phosphate-bearing matrices induce osteogenic differentiation of stem cells through adenosine signaling. Proceedings of the National Academy of Sciences, 2014, 111, 990-995.
[124] Müller P, Bulnheim U, Diener A, Lüthen F, Teller M, Klinkenberg E-D, Neumann H-G, Nebe B, Liebold A, Steinhoff G and others. Calcium phosphate surfaces promote osteogenic differentiation of mesenchymal stem cells. Journal of Cellular and Molecular Medicine, 2008, 12, 281-291.
[125] Jeong J, Kim JH, Shim JH, Hwang NS, Heo CY. Bioactive calcium phosphate materials and applications in bone regeneration. Biomaterials Research, 2019, 23, 4.
[126] Uskoković V, Janković-Častvan I, Wu VM. Bone mineral crystallinity governs the orchestration of ossification and resorption during bone remodeling. ACS Biomaterials Science & Engineering, 2019, 5, 3483-3498.
[127] Whited BM, Skrtic D, Love BJ, Goldstein AS. Osteoblast response to zirconia-hybridized pyrophosphate-stabilized amorphous calcium phosphate. Journal of Biomedical Materials Research Part A, 2006, 76A, 596-604.
[128] Ogata K, Imazato S, Ehara A, Ebisu S, Kinomoto Y, Nakano T, Umakoshi Y. Comparison of osteoblast responses to hydroxyapatite and hydroxyapatite/soluble calcium phosphate composites. Journal of Biomedical Materials Research Part A, 2005, 72A, 127-135.
[129] Lutolf MP, Lauer-Fields JL, Schmoekel HG, Metters AT, Weber FE, Fields GB, Hubbell JA. Synthetic matrix metalloproteinase-sensitive hydrogels for the conduction of tissue regeneration: engineering cell-

invasion characteristics. Proceedings of the National Academy of Sciences of the United States of America, 2003, 100, 5413-5418.
[130] Azagarsamy MA, Anseth KS. Bioorthogonal click chemistry: An indispensable tool to create multifaceted cell culture scaffolds. ACS Macro Letters, 2013, 2, 5-9.
[131] Nair DP, Podgórski M, Chatani S, Gong T, Xi W, Fenoli CR, Bowman CN. The thiol-michael addition click reaction: A powerful and widely used tool in materials chemistry. Chemistry of Materials, 2014, 26, 724-744.
[132] Kim J, Kong YP, Niedzielski SM, Singh RK, Putnam AJ, Shikanov A. Characterization of the crosslinking kinetics of multi-arm poly(ethylene glycol) hydrogels formed via Michael-type addition. Soft Matter, 2016, 12, 2076-2085.
[133] Phelps EA, Enemchukwu NO, Fiore VF, Sy JC, Murthy N, Sulchek TA, Barker TH, Garcia AJ. Maleimide cross-linked bioactive PEG hydrogel exhibits improved reaction kinetics and cross-linking for cell encapsulation and in situ delivery. Advanced Materials, 2012, 24, 64-70.
[134] Schweikle M, Zinn T, Lund R, Tiainen H. Injectable synthetic hydrogel for bone regeneration: Physicochemical characterisation of a high and a low pH gelling system. Materials Science and Engineering: C, 2018, 90, 67-76.
[135] Jansen LE, Negrón-Piñeiro LJ, Galarza S, Peyton SR. Control of thiol-maleimide reaction kinetics in PEG hydrogel networks. Acta Biomaterialia, 2018, 70, 120-128.
[136] Adelöw C, Segura T, Hubbell JA, Frey P. The effect of enzymatically degradable poly(ethylene glycol) hydrogels on smooth muscle cell phenotype. Biomaterials, 2008, 29, 314-326.
[137] Chung IM, Enemchukwu NO, Khaja SD, Murthy N, Mantalaris A, García AJ. Bioadhesive hydrogel microenvironments to modulate epithelial morphogenesis. Biomaterials, 2008, 29, 2637-2645.
[138] Kraehenbuehl TP, Zammaretti P, Van der Vlies AJ, Schoenmakers RG, Lutolf MP, Jaconi ME, Hubbell JA. Three-dimensional extracellular matrix-directed cardioprogenitor differentiation: systematic modulation of a synthetic cell-responsive PEG-hydrogel. Biomaterials, 2008, 29, 2757-2766.
[139] Schweikle M, Bjørnøy SH, van Helvoort ATJ, Haugen HJ, Sikorski P, Tiainen H. Stabilisation of amorphous calcium phosphate in polyethylene glycol hydrogels. Acta Biomaterialia, 2019, 90, 132-145.
[140] Ruoslahti E. RGD and other recognition sequences for integrins. Annual Review of Cell and Developmental Biology, 1996, 12, 697-715.
[141] Burdick JA, Anseth KS. Photoencapsulation of osteoblasts in injectable RGD-modified PEG hydrogels for bone tissue engineering. Biomaterials, 2002, 23, 4315-4323.
[142] Haubner R, Gratias R, Diefenbach B, Goodman SL, Jonczyk A, Kessler H. Structural and functional aspects of RGD-containing cyclic pentapeptides as highly potent and selective integrin $\alpha_V\beta_3$ antagonists. Journal of the American Chemical Society, 1996, 118, 7461-7472.
[143] Rodda AE, Meagher L, Nisbet DR, Forsythe JS. Specific control of cell–material interactions: targeting cell receptors using ligand-functionalized polymer substrates. Progress in Polymer Science, 2014, 39, 1312-1347.
[144] Salinas CN, Anseth KS. The influence of the RGD peptide motif and its contextual presentation in PEG gels on human mesenchymal stem cell viability. Journal of Tissue Engineering and Regenerative Medicine, 2008, 2, 296-304.
[145] Kyburz KA, Anseth KS. Three-dimensional hMSC motility within peptide-functionalized PEG-based hydrogels of varying adhesivity and crosslinking density. Acta Biomaterialia, 2013, 9, 6381-6392.
[146] Bae M-S, Lee KY, Park YJ, Mooney DJ. RGD island spacing controls phenotype of primary human fibroblasts adhered to ligand-organized hydrogels. Macromolecular Research, 2007, 15, 469-472.
[147] Cavalcanti-Adam EA, Volberg T, Micoulet A, Kessler H, Geiger B, Spatz JP. Cell spreading and focal adhesion dynamics are regulated by spacing of integrin ligands. Biophysical Journal, 2007, 92, 2964-2974.
[148] Zheng Y, Ji S, Czerwinski A, Valenzuela F, Pennington M, Liu S. FITC-conjugated cyclic RGD peptides as fluorescent probes for staining integrin αvβ3/αvβ5 in tumor tissues. Bioconjugate Chemistry, 2014, 25, 1925-1941.
[149] Cheng Z, Wu Y, Xiong Z, Gambhir SS, Chen X. Near-infrared fluorescent RGD peptides for optical imaging of integrin alphavbeta3 expression in living mice. Bioconjugate Chemistry, 2005, 16, 1433-1441.
[150] Beniash E, Metzler RA, Lam RS, Gilbert PU. Transient amorphous calcium phosphate in forming enamel. Journal of Structural Biology, 2009, 166, 133-143.
[151] Sauer GR, Zunic WB, Durig JR, Wuthier RE. Fourier transform raman spectroscopy of synthetic and biological calcium phosphates. Calcified Tissue International, 1994, 54, 414-420.
[152] Crane NJ, Popescu V, Morris MD, Steenhuis P, Ignelzi MA. Raman spectroscopic evidence for octacalcium phosphate and other transient mineral species deposited during intramembranous mineralization. Bone, 2006, 39, 434-442.
[153] Olszta MJ, Cheng X, Jee SS, Kumar R, Kim Y-Y, Kaufman MJ, Douglas EP, Gower LB. Bone structure and formation: a new perspective. Materials Science and Engineering: R: Reports, 2007, 58, 77-116.

[154] Brès EF, Moebus G, Kleebe HJ, Pourroy G, Werkmann J, Ehret G. High resolution electron microscopy study of amorphous calcium phosphate. Journal of Crystal Growth, 1993, 129, 149-162.
[155] Bohner M. Calcium orthophosphates in medicine: from ceramics to calcium phosphate cements. Injury, 2000, 31, D37-D47.
[156] Chow LC, Eanes E. Solubility of calcium phosphates. Monographs in Oral Science, 2001, 18, 94-111.
[157] Wu VM, Uskoković V. Is there a relationship between solubility and resorbability of different calcium phosphate phases in vitro? Biochimica et biophysica acta, 2016, 1860, 2157-2168.
[158] LeGeros RZ, Bleiwas CB, Retino M, Rohanizadeh R, LeGeros JP. Zinc effect on the in vitro formation of calcium phosphates: relevance to clinical inhibition of calculus formation. American Journal of Dentistry, 1999, 12, 65-71.
[159] Boanini E, Gazzano M, Bigi A. Ionic substitutions in calcium phosphates synthesized at low temperature. Acta Biomaterialia, 2010, 6, 1882-1894.
[160] Chatzipanagis K, Iafisco M, Roncal-Herrero T, Bilton M, Tampieri A, Kröger R, Delgado-López JM. Crystallization of citrate-stabilized amorphous calcium phosphate to nanocrystalline apatite: a surface-mediated transformation. CrystEngComm, 2016, 18, 3170-3173.
[161] Ma PX, Elisseeff J. Injectable systems for cartilage tissue engineering. Scaffolding in Tissue Engineering: CRC Press; 2005. p 169-184.
[162] Lin C-C, Anseth KS. PEG hydrogels for the controlled release of biomolecules in regenerative medicine. Pharmaceutical Research, 2009, 26, 631-643.
[163] Engler AJ, Sen S, Sweeney HL, Discher DE. Matrix elasticity directs stem cell lineage specification. Cell, 2006, 126, 677-689.
[164] Wen JH, Vincent LG, Fuhrmann A, Choi YS, Hribar KC, Taylor-Weiner H, Chen S, Engler AJ. Interplay of matrix stiffness and protein tethering in stem cell differentiation. Nature Materials, 2014, 13, 979-987.
[165] Chen J. Nanobiomechanics of living cells: a review. Interface Focus, 2014, doi: 10.1098/rsfs.2013.0055.
[166] Ludwig T, Kirmse R, Poole K, Schwarz US. Probing cellular microenvironments and tissue remodeling by atomic force microscopy. Pflugers Archive: European Journal of Physiology, 2008, 456, 29-49.
[167] Frey MT, Engler A, Discher DE, Lee J, Wang YL. Microscopic methods for measuring the elasticity of gel substrates for cell culture: microspheres, microindenters, and atomic force microscopy. Methods in Cell Biology, 2007, 83, 47-65.
[168] Lin D, Dimitriadis E, Horkay F. Elasticity of rubber-like materials measured by AFM nanoindentation. Express Polymer Letters, 2007, 1, 576-584.
[169] Horzum U, Ozdil B, Pesen-Okvur D. Step-by-step quantitative analysis of focal adhesions. MethodsX, 2014, 1, 56-59.
[170] Zuidema JM, Rivet CJ, Gilbert RJ, Morrison FA. A protocol for rheological characterization of hydrogels for tissue engineering strategies. Journal of Biomedical Materials Research Part B: Applied Biomaterials, 2014, 102, 1063-1073.
[171] Franck A. Viscoelasticity and dynamic mechanical testing. Volume AN004. Germany: TA Instruments. p 1-7.
[172] Fernández B, Lobo L, Pereiro R. Atomic absorpton spectrometry | fundamentals, instrumentation and capabilities. In: Worsfold P, Poole C, Townshend A, Miró M, editors. Encyclopedia of Analytical Science (Third Edition). Oxford: Academic Press; 2019. p 137-143.
[173] Smith PK, Krohn RI, Hermanson G, Mallia A, Gartner F, Provenzano M, Fujimoto E, Goeke N, Olson B, Klenk D. Measurement of protein using bicinchoninic acid. Analytical Biochemistry, 1985, 150, 76-85.
[174] Chang SK, Zhang Y. Protein analysis. Food analysis: Springer; 2017. p 315-331.
[175] Strioga M, Viswanathan S, Darinskas A, Slaby O, Michalek J. Same or not the same? Comparison of adipose tissue-derived versus bone marrow-derived mesenchymal stem and stromal cells. Stem Cells and Development, 2012, 21, 2724-52.
[176] Baxter MA, Wynn RF, Jowitt SN, Wraith JE, Fairbairn LJ, Bellantuono I. Study of telomere length reveals rapid aging of human marrow stromal cells following in vitro expansion. Stem Cells, 2004, 22, 675-682.
[177] Vacanti V, Kong E, Suzuki G, Sato K, Canty JM, Lee T. Phenotypic changes of adult porcine mesenchymal stem cells induced by prolonged passaging in culture. Journal of Cellular Physiology, 2005, 205, 194-201.
[178] Zengel P, Nguyen-Hoang A, Schildhammer C, Zantl R, Kahl V, Horn E. μ-Slide chemotaxis: a new chamber for long-term chemotaxis studies. BMC Cell Biology, 2011, 12, 21-21.
[179] Park S, Jang H, Kim BS, Hwang C, Jeong GS, Park Y. Directional migration of mesenchymal stem cells under an SDF-1α gradient on a microfluidic device. PLoS ONE, 2017, 12, e0184595.
[180] Bartosh TJ, Ylöstalo JH, Mohammadipoor A, Bazhanov N, Coble K, Claypool K, Lee RH, Choi H, Prockop DJ. Aggregation of human mesenchymal stromal cells (MSCs) into 3D spheroids enhances their antiinflammatory properties. Proceedings of the National Academy of Sciences of the United States of America, 2010, 107, 13724-13729.
[181] Pawley J. Handbook of Biological Confocal Microscopy: Springer US; 2010.

[182] Atherton P, Stutchbury B, Jethwa D, Ballestrem C. Mechanosensitive components of integrin adhesions: role of vinculin. Experimental Cell Research, 2016, 343, 21-27.
[183] Case LB, Baird MA, Shtengel G, Campbell SL, Hess HF, Davidson MW, Waterman CM. Molecular mechanism of vinculin activation and nanoscale spatial organization in focal adhesions. Nature Cell Biology, 2015, doi: 10.1038/ncb3180.
[184] Elosegui-Artola A, Oria R, Chen Y, Kosmalska A, Pérez-González C, Castro N, Zhu C, Trepat X, Roca-Cusachs P. Mechanical regulation of a molecular clutch defines force transmission and transduction in response to matrix rigidity. Nature Cell Biology, 2016, doi: 10.1038/ncb3336.
[185] Swaminathan V, Waterman CM. The molecular clutch model for mechanotransduction evolves. Nature Cell Biology, 2016, 18, 459.
[186] Wulf E, Deboben A, Bautz FA, Faulstich H, Wieland T. Fluorescent phallotoxin, a tool for the visualization of cellular actin. Proceedings of the National Academy of Sciences of the United States of America, 1979, 76, 4498-4502.
[187] Tarnowski BI, Spinale FG, Nicholson JH. DAPI as a useful stain for nuclear quantitation. Biotechnic & Histochemistry, 1991, 66, 296-302.
[188] Clark PJ, Evans FC. Distance to nearest neighbor as a measure of spatial relationships in populations. Ecology, 1954, 35, 445-453.
[189] Eidet JR, Pasovic L, Maria R, Jackson CJ, Utheim TP. Objective assessment of changes in nuclear morphology and cell distribution following induction of apoptosis. Diagnostic Pathology, 2014, 9, 92-92.
[190] Aslantürk ÖS. In vitro cytotoxicity and cell viability assays: Principles, advantages, and disadvantages: InTech; 2018.
[191] Rampersad SN. Multiple applications of Alamar Blue as an indicator of metabolic function and cellular health in cell viability bioassays. Sensors, 2012, 12, 12347-12360.
[192] O'Brien J, Wilson I, Orton T, Pognan F. Investigation of the Alamar Blue (resazurin) fluorescent dye for the assessment of mammalian cell cytotoxicity. European Journal of Biochemistry, 2000, 267, 5421-5426.
[193] Johannisson A, Jonasson R, Dernfalk J, Jensen-Waern M. Simultaneous detection of porcine proinflammatory cytokines using multiplex flow cytometry by the xMAP™ technology. Cytometry Part A, 2006, 69A, 391-395.
[194] Baker HN, Murphy R, Lopez E, Garcia C. Conversion of a capture ELISA to a Luminex xMAP assay using a multiplex antibody screening method. Journal of Visualized Experiments, 2012, doi, e4084.
[195] Elshal MF, McCoy JP. Multiplex bead array assays: performance evaluation and comparison of sensitivity to ELISA. Methods, 2006, 38, 317-323.
[196] Wagner ER, Luther G, Zhu G, Luo Q, Shi Q, Kim SH, Gao J-L, Huang E, Gao Y, Yang K. Defective osteogenic differentiation in the development of osteosarcoma. Sarcoma, 2011, doi: 10.1155/2011/325238.
[197] Simms D, Cizdziel PE, Chomczynski P. TRIzol: A new reagent for optimal single-step isolation of RNA. Focus, 1993, 15, 532-535.
[198] Zhao X, Zhou Q, Zhang L, Yan W, Sun N, Liang X, Deng C. Comparison of three magnetic-bead-based RNA extraction methods for detection of cucumber green mottle mosaic virus by real-time RT-PCR. Archives of Virology, 2015, 160, 1791-1796.
[199] Tan SC, Yiap BC. DNA, RNA, and protein extraction: the past and the present. BioMed Research International, 2009, doi: 10.1155/2009/574398.
[200] Taylor S, Wakem M, Dijkman G, Alsarraj M, Nguyen M. A practical approach to RT-qPCR—publishing data that conform to the MIQE guidelines. Methods, 2010, 50, S1-S5.
[201] Singh VK, Kumar A. PCR primer design. Molecular Biology Today, 2001, 2, 27-32.
[202] Barber RD, Harmer DW, Coleman RA, Clark BJ. GAPDH as a housekeeping gene: analysis of GAPDH mRNA expression in a panel of 72 human tissues. Physiological Genomics, 2005, 21, 389-395.
[203] Kozera B, Rapacz M. Reference genes in real-time PCR. Journal of Applied Genetics, 2013, 54, 391-406.
[204] Stein GS, Lian JB, Stein JL, Van Wijnen AJ, Montecino M. Transcriptional control of osteoblast growth and differentiation. Physiological Reviews, 1996, 76, 593-629.
[205] Sabokbar A, Millett PJ, Myer B, Rushton N. A rapid, quantitative assay for measuring alkaline phosphatase activity in osteoblastic cells in vitro. Bone and Mineral, 1994, 27, 57-67.
[206] Sanikop S, Patil S, Agrawal P. Gingival crevicular fluid alkaline phosphatase as a potential diagnostic marker of periodontal disease. Journal of Indian Society of Periodontology, 2012, 16, 513-518.
[207] Puchtler H, Meloan SN, Terry MS. On the history and mechanism of alizarin and alizarin red stains for calcium. Journal of Histochemistry & Cytochemistry, 1969, 17, 110-124.
[208] Wang Y-H, Liu Y, Maye P, Rowe DW. Examination of mineralized nodule formation in living osteoblastic cultures using fluorescent dyes. Biotechnology Progress, 2006, 22, 1697-1701.
[209] Lee JTY, Chow KL. SEM sample preparation for cells on 3D scaffolds by freeze-drying and HMDS. Scanning, 2012, 34, 12-25.

[210] Alhede M, Qvortrup K, Liebrechts R, Høiby N, Givskov M, Bjarnsholt T. Combination of microscopic techniques reveals a comprehensive visual impression of biofilm structure and composition. FEMS Immunology & Medical Microbiology, 2012, 65, 335-342.
[211] Panchal V, Yang Y, Cheng G, Hu J, Kruskopf M, Liu C-I, Rigosi AF, Melios C, Hight Walker AR, Newell DB and others. Confocal laser scanning microscopy for rapid optical characterization of graphene. Communications Physics, 2018, doi: 10.1038/s42005-018-0084-6.
[212] Boyden S. The chemotactic effect of mixtures of antibody and antigen on polymorphonuclear leucocytes. The Journal of Experimental Medicine, 1962, 115, 453-466.
[213] Kim YH, He S, Kase S, Kitamura M, Ryan SJ, Hinton DR. Regulated secretion of complement factor H by RPE and its role in RPE migration. Graefe's Archive for Clinical and Experimental Ophthalmology, 2009, 247, 651-659.
[214] Kobayashi N, Yamada Y, Ito W, Ueki S, Kayaba H, Nakamura H, Yodoi J, Chihara J. Thioredoxin reduces C-C chemokine-induced chemotaxis of human eosinophils. Allergy, 2009, 64, 1130-1135.
[215] Chen H-C. Boyden chamber assay. In: Guan J-L, editor. Cell Migration: Developmental Methods and Protocols. Totowa, NJ: Humana Press; 2005. p 15-22.
[216] Foxman EF, Kunkel EJ, Butcher EC. Integrating conflicting chemotactic signals. The role of memory in leukocyte navigation. The Journal of Cell Biology, 1999, 147, 577-588.
[217] McCutcheon M. Chemotaxis in leukocytes. Physiological Reviews, 1946, 26, 319-336.
[218] Mardia KV. Test for samples from Von Mises populations. In: Mardia KV, editor. Statistics of Directional Data: Academic Press; 1972. p 131-170.
[219] Demuth T, Hopf NJ, Kempski O, Sauner D, Herr M, Giese A, Perneczky A. Migratory activity of human glioma cell lines in vitro assessed by continuous single cell observation. Clinical & Experimental Metastasis, 2000, 18, 589-597.
[220] Cordelières FP. Manual tracking. Institut Curie, Orsay (France), 2005, doi.
[221] Hand AJ, Sun T, Barber DC, Hose DR, Macneil S. Automated tracking of migrating cells in phase-contrast video microscopy sequences using image registration. Journal of Microscopy, 2009, 234, 62-79.
[222] Cantarella C, Sepe L, Fioretti F, Ferrari MC, Paolella G. Analysis and modelling of motility of cell populations with MotoCell. BMC Bioinformatics, 2009, doi: 10.1186/1471-2105-10-S12-S12.
[223] Germain F, Doisy A, Ronot X, Tracqui P. Characterization of cell deformation and migration using a parametric estimation of image motion. IEEE Transactions on Biomedical Engineering, 1999, 46, 584-600.
[224] Williams DF. There is no such thing as a biocompatible material. Biomaterials, 2014, 35, 10009-10014.
[225] Williams DF. Titanium for medical applications. Titanium in Medicine: Material Science, Surface Science, Engineering, Biological Responses and Medical Applications. Berlin, Heidelberg: Springer Berlin Heidelberg; 2001. p 13-24.
[226] Ou K-L, Hosseinkhani H. Development of 3D in vitro technology for medical applications. International Journal of Molecular Sciences, 2014, 15, 17938-17962.
[227] Hoarau-Véchot J, Rafii A, Touboul C, Pasquier J. Halfway between 2D and animal models: Are 3D cultures the ideal tool to study cancer-microenvironment interactions? International Journal of Molecular Sciences, 2018, doi: 10.3390/ijms19010181.
[228] Yamada KM, Cukierman E. Modeling tissue morphogenesis and cancer in 3D. Cell, 2007, 130, 601-610.
[229] Duval K, Grover H, Han L-H, Mou Y, Pegoraro AF, Fredberg J, Chen Z. Modeling physiological events in 2D vs. 3D cell culture. Physiology, 2017, 32, 266-277.
[230] Fang Y, Eglen RM. Three-dimensional cell cultures in drug discovery and development. SLAS Discovery, 2017, 22, 456-472.
[231] Hughes CS, Postovit LM, Lajoie GA. Matrigel: a complex protein mixture required for optimal growth of cell culture. Proteomics, 2010, 10, 1886-1890.
[232] Vukicevic S, Kleinman HK, Luyten FP, Roberts AB, Roche NS, Reddi AH. Identification of multiple active growth factors in basement membrane matrigel suggests caution in interpretation of cellular activity related to extracellular matrix components. Experimental Cell Research, 1992, 202, 1-8.
[233] Abagnale G, Sechi A, Steger M, Zhou Q, Kuo C-C, Aydin G, Schalla C, Müller-Newen G, Zenke M, Costa IG and others. Surface topography guides morphology and spatial patterning of induced pluripotent stem cell colonies. Stem Cell Reports, 2017, 9, 654-666.
[234] Dalby MJ, Gadegaard N, Oreffo ROC. Harnessing nanotopography and integrin-matrix interactions to influence stem cell fate. Nature Materials, 2014, 13, 558-569.
[235] Ladoux B, Mege RM, Trepat X. Front-rear polarization by mechanical cues: From single cells to tissues. Trends in Cell Biology, 2016, 26, 420-433.
[236] Wilson MJ, Liliensiek SJ, Murphy CJ, Murphy WL, Nealey PF. Hydrogels with well-defined peptide-hydrogel spacing and concentration: impact on epithelial cell behavior. Soft Matter, 2012, 8, 390-398.
[237] Wolfenson H, Iskratsch T, Sheetz Michael P. Early events in cell spreading as a model for quantitative analysis of biomechanical events. Biophysical Journal, 2014, 107, 2508-2514.

[238] Maheshwari G, Brown G, Lauffenburger DA, Wells A, Griffith LG. Cell adhesion and motility depend on nanoscale RGD clustering. Journal of Cell Science, 2000, 113, 1677-1686.
[239] Singh SP, Schwartz MP, Lee JY, Fairbanks BD, Anseth KS. A peptide functionalized poly (ethylene glycol)(PEG) hydrogel for investigating the influence of biochemical and biophysical matrix properties on tumor cell migration. Biomaterials Science, 2014, 2, 1024-1034.
[240] Simona BR, Hirt L, Demkó L, Zambelli T, Vörös J, Ehrbar M, Milleret V. Density gradients at hydrogel interfaces for enhanced cell penetration. Biomaterials Science, 2015, 3, 586-591.
[241] Deuel TF, Huang J. Platelet-derived growth factor. Structure, function, and roles in normal and transformed cells. The Journal of Clinical Investigation, 1984, 74, 669-676.
[242] Pillarisetti K, Gupta SK. Cloning and relative expression analysis of rat stromal cell derived factor-1 (SDF-1): SDF-1 α mRNA is selectively induced in rat model of myocardial infarction. Inflammation, 2001, 25, 293-300.
[243] Seppä H, Grotendorst G, Seppä S, Schiffmann E, Martin GR. Platelet-derived growth factor in chemotactic for fibroblasts. The Journal of Cell Biology, 1982, 92, 584-588.
[244] Burnouf T, Strunk D, Koh MBC, Schallmoser K. Human platelet lysate: replacing fetal bovine serum as a gold standard for human cell propagation? Biomaterials, 2016, 76, 371-387.
[245] Re F, Sartore L, Moulisova V, Cantini M, Almici C, Bianchetti A, Chinello C, Dey K, Agnelli S, Manferdini C and others. 3D gelatin-chitosan hybrid hydrogels combined with human platelet lysate highly support human mesenchymal stem cell proliferation and osteogenic differentiation. Journal of Tissue Engineering, 2019, 10, 2041731419845852.
[246] Liu X, Yang Y, Niu X, Lin Q, Zhao B, Wang Y, Zhu L. An in situ photocrosslinkable platelet rich plasma – complexed hydrogel glue with growth factor controlled release ability to promote cartilage defect repair. Acta Biomaterialia, 2017, 62, 179-187.
[247] Ito R, Morimoto N, Pham LH, Taira T, Kawai K, Suzuki S. Efficacy of the controlled release of concentrated platelet lysate from a collagen/gelatin scaffold for dermis-like tissue regeneration. Tissue Engineering Part A, 2013, 19, 1398-1405.
[248] Donnelly H, Salmeron-Sanchez M, Dalby MJ. Designing stem cell niches for differentiation and self-renewal. Journal of The Royal Society Interface, 2018, 15, 20180388.
[249] Ort C, Dayekh K, Xing M, Mequanint K. Emerging strategies for stem cell lineage commitment in tissue engineering and regenerative medicine. ACS Biomaterials Science & Engineering, 2018, 4, 3644-3657.
[250] Livak KJ, Schmittgen TD. Analysis of relative gene expression data using real-time quantitative PCR and the 2−ΔΔCT method. Methods, 2001, 25, 402-408.
[251] Rao X, Huang X, Zhou Z, Lin X. An improvement of the 2ˆ(-delta delta CT) method for quantitative real-time polymerase chain reaction data analysis. Biostatistics, Bioinformatics and Biomathematics, 2013, 3, 71-85.
[252] Persson M, Lehenkari PP, Berglin L, Turunen S, Finnilä MAJ, Risteli J, Skrifvars M, Tuukkanen J. Osteogenic differentiation of human mesenchymal stem cells in a 3D woven scaffold. Scientific Reports, 2018, 8, 10457.
[253] Polini A, Pisignano D, Parodi M, Quarto R, Scaglione S. Osteoinduction of human mesenchymal stem cells by bioactive composite scaffolds without supplemental osteogenic growth factors. PLoS ONE, 2011, 6, e26211.
[254] Langenbach F, Handschel J. Effects of dexamethasone, ascorbic acid and beta-glycerophosphate on the osteogenic differentiation of stem cells in vitro. Stem Cell Research & Therapy, 2013, doi: 10.1186/scrt328.
[255] Murad S, Grove D, Lindberg KA, Reynolds G, Sivarajah A, Pinnell SR. Regulation of collagen synthesis by ascorbic acid. Proceedings of the National Academy of Sciences of the United States of America, 1981, 78, 2879-2882.
[256] Hamidouche Z, Haÿ E, Vaudin P, Charbord P, Schüle R, Marie PJ, Fromigué O. FHL2 mediates dexamethasone-induced mesenchymal cell differentiation into osteoblasts by activating Wnt/β-catenin signaling-dependent Runx2 expression. The FASEB Journal, 2008, 22, 3813-3822.
[257] Ghali O, Broux O, Falgayrac G, Haren N, van Leeuwen JPTM, Penel G, Hardouin P, Chauveau C. Dexamethasone in osteogenic medium strongly induces adipocyte differentiation of mouse bone marrow stromal cells and increases osteoblast differentiation. BMC Cell Biology, 2015, doi: 10.1186/s12860-015-0056-6.
[258] Pan J-M, Wu L-G, Cai J-W, Wu L-T, Liang M. Dexamethasone suppresses osteogenesis of osteoblast via the PI3K/Akt signaling pathway in vitro and in vivo. Journal of Receptors and Signal Transduction, 2019, 39, 80-86.
[259] Tenenbaum HC, Heersche JN. Dexamethasone stimulates osteogenesis in chick periosteum in vitro. Endocrinology, 1985, 117, 2211-2217.

[260] Panek M, Antunović M, Pribolšan L, Ivković A, Gotić M, Vukasović A, Caput Mihalić K, Pušić M, Jurkin T, Marijanović I. Bone tissue engineering in a perfusion bioreactor using dexamethasone-loaded peptide hydrogel. Materials, 2019, doi: 10.3390/ma12060919.
[261] Hu Q, Tan Z, Liu Y, Tao J, Cai Y, Zhang M, Pan H, Xu X, Tang R. Effect of crystallinity of calcium phosphate nanoparticles on adhesion, proliferation, and differentiation of bone marrow mesenchymal stem cells. Journal of Materials Chemistry, 2007, 17, 4690-4698.
[262] Dimitriou R, Mataliotakis GI, Calori GM, Giannoudis PV. The role of barrier membranes for guided bone regeneration and restoration of large bone defects: current experimental and clinical evidence. BMC Medicine, 2012, doi: 10.1186/1741-7015-10-81.
[263] Retzepi M, Donos N. Guided bone regeneration: Biological principle and therapeutic applications. Clinical Oral Implants Research, 2010, 21, 567-576.
[264] Kim JH, Park CH, Perez RA, Lee HY, Jang JH, Lee HH, Wall IB, Shi S, Kim HW. Advanced biomatrix designs for regenerative therapy of periodontal tissues. Journal of Dental Research, 2014, 93, 1203-1211.
[265] Babo PS, Cai X, Plachokova AS, Reis RL, Jansen JA, Gomes ME, Walboomers XF. The role of a platelet lysate-based compartmentalized system as a carrier of cells and platelet-origin cytokines for periodontal tissue regeneration. Tissue Engineering Part A, 2016, 22, 1164-1175.
[266] Iwata T, Yamato M, Tsuchioka H, Takagi R, Mukobata S, Washio K, Okano T, Ishikawa I. Periodontal regeneration with multi-layered periodontal ligament-derived cell sheets in a canine model. Biomaterials, 2009, 30, 2716-2723.
[267] Requicha JF, Viegas CA, Muñoz F, Azevedo JM, Leonor IB, Reis RL, Gomes ME. A tissue engineering approach for periodontal regeneration based on a biodegradable double-layer scaffold and adipose-derived stem cells. Tissue Engineering Part A, 2014, 20, 2483-2492.
[268] Liu H, Li M, Du L, Yang P, Ge S. Local administration of stromal cell-derived factor-1 promotes stem cell recruitment and bone regeneration in a rat periodontal bone defect model. Materials Science and Engineering: C, 2015, 53, 83-94.
[269] Ji B, Sheng L, Chen G, Guo S, Xie L, Yang B, Guo W, Tian W. The combination use of platelet-rich fibrin and treated dentin matrix for tooth root regeneration by cell homing. Tissue Engineering Part A, 2015, 21, 26-34.
[270] El-Sharkawy H, Kantarci A, Deady J, Hasturk H, Liu H, Alshahat M, Van Dyke TE. Platelet-rich plasma: growth factors and pro- and anti-inflammatory properties. Journal of Periodontology, 2007, 78, 661-669.
[271] Abdul Ameer LA, Raheem ZJ, Abdulrazaq SS, Ali BG, Nasser MM, Aldeen Khairi AW. The anti-inflammatory effect of the platelet-rich plasma in the periodontal pocket. European Journal of Dentistry, 2018, 12, 528-531.

# Appendix

Appendix 1: Image of hMSCs cultured on the surface of RGD functionalised PEG-M hydrogels for 30 days.

# I

Journal of the Mechanical Behavior of Biomedical Materials 84 (2018) 46–53

Contents lists available at ScienceDirect

Journal of the Mechanical Behavior of Biomedical Materials

journal homepage: www.elsevier.com/locate/jmbbm

# Attachment and spatial organisation of human mesenchymal stem cells on poly(ethylene glycol) hydrogels

Aman S. Chahal, Manuel Schweikle, Catherine A. Heyward, Hanna Tiainen*

*Department of Biomaterials, Institute of Clinical Dentistry, University of Oslo, Norway*

ARTICLE INFO

*Keywords:*
Cell attachment
RGD
PEG
Hydrogel
Human mesenchymal stem cells
Tissue engineering

ABSTRACT

Strategies that enable hydrogel substrates to support cell attachment typically incorporate either entire extracellular matrix proteins or synthetic peptide fragments such as the RGD (arginine–glycine–aspartic acid) motif. Previous studies have carefully analysed how material characteristics can affect single cell morphologies. However, the influence of substrate stiffness and ligand presentation on the spatial organisation of human mesenchymal stem cells (hMSCs) have not yet been examined. In this study, we assessed how hMSCs organise themselves on soft ($E$ = 7.4–11.2 kPa) and stiff ($E$ = 27.3–36.8 kPa) poly(ethylene glycol) (PEG) hydrogels with varying concentrations of RGD (0.05–2.5 mM). Our results indicate that hMSCs seeded on soft hydrogels clustered with reduced cell attachment and spreading area, irrespective of RGD concentration and isoform. On stiff hydrogels, in contrast, cells spread with high spatial coverage for RGD concentrations of 0.5 mM or higher. In conclusion, we identified that an interplay of hydrogel stiffness and the availability of cell attachment motifs are important factors in regulating hMSC organisation on PEG hydrogels. Understanding how cells initially interact and colonise the surface of this material is a fundamental prerequisite for the design of controlled platforms for tissue engineering and mechanobiology studies.

## 1. Introduction

The mechanical properties of biomaterial substrates are known to alter cellular behaviour in many ways (Fusco et al., 2015). Changes in substrate stiffness are capable of altering cellular morphologies as well as guiding cells towards a specific fate (Chicurel et al., 1998; El-Sherbiny and Yacoub, 2013; Engler et al., 2006). This has revolutionised researchers' approaches towards tailoring substrates that communicate with and instruct cells in a manner that supports the application of the biomaterial itself (Li et al., 2017). In addition to the mechanical properties, the presence of anchored biochemical ligands within the substrate can have a significant impact on various cellular behaviours (Bae et al., 2007; Engler et al., 2004; Hsiong et al., 2008; Kilian and Mrksich, 2012; Wen et al., 2014). Cellular structure, motility and proliferation rates can be influenced by altering substrate stiffness or the availability of biochemical ligands (Frith et al., 2012; Mathieu and Loboa, 2012). Poly(ethylene glycol) (PEG) hydrogels are excellent platforms for mechanobiology studies by providing robust and highly controllable systems, allowing for regulated ligand tethering while permitting stiffness tunability (Herrick et al., 2013).

While elaborate studies have investigated changes in single cell morphologies linked to alterations in nanotopography, mechanics and functionality of various substrates, the way in which cells organise in groups or colonies on these substrates has not yet been investigated (Engler et al., 2004; Kim et al., 2012; Schwarz and Bischofs, 2005; Yim et al., 2010). Various studies have controlled the presentation of synthetic cell attachment ligands on patterned surfaces, providing insight into mechanosensing and mechanotransductive processes (Arnold et al., 2004; Deeg et al., 2011; Frith et al., 2012). Studies that have successfully incorporated various concentrations of RGD peptides within hydrogels often encapsulate cells within the gel and test for fate-priming without analysing how cells organise themselves as groups upon initial contact (Anderson et al., 2011; Kyburz and Anseth, 2013; Nuttelman et al., 2004). However, the encapsulation of autologous cells typically requires isolation and expansion, substantially limiting its potential translation to the clinic. Cell-free systems relying on recruitment and attachment of cells from adjacent tissues to the substrate promise a more feasible solution regarding clinical application. To maximise the potential of such approaches, it is crucial that we define a minimum concentration of RGD required in order to accommodate cell attachment.

The low protein adsorption of PEG is advantageous when engineering controlled cell-responsive systems, but requires tethering of sufficient levels of cell attachment motifs in order for the substrate to

* Corresponding author.
*E-mail address:* hanna.tiainen@odont.uio.no (H. Tiainen).

https://doi.org/10.1016/j.jmbbm.2018.04.025
Received 17 January 2018; Received in revised form 18 April 2018; Accepted 30 April 2018
Available online 03 May 2018

support cellular adhesion (Hern and Hubbell, 1998). The incorporation of RGD peptides in hydrogel systems have shown to enhance cellular attachment, spreading and proliferation (Shu et al., 2004). Both linear and cyclic isoforms of synthetic RGD peptides have been used in the past (Hersel et al., 2003; Verrier et al., 2002). It is known that the cyclic isoform is selective in binding to the $\alpha_v\beta_3$ integrin subunit, while the linear form is specific to the $\alpha_5\beta_1$ subunit, resulting in the onset of different downstream cascades within the cell (Hersel et al., 2003). Studies related to tissue engineering and stem cell-based regenerative medicine often use cyclic isoforms to guide differentiation processes, since the cyclic isoform is also known to have high stability in vivo (Haubner et al., 1996; Hersel et al., 2003; Kantlehner et al., 2000; Zhang et al., 2016). Additional evidence suggests that $\alpha_v\beta_3$ integrin exhibits significantly higher binding affinity and specificity to the cyclic isoform than the linear one (Haubner et al., 1996; Rodda et al., 2014). This proposes that lower concentrations of the cyclic isoform may be required in hydrogels for efficient cell adhesion and survival, compared to the linear isoform, which could in turn also have an impact on the stiffness of the substrate. As indicated by Bellis, many confounding factors make the selection of RGD peptide concentrations and isoforms a complex decision when designing hydrogels (Bellis, 2011).

In this study, we use a hydrogel system based on PEG star macromeres. Maleimide groups at the chain ends serve as functional groups for end-linking of the macromeres into hydrogels as well as ligation sites for tethering RGD peptides. Since the same functional groups are used for tethering RGD peptides as for cross-linking of the hydrogel backbone, one can expect a correlation of RGD peptide concentration and gel stiffness as less elastically active links might be formed when fewer unreacted functional groups are available. We investigate potential changes in substrate stiffness due to increased RGD tethering within this system via nanoindentation, using atomic force microscopy (AFM). We hypothesize that higher RGD concentrations and stiffer gels promote human mesenchymal stem cell (hMSC) attachment and spreading. Hence, we study how hMSCs attach and organise themselves on PEG hydrogels functionalised with varying concentrations of linear or cyclic RGD peptides (linRGD and cycRGD respectively) while implementing image analysis tools to assess organisational changes of cells as initial indicators of how they interact with PEG hydrogels.

## 2. Methods

### 2.1. Hydrogel preparation

Hydrogels of distinct stiffness were made from maleimide functionalised PEG star macromeres (PEG-MAL) varying in molecular weight and functionality. All polymers were purchased from JenKem Technology USA. Four-armed PEG-MAL (20 kDa) was dissolved in citrate phosphate buffer with a final buffer concentration of 100 mM within the polymer mix (pH 3), whereas 4-armed PEG-MAL (10 kDa) and 8-arm PEG-MAL (20 kDa) were dissolved in citrate phosphate buffer at pH 2.5. Prior to gel formation, macromeres were either functionalized with Cyclo(RGD(dF)C) produced by AnaSpec or linear RGD peptide (Ac-GCGYGRGDSPG-$NH_2$) produced by Pepmic, at final concentrations of 0.05, 0.5, 1.5 or 2.5 mM. Four-arm (20 kDa) and 8-arm (20 kDa) gels without any RGD peptides were prepared as controls. A linking peptide (Ac-GCRDVPMSMRGGDRCG-NH2) synthesized by Pepmic was used to end-link the macromeres into gels. In brief, 20 μL of RGD-functionalised PEG-MAL-end-linker mixtures were pipetted between two hydrophobic glass slides separated by a 1 mm spacer and allowed to react at 37 °C for 20 min. All gels were swollen for 1 h in 1 mL of mesenchymal stem cell growth media (MSCGM, Lonza) at 37 °C in 24-well plates. After swelling, excess medium was discarded in preparation for cell seeding. Three gels were prepared for each RGD concentration, in preparation for cell seeding. Four-arm PEG-MAL (20 kDa) hydrogels are referred to as 'soft' hydrogels, whereas 8-arm PEG-MAL (20 kDa) hydrogels are referred to as 'stiff' hydrogels in the results and discussion of this paper.

### 2.2. Swelling ratio measurements

The swelling ratio was defined as the ratio of swollen ($V_s$) to non-swollen ($V_r$) volume. Volumes were determined using an analytical scale equipped with a buoyancy kit. Hydrogels were weighed first in air and then in phosphate buffered saline (PBS) immediately after curing. Swollen gels were weighed again at 1.5 h and 48 h after swelling in PBS. Triplicates were prepared for each group and experiments were conducted twice independently (n = 6). All measurements were performed at room temperature.

### 2.3. AFM nanoindentation

Gel stiffness was determined on micro-scale via nanoindentation using a JPK Nanowizard 4 atomic force microscope (AFM). Indentation was performed with colloidal probes with 2 μm $SiO_2$ spheres attached to tip-less silicon nitride cantilevers (PNP-TR-TL, NanoWorld AG), which were purchased from sQube. Each cantilever was calibrated in a two-step procedure in PBS. First, the optical lever sensitivity was defined by deflecting the cantilever against a hard glass surface, then, the cantilever spring constant was determined using the thermal noise method. Spring constants were typically found around 0.06 N/m.

For nanoindentation experiments, hydrogel disks were prepared as described above and swollen to equilibrium in PBS at 37 °C. The disks were placed on glass slides and covered with a PBS droplet. Three force maps of 8 × 8 indentations on an area of 50 × 50 $\mu m^2$ were recorded on random spots. A minimum of three gels from independent experiments were tested per group. Maximal indentation force was controlled to 2 nN. E-modulus was determined from the force-indentation curves using the Hertz model. All samples were assumed to behave like ideal gels (Poisson's ratio of 0.5).

### 2.4. Cell culture and seeding

Experiments were performed using hMSCs purchased from Lonza (lot #0000451491, tissue acquisition #28386). Cells were cultured (passage ≤ 5) at 37 °C in a 5% $CO_2$ incubator in Lonza's Poetics Mesenchymal Stem Cell Basal Medium (catalog no. PT-3238) supplemented with Poetics MSCGM™ hMSC SingleQuot Kit (catalog no. PT-4105) to maintain cells in an undifferentiated state. Once cells were 70% confluent, they were trypsinized for seeding onto glass coverslips and onto hydrogels. A seeding density of 4700 cells/$cm^2$ of hydrogel surface area (3000 per gel in a 30 μL droplet) was used. The surface area covered by the droplets was assessed using contact angle measurements to ensure uniform initial cell seeding density across the gel and glass surfaces. Cells were allowed to attach for 1.5 h before 1 mL of MSCGM was added to each well. hMSCs were cultured on hydrogels and glass substrates for 48 h prior to fixation. Two independent experiments were conducted, each containing triplicates and data for triplicates from each group was pooled.

### 2.5. Immunolabeling and confocal microscopy

hMSCs were fixed by first adding a 4% paraformaldehyde (PFA) solution directly to the medium (1:1 ratio) for 10 min, before all liquid was discarded. Subsequently, 4% PFA was added to the wells for 20 min. The PFA was discarded and cells were washed with Dulbecco's Phosphate-buffered saline (DPBS) three times. hMSCs were then permeabilized using 0.1% Triton X-100 for 10 min, followed by a DPBS rinse. All samples were blocked with 5% bovine serum albumin (BSA) in DPBS blocking buffer for 2 h at room temperature. Blocking buffer was discarded and cells were rinsed three times with DPBS. Mouse anti-human vinculin primary antibody (ABfinity, Thermo Fischer) was diluted 1:100 in 1% DPBS-BSA solution. Cells were incubated overnight

at 4 °C with primary antibodies. The primary antibodies were discarded, followed by three DPBS rinses, before the secondary antibodies and phalloidin were added to the wells. Phalloidin and all secondary antibodies (Thermo Fischer Scientific) were diluted in 1% BSA-DPBS solution to obtain working dilutions of 1:400. Alexa Fluor® 647 Phalloidin was used for fluorescent labelling of actin and cytoskeleton. Goat anti-mouse IgG secondary antibody Alexa Fluor® 488 was used to fluorescently label anti-vinculin primary antibodies. DAPI was used at a 1:1000 working dilution to stain the nuclei. Gels and glass cover slips were viewed with a 20×/0.40 HCX PL APO CS objective lens on a Leica SP8 confocal microscope using 638 nm excitation and 643–710 nm emission filters for phalloidin and with 488 nm excitation and 493–560 nm emission filters for vinculin. Two additional images were taken per replicate with the same lens and an additional 2× electronic zoom to obtain images for focal adhesion analysis. Z-stacks were generated where cells in the same field of view did not appear on the same plane due to sample topography.

### 2.6. Data extraction and image analysis

For all data obtained via confocal imaging, 60 fields of view (F.O.V) were analysed per gel group (n = 60). However, these 60 F.O.Vs were obtained from two independent experiments, each consisting of triplicates, from which 10 images were taken per replicate. Maximal intensity projections were generated for regions of interest that were imaged as z-stacks. Confocal microscopy images were imported into FIJI Software (ImageJ, NIH) for automated cell area analysis using a custom macro. Briefly, the macro consisted of removal of outlier pixels, median blur and rolling ball background subtraction, followed by merging of the nuclear and vinculin channels to generate images for whole cell area measurements. Otsu intensity thresholding produced a binary image to allow counting and measuring of all objects above a defined size threshold. Data was expressed as the mean proportion of field of view area covered by cells. Separately, the DAPI channel images were imported into Cell Profiler 2.2.0 for nuclei counting and nearest neighbour analysis. The pipeline comprised of image smoothening with a median blur, background subtraction and rescaling of the image intensities, followed by automatic Otsu thresholding to identify the nuclei and allow assessment of the nearest neighbour distance. We employed a nearest neighbour analysis methodology from Eidet et al. (2014) to analyse the spatial arrangement of cells in relation to their neighbours. This was first described by Clark and Evans to measure spatial relationships in populations (Clark and Evans, 1954). This enabled the assessment of the cell distribution within each field of view with parameter R, which can vary from 0 (clustered) to 2.15 (hexagonal distribution), with R = 1 indicating a random distribution. A sample of this methodology is provided in the Supplementary information of this manuscript (Fig. S1).

### 2.7. Statistical analysis

Statistical analysis was conducted using the software Sigma Plot 13.0 (Systat Software Inc.) One-way ANOVA was performed along with the Dunn's method on all data sets to test for statistical significance. The only exception to this was for swelling ratio data, where *t*-tests were performed to determine significant differences. Statistic tests were performed where differences between groups show $p < 0.05$. Significant statistical differences are represented in figures by a single asterisk symbol. The spread of data points for all box plots are represented by a central solid line (median), box limits (25th and 75th percentiles) and whiskers denoting upper (90th) and lower (10th) percentiles.

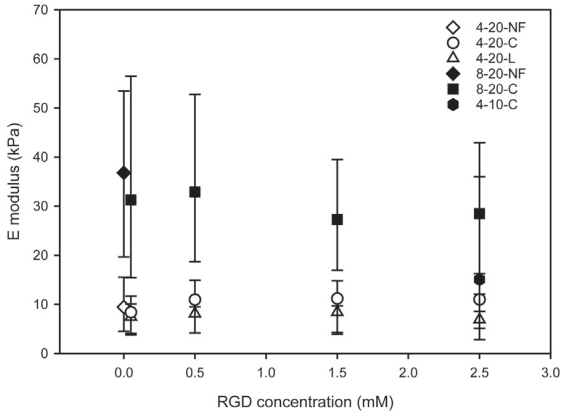


**Fig. 1.** Differences in stiffness between 4-arm (20 kDa), 8-arm (20 kDa) and 4-arm (10 kDa) hydrogels (n ≥ 3). Increased RGD tethering did not influence the overall stiffness of the hydrogels. However, 8-arm gels were significantly stiffer compared to the 4-arm gels ($p < 0.05$). Median with 90th and 10th percentiles. C: cyclic RGD, L: linear RGD, NF: non- functionalised.

## 3. Results

### 3.1. Mechanical properties of the hydrogel substrates

Stiffness of 4-arm (20 kDa) and 8-arm (20 kDa) PEG hydrogels as measured by AFM nanoindentation is shown in Fig. 1. As a control, we also performed nanoindentation on gels without RGD functionalisation (NF gels) as well as 4-arm gels of lower molecular weight (10 kDa). A prominent difference in stiffness can be observed between 4-arm and 8-arm gels. 4-arm "soft" hydrogels show *E* moduli ranging from 7.4 to 11.2 kPa, whereas 8-arm "stiff" hydrogels feature *E* moduli ranging from 27.3 to 36.8 kPa. However, we observe no statistically significant differences in stiffness between gels with varying RGD concentrations for neither the 4-arm nor the 8-arm gels. A noticeably wide spread of data points is seen for all gels, indicative of variations in stiffness of gel batches produced from different reaction mixtures.

In addition to assessing the stiffness of hydrogels, the degree of swelling was determined as a measure of gel topology. Soft hydrogels show a significantly larger increase in volume 48 h after swelling compared to 1.5 h after swelling (Fig. 2). However, 8-arm gels did not swell more at 48 h versus 1.5 h. The data also shows that increased RGD tethering does not result in significant differences in swelling ratios for both soft and stiff gel groups, which is consistent with the AFM nanoindentation results (Fig. 1). 4-arm (10 kDa) gels display intermediate gel stiffness, with mean swelling ratios higher than those of stiff gels but lower than those of soft gels at both time points.

### 3.2. Attachment and spatial organisation of hMSCs

Fig. 3 displays the median number of cells attached to the hydrogels per field of view. On soft RGD-functionalised hydrogels, fewer than 40 cells attached per field of view. Additionally, we observe increased hMSC attachment on soft hydrogels with an increase in RGD concentration. However, there is no significant difference in cell attachment between gels with linear versus cyclic RGDs at each concentration tested. Interestingly, there is a significant increase in cell attachment for stiff hydrogels beyond 0.5 mM of RGD, whereas stiff gels functionalised with RGD concentrations as low as 0.05 mM support cell adhesion in a similar manner as seen for the soft gels. NF gels lack RGD functionality and show minimal cell attachment overall, irrespective of differences in stiffness between the 4-arm and 8-arm counterparts. Interestingly, 4-arm (10 kDa) gels functionalised with 2.5 mM of cyclic RGD, which feature a stiffness between the soft and stiff gels ($E \approx 15$ kPa), exhibit significantly fewer number of attached cells compared to all 8-arm gels

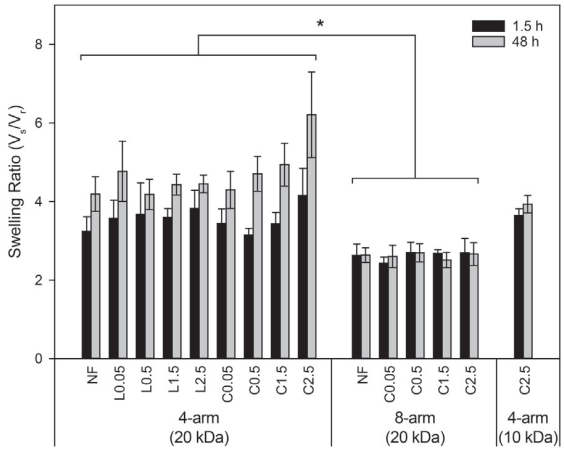


**Fig. 2.** Average swelling ratios ( ± SD) of PEG-MAL hydrogels swollen for 1.5 h and 48 h (n = 6). Increased RGD tethering does not have a significant effect on swelling for any gel type. Furthermore, after 1.5 h no significant differences in swelling can be observed between stiff and soft gels. Statistically, 4-arm gels exhibit increased swelling at 48 h in comparison to 8-arm counterparts (*$p < 0.05$). 8-arm gels appear to reach maximal swelling at 1.5 h and do not swell further at 48 h. C: cyclic RGD, L: linear RGD, NF: non- functionalised.

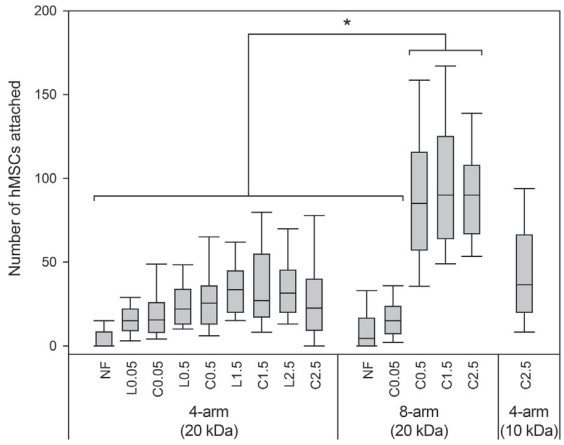


**Fig. 3.** Number of hMSCs observed per field of view (F.O.V) via confocal microscopy (n = 60). A significantly higher cell attachment number was evident for 8-arm gels with RGD concentration of 0.5 mM or more (*$p < 0.05$). Stiff gels with 0.05 mM RGD show cell attachment numbers similar to those observed on soft gels. C: cyclic RGD, L: linear RGD, NF: non- functionalised.

($p < 0.05$). Variation between independent experiments have been accounted for and results from individual experiments are shown in Supplementary information Fig. 2.

Fig. 4 shows qualitative differences in hMSC organisation based on the substrate stiffness and availability of RGD motifs. These images indicate spreading on gels of sufficient stiffness in conjunction with an adequate concentration of RGD motifs (≥ 0.5 mM). On all soft hydrogels, cells cluster and organise themselves in close proximity to each other, irrespective of concentration and type of RGD. Fig. 4 also shows that cells do not spread on 4-arm (10 kDa) gels, despite an ample amount of RGD and a higher stiffness compared to 4-arm (20 kDa) gels. Furthermore, on soft 4-arm gels we generally observe an increased cluster size with increased concentration of RGD for both linear and cyclic RGD.

In order to quantify the manner in which cells organise themselves, we measured the proximity of each cell in relation to the cells around it. This results in an R-value indicative of each hMSC's association with its neighbours (Fig. 5A). When assessing spatial organisation of hMSCs, we see higher R-values for stiff hydrogels. R-values were distinctively high in stiff gels with an RGD concentration of up to 0.5 mM, indicating a more random cell distribution compared to cells seeded on the soft gels, which exhibit lower R-values denoting clustering. Overall, stiff gels feature significantly higher R-values with increased RGD concentrations, indicative of greater spreading ($p < 0.05$). Finally, though few hMSCs attached to NF gels, R-values are less than 0.32, indicating clustering which can also be seen qualitatively in Fig. 4.

An additional parameter assessed is the surface area covered by attached cells. This enables quantifying the extent of spreading while also providing an overview of the degree of clustering on softer hydrogels. hMSCs attached to stiff hydrogels with more than 0.5 mM RGD cover approximately 40% of the surface area of the gel. This is a significantly higher coverage compared to groups where cells cluster (Fig. 5B). Groups that exhibit clustering show minimal coverage on the surface of the gel, implying that clusters are relatively small.

To further investigate cellular interactions with the PEG hydrogels, cells were immunolabeled with an anti-vinculin primary antibody (Fig. 6). For all gel types, irrespective of stiffness or RGD concentration, no peripheral recruitment of vinculin was observed. Vinculin appears across the cytoplasm with no indication of mature focal adhesion formation. However, cells seeded on glass cover slips showed distinct peripheral localisation of vinculin as part of mature focal adhesions complexes.

## 4. Discussion

Mesenchymal stem cells are an adherent-dependent cell type, implying that physical and biochemical interactions with their microenvironment can influence cell survival, growth, migration and differentiation (Dominici et al., 2006; Park et al., 2012). Salinas and Anseth have previously tested MSC affinity for different RGD peptide sequences and their contextual presentation in PEG hydrogels (Salinas and Anseth, 2008). However, the combined influence of RGD concentration and stiffness on the spatial organisation of hMSCs on hydrogel substrates has not yet been investigated.

We first determined whether increased RGD tethering affects hydrogel stiffness. Since maleimide groups functionalised with RGD peptides are no longer available for end-linking, one might expect a decreased number of elastically effective chains in the network and thus a reduced stiffness. However, we do not see any statistically significant differences within either of the gel groups when varying RGD concentrations. This means that despite the different numbers of maleimide groups available for end-linking, a comparable number of end-links is formed. This observation can be explained by the fact that the architecture of the used hydrogels is non-ideal in the sense that just a fraction of the available functional groups ultimately forms elastically effective links. Thus, the number of ultimately formed end-links can well be very similar, irrespective of a fraction of the maleimide groups being consumed for tethering RGD motifs. However, the large variation of measured stiffness values makes it difficult to draw any definite conclusions. Though we do not see changes in stiffness upon RGD functionalization, it is important to acknowledge the possibilities of alterations in network architecture, such as entanglements and changes in hydrophobicity that may occur. However, analysis of this is beyond the scope of this study. Zustiak et al. (2010) successfully tested different peptides and studied the effects on a variety of gel parameters. However, no previous studies have investigated the effects of different RGD isoforms on substrate stiffness.

Unsurprisingly, we observed substantial differences in stiffness between the 4-arm and 8-arm gel groups. It is also worth noting the large spread in measured stiffness for each of the groups. This represents a substantial variation when producing the gels independently. However, replicates for any given gel group produced from the same reaction mix did not exhibit such large variations. In contrast, we see consistent results in cell attachment and organisation for independent batches of

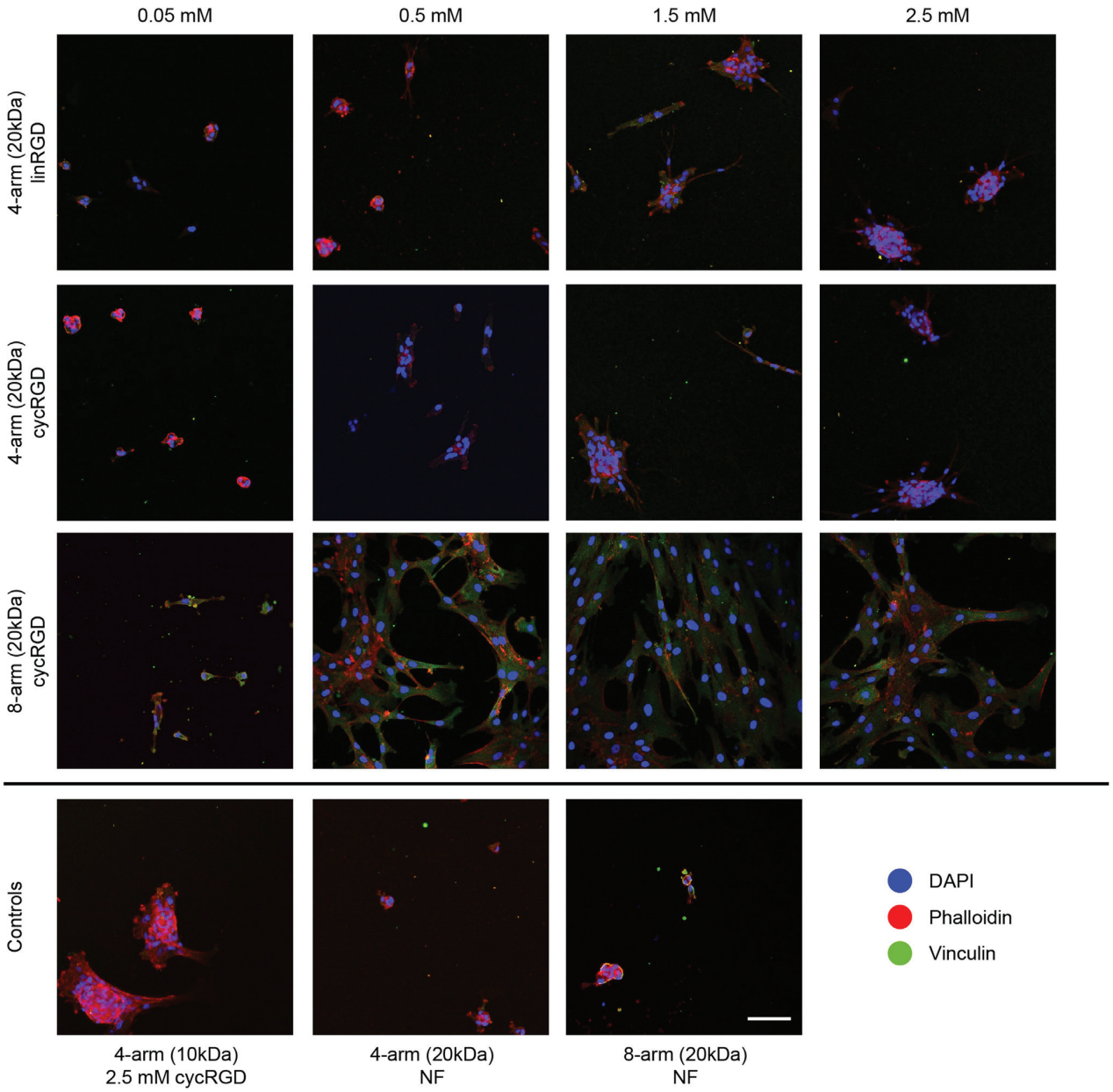


**Fig. 4.** Confocal images of hMSCs immunolabeled with DAPI (nucleus), phalloidin (actin) and vinculin (focal adhesions) (scale bar: 100 μm). hMSCs organised themselves as clusters on soft substrates, irrespective of RGD conformation or concentration. Furthermore, a shift in hMSC organisation is evident on stiff hydrogels with 0.5 mM of cycRGD or more. cyc: cyclic RGD, lin: linear RGD, NF: non-functionalised.

the gel. To our best knowledge, there have been two previous studies on changes in substrate compliance with increased ligand tethering for PEG hydrogels (Missirlis and Spatz, 2014; Zustiak et al., 2010). Zustiak and colleagues tested the effects of 0.1, 1.0 and 3.0 mM RGD on the swelling ratios and shear moduli of PEG gels. They found that swelling ratios were increased by 12% only in gels functionalised with 3.0 mM of RGD compared to hydrogels with no RGD, and shear moduli were not altered for concentrations below 3.0 mM (Zustiak et al., 2010). In a different study, Missirlis and Spatz tested gels of similar stiffness as in our study and report that increased RGD concentrations only resulted in a slight increase in $E$ modulus for 'medium' ($E \approx 33.2$ kPa) and 'stiff' ($E \approx 65.4$ kPa) gels (Missirlis and Spatz, 2014). Considering we here incorporate a maximum of 2.5 mM RGD, our results are in good accordance with those reported. Contradictory to observations from Missirlis and Spatz, we report a significant increase in cell attachment with increased substrate stiffness. This effect is enhanced upon increasing RGD concentrations on stiff substrates (Fig. 3). Even though we did not see major effects on substrate stiffness with increased RGD tethering, cells do sense a combination of these factors and exhibit organisational differences.

hMSCs on soft PEG gels cluster rather than spread, irrespective of RGD peptide concentrations or isoforms (Fig. 4). It is likely that a variety of factors contribute to this observation. For instance, cells require sufficient traction to enable spreading which may be inadequate on the soft gels (Fang and Lai, 2016). Additionally, due to significantly greater swelling for soft gels (Fig. 2), RGDs are spaced further apart than those on the stiff gels, despite identical nominal concentrations. Assuming that peptides within 5 nm from the surface are available for cell interaction, we found 30–1690 peptides/μm$^2$ for soft gels and 60–2830 peptides/μm$^2$ for stiff gels based on the nominal RGD

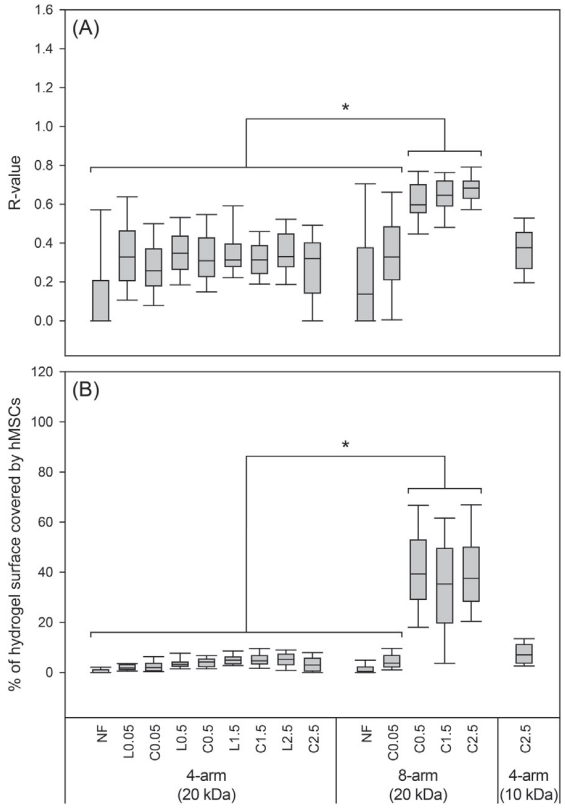


**Fig. 5.** (A) R-values classifying spatial organisation of hMSCs across the field of view (n = 60). On soft gels, hMSCs exhibit significantly higher clustering irrespective of RGD concentrations with R-values ≤ 0.3 ($*p < 0.05$). NF gels also exhibit clustering with even lower R-values. Stiff gels exhibit decreased clustering as RGD concentrations increase, with an evident shift in cellular organisation between 0.05 and 0.5 mM. (B) Surface area of the gel covered by hMSCs. Differences in cell organisation leads to distinct differences in cell coverage. Cells attached on stiff substrates functionalized with sufficient RGD tend to spread, resulting in higher surface coverage (≈ 40%). However, on soft gels clustered cells cover a smaller surface area (< 8%). C: cyclic RGD, L: linear RGD, NF: non- functionalised.

concentrations ranging from 0.05 to 2.5 mM. Previous studies controlled RGD presentation and found that cell spreading is highly sensitive to slight changes in ligand spacing (Arnold et al., 2004; Wilson et al., 2012; Wolfenson et al., 2014). They identified a critical spacing of 60–70 nm to be required for stable integrin mediated adhesion. Elsewhere, Frith et al. studied the influence of lateral spacing of RGD on hMSCs and found that cells were less spread for ligand spacing greater than 62 nm (Frith et al., 2012). Based on a theoretical estimate, soft hydrogels used in our study with RGD concentrations of 0.5 mM or higher are below this threshold, indicating that RGD concentration alone does not govern the cell morphology.

Missirlis and Spatz observed similar rounded cell morphologies when seeding REF52 cells on hydrogels functionalized with up to 0.5 mM RGD (Missirlis and Spatz, 2014). However, in contrast to our findings, these cells were not clustered. Two primary reasons may contribute to the cluster morphologies of hMSCs on soft gels. First, the lack of traction prevents the cells from spreading and thus limiting the movement of cells on the surface. Second, the lack of sufficient available anchoring points may cause the cells to cluster. As a result, cells in close proximity with each other appear to attach to their neighbours in order to survive and form clusters. For stiffer gels providing sufficient traction, 0.05 mM RGD is inadequate to prevent clustering. However, stiff gels with RGD concentrations of 0.5 mM or higher support hMSC spreading. As a result, a combination of sufficient stiffness to provide traction and adequate RGD motifs seems to be required to enable cell adhesion and prevent clustering.

Although the presence or absence of ligands plays an independent role, previous studies have shown that cell shape and spreading are greatly regulated by substrate stiffness (Han et al., 2012). Engler et al. demonstrated that cells on soft substrates are insensitive to adhesion ligand density (Engler et al., 2004). We observed a similar scenario here, where the presence of RGD alone does not enable cells to spread if the substrate is not sufficiently stiff. The cytoskeleton plays a central role in cell spreading, and as a response to mechanical stimuli, proteins assemble at the periphery of the cytoskeleton to form focal complexes (Engler et al., 2004). Confocal images taken of hMSCs seeded on soft gels in Fig. 6 showed no punctuations of large, mature focal adhesions akin to those observed on glass controls. Instead, we observe dot-like expression of vinculin throughout the cell body of cells seeded on hydrogels. Intriguingly, Fig. 6 also shows hMSCs spread on stiff hydrogels, but there is no indication of vinculin at the cell membrane to represent mature focal adhesions. One possible reason leading to the absence of mature focal adhesions may be attributed to the lack of mechanical forces to drive the recruitment of vinculin associated with mechanosensing at focal complexes. Other studies also suggest vinculin recruitment to focal adhesions in cells on substrates with Young's moduli of at least 200 kPa (Kocgozlu et al., 2010). This would explain the lack of mature focal adhesions on soft hydrogels. However, hMSCs did not form mature focal adhesions on stiff hydrogels either. This is likely due to the insufficient binding of integrin to the substrate, since vinculin is known to play a vital role in physically linking integrins to the cytoskeleton (Berrier and Yamada, 2007).

Cavalcanti-Adam and colleagues have previously observed a lack of focal adhesions on substrates with RGD spaced 108 nm or further apart. However, integrin-based adhesion may still occur at this point, leading to what has been referred to as cryptic adhesions forming under protruding lamellae (Cavalcanti-Adam et al., 2007). In the study conducted by Missirlis and Spatz, REF52 cells were seeded on to PEG hydrogels functionalised with 0.1–2.0 mM RGD (Missirlis and Spatz, 2014). They observed localisation of vinculin to the periphery on gels with RGD concentrations of at least 0.25 mM. However, we observed neither focal adhesion formation nor vinculin recruitment at the cell periphery, irrespective of RGD presentation. The PEG gels used in their study feature a similar stiffness as the soft and stiff gels tested in our study. However, since the cells they used are of rat origin, there may be interspecies differences to consider in the regulation of vinculin when compared to hMSCs. However, we observed vinculin throughout the cytoplasm. One possible explanation is that we are observing nascent focal adhesions, since evidence suggest that they occur independent of substrate rigidity (Changede et al., 2015). However, definite verification of nascent focal adhesions is complicated and previous studies suggested localisation at the lamellipodium (Choi et al., 2008). The lack of mature focal adhesions has further been attributed to increased cell motility (Rodriguez Fernandez et al., 1992), contributing to the observed formation of cell clusters.

Previous studies typically encapsulate cells into PEG hydrogels in order to study how cells interact with their 3D environment (Pfaff et al., 1994; Wang et al., 2013; Yang et al., 2005). However, few studies have seeded cells onto the surface of hydrogels (Huebsch et al., 2010). In clinical situations, access and isolation of patient's stem cells can be expensive and limited. As a result, it is important to recognize alternative approaches that are capable of inducing local host stem cell migration towards the site of damage using injectable, cell-responsive, biodegradable scaffolds. There has been increasing evidence that mesenchymal stem cells have immense migratory potential in various regenerative scenarios, both in vitro and in vivo (Cornelissen et al., 2015). In order to orchestrate the function of MSCs, it is necessary to understand how these cells attach, colonise and organise themselves on compliant materials. Therefore, the minimum requirements for efficient adhesion and the optimal mechanical stiffness need to be determined.

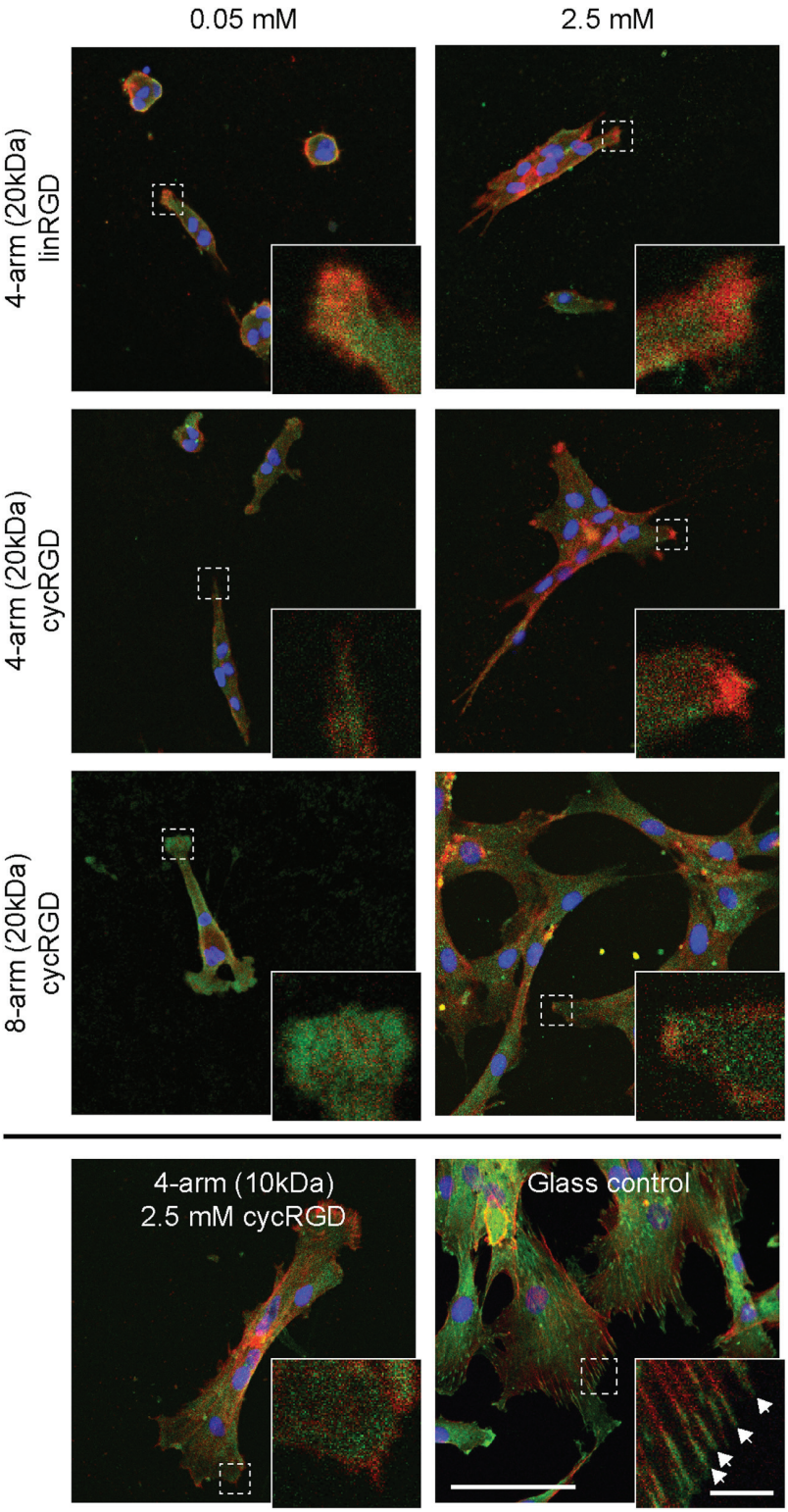


**Fig. 6.** hMSCs immunolabeled with DAPI (blue), phalloidin (red) anti-vinculin antibodies (green) (scale bar: 100 μm). Inlet images highlight cell peripheries (inlet scale bar: 10 μm). No recruitment of vinculin was observed as part of mature focal adhesion formation for all gel types. Instead, vinculin was observed across the cytoplasm of cells, without particular localisation at the periphery. Cells seeded on glass coverslips clearly exhibit mature focal adhesion formation with vinculin distinctively localised to complexes at the periphery of the cell body (white arrows). cyc: cyclic RGD, lin: linear RGD. (For interpretation of the references to color in this figure legend, the reader is referred to the web version of this article.)

Our study, however, shows that these processes are multifaceted and do not solely depend on substrate stiffness or RGD presentation independently. This fundamental understanding constitutes a prerequisite for a future class of acellular scaffolds.

## 5. Conclusions

This study extends the current knowledge for cell-based applications that utilize PEG. We provide a basis for selecting specific stiffness and ligand presentation that contribute to hMSCs attachment and colonisation on PEG hydrogels. In order to attach large numbers of hMSCs in a

spread manner, both substrate stiffness and attachment ligand concentrations need to be above a certain threshold. Cells seeded on soft hydrogels exhibited significantly fewer attached cells, with the formation of cell clusters, irrespective of RGD concentrations. In contrast, hMSCs attached in large numbers and spread on stiff hydrogels with RGD concentrations of 0.5 mM or higher, suggesting that cell attachment and spreading are both multifaceted phenomena. We observed that increased RGD tethering has no significant effect on the stiffness of both soft and stiff hydrogels. Additionally, we found no differences in the number of hMSCs attaching to gels functionalised with either linear or cyclic RGD.

## Acknowledgements

The authors are grateful to Dr. Nick J. Walters for the constructive discussions and his critical review of this manuscript. This research did not receive any specific grant from funding agencies in the public, commercial, or not-for-profit sectors.

## Appendix A. Supplementary information

Supplementary data associated with this article can be found in the online version at http://dx.doi.org/10.1016/j.jmbbm.2018.04.025.

## References

Anderson, S.B., Lin, C.C., Kuntzler, D.V., Anseth, K.S., 2011. The performance of human mesenchymal stem cells encapsulated in cell-degradable polymer-peptide hydrogels. Biomaterials 32, 3564–3574.
Arnold, M., Cavalcanti-Adam, E.A., Glass, R., Blümmel, J., Eck, W., Kantlehner, M., Kessler, H., Spatz, J.P., 2004. Activation of integrin function by nanopatterned adhesive interfaces. ChemPhysChem 5, 383–388.
Bae, M.-S., Lee, K.Y., Park, Y.J., Mooney, D.J., 2007. RGD island spacing controls phenotype of primary human fibroblasts adhered to ligand-organized hydrogels. Macromol. Res. 15, 469–472.
Bellis, S.L., 2011. Advantages of RGD peptides for directing cell association with biomaterials. Biomaterials 32, 4205–4210.
Berrier, A.L., Yamada, K.M., 2007. Cell–matrix adhesion. J. Cell Physiol. 213, 565–573.
Cavalcanti-Adam, E.A., Volberg, T., Micoulet, A., Kessler, H., Geiger, B., Spatz, J.P., 2007. Cell spreading and focal adhesion dynamics are regulated by spacing of integrin ligands. Biophys. J. 92, 2964–2974.
Changede, R., Xu, X., Margadant, F., Sheetz, Michael, P., 2015. Nascent integrin adhesions form on all matrix rigidities after integrin activation. Dev. Cell 35, 614–621.
Chicurel, M.E., Chen, C.S., Ingber, D.E., 1998. Cellular control lies in the balance of forces. Curr. Opin. Cell Biol. 10, 232–239.
Choi, C.K., Vicente-Manzanares, M., Zareno, J., Whitmore, L.A., Mogilner, A., Horwitz, A.R., 2008. Actin and α-actinin orchestrate the assembly and maturation of nascent adhesions in a myosin II motor-independent manner. Nat. Cell Biol. 10, 1039.
Clark, P.J., Evans, F.C., 1954. Distance to nearest neighbor as a measure of spatial relationships in populations. Ecology 35, 445–453.
Cornelissen, A.S., Maijenburg, M.W., Nolte, M.A., Voermans, C., 2015. Organ-specific migration of mesenchymal stromal cells: Who, when, where and why? Immunol. Lett 168, 159–169.
Deeg, J.A., Louban, I., Aydin, D., Selhuber-Unkel, C., Kessler, H., Spatz, J.P., 2011. Impact of local versus global ligand density on cellular adhesion. Nano Lett. 11, 1469–1476.
Dominici, M., Le Blanc, K., Mueller, I., Slaper-Cortenbach, I., Marini, F., Krause, D., Deans, R., Keating, A., Prockop, D., Horwitz, E., 2006. Minimal criteria for defining multipotent mesenchymal stromal cells. The International Society for Cellular Therapy position statement. Cytotherapy 8, 315–317.
Eidet, J.R., Pasovic, L., Maria, R., Jackson, C.J., Utheim, T.P., 2014. Objective assessment of changes in nuclear morphology and cell distribution following induction of apoptosis. Diagn. Pathol. 9 (92-92).
El-Sherbiny, I.M., Yacoub, M.H., 2013. Hydrogel scaffolds for tissue engineering: progress and challenges. Glob. Cardiol. Sci. Pract. 2013, 316–342.
Engler, A., Bacakova, L., Newman, C., Hategan, A., Griffin, M., Discher, D., 2004. Substrate compliance versus ligand density in cell on gel responses. Biophys. J. 86, 617–628.
Engler, A.J., Sen, S., Sweeney, H.L., Discher, D.E., 2006. Matrix elasticity directs stem cell lineage specification. Cell 126, 677–689.
Fang, Y., Lai, K.W.C., 2016. Modeling the mechanics of cells in the cell-spreading process driven by traction forces. Phys. Rev. E 93, 042404.
Frith, J.E., Mills, R.J., Cooper-White, J.J., 2012. Lateral spacing of adhesion peptides influences human mesenchymal stem cell behaviour. J. Cell Sci. 125, 317–327.
Fusco, S., Panzetta, V., Embrione, V., Netti, P.A., 2015. Crosstalk between focal adhesions and material mechanical properties governs cell mechanics and functions. Acta Biomater. 23, 63–71.
Han, Sangyoon J., Bielawski, Kevin S., Ting, Lucas H., Rodriguez, Marita L., Sniadecki, Nathan J., 2012. Decoupling substrate stiffness, spread area, and micropost density: a close spatial relationship between traction forces and focal adhesions. Biophys. J. 103, 640–648.
Haubner, R., Gratias, R., Diefenbach, B., Goodman, S.L., Jonczyk, A., Kessler, H., 1996. Structural and functional aspects of RGD-containing cyclic pentapeptides as highly potent and selective integrin $\alpha_V\beta_3$ antagonists. J. Am. Chem. Soc. 118, 7461–7472.
Hern, D.L., Hubbell, J.A., 1998. Incorporation of adhesion peptides into nonadhesive hydrogels useful for tissue resurfacing. J. Biomed. Mater. Res. 39, 266–276.
Herrick, W.G., Nguyen, T.V., Sleiman, M., McRae, S., Emrick, T.S., Peyton, S.R., 2013. PEG-phosphorylcholine hydrogels as tunable and versatile platforms for mechanobiology. Biomacromolecules 14, 2294–2304.
Hersel, U., Dahmen, C., Kessler, H., 2003. RGD modified polymers: biomaterials for stimulated cell adhesion and beyond. Biomaterials 24, 4385–4415.
Hsiong, S.X., Carampin, P., Kong, H.J., Lee, K.Y., Mooney, D.J., 2008. Differentiation stage alters matrix control of stem cells. J. Biomed. Mater. Res. A 85, 145–156.
Huebsch, N., Arany, P.R., Mao, A.S., Shvartsman, D., Ali, O.A., Bencherif, S.A., Rivera-Feliciano, J., Mooney, D.J., 2010. Harnessing traction-mediated manipulation of the cell/matrix interface to control stem-cell fate. Nat. Mater. 9, 518–526.
Kantlehner, M., Schaffner, P., Finsinger, D., Meyer, J., Jonczyk, A., Diefenbach, B., Nies, B., Holzemann, G., Goodman, S.L., Kessler, H., 2000. Surface coating with cyclic RGD peptides stimulates osteoblast adhesion and proliferation as well as bone formation. ChemBioChem 1, 107–114.
Kilian, K.A., Mrksich, M., 2012. Directing stem cell fate by controlling the affinity and density of ligand–receptor interactions at the biomaterials interface. Angew. Chem. Int. Ed. 51, 4891–4895.
Kim, D.-H., Provenzano, P.P., Smith, C.L., Levchenko, A., 2012. Matrix nanotopography as a regulator of cell function. J. Cell Biol. 197, 351.
Kocgozlu, L., Lavalle, P., Koenig, G., Senger, B., Haikel, Y., Schaaf, P., Voegel, J.-C., Tenenbaum, H., Vautier, D., 2010. Selective and uncoupled role of substrate elasticity in the regulation of replication and transcription in epithelial cells. J. Cell Sci. 123, 29–39.
Kyburz, K.A., Anseth, K.S., 2013. Three-dimensional hMSC motility within peptide-functionalized PEG-based hydrogels of varying adhesivity and crosslinking density. Acta Biomater. 9, 6381–6392.
Li, L., Eyckmans, J., Chen, C.S., 2017. Designer biomaterials for mechanobiology. Nat. Mater. 16, 1164.
Mathieu, P.S., Loboa, E.G., 2012. Cytoskeletal and focal adhesion influences on mesenchymal stem cell shape, mechanical properties, and differentiation down osteogenic, adipogenic, and chondrogenic pathways. Tissue Eng. B 18, 436–444.
Missirlis, D., Spatz, J.P., 2014. Combined effects of PEG hydrogel elasticity and cell-adhesive coating on fibroblast adhesion and persistent migration. Biomacromolecules 15, 195–205.
Nuttelman, C.R., Tripodi, M.C., Anseth, K.S., 2004. In vitro osteogenic differentiation of human mesenchymal stem cells photoencapsulated in PEG hydrogels. J. Biomed. Mater. Res. A 68, 773–782.
Park, J., Kim, P., Helen, W., Engler, A.J., Levchenko, A., Kim, D.-H., 2012. Control of stem cell fate and function by engineering physical microenvironments. Integr. Biol. 4, 1008–1018.
Pfaff, M., Tangemann, K., Muller, B., Gurrath, M., Muller, G., Kessler, H., Timpl, R., Engel, J., 1994. Selective recognition of cyclic RGD peptides of NMR defined conformation by alpha IIb beta 3, alpha V beta 3, and alpha 5 beta 1 integrins. J. Biol. Chem. 269, 20233–20238.
Rodda, A.E., Meagher, L., Nisbet, D.R., Forsythe, J.S., 2014. Specific control of cell–material interactions: targeting cell receptors using ligand-functionalized polymer substrates. Prog. Polym. Sci. 39, 1312–1347.
Rodriguez Fernandez, J.L., Geiger, B., Salomon, D., Sabanay, I., Zoller, M., Ben-Ze'ev, A., 1992. Suppression of tumorigenicity in transformed cells after transfection with vinculin cDNA. J. Cell Biol. 119, 427–438.
Salinas, C.N., Anseth, K.S., 2008. The influence of the RGD peptide motif and its contextual presentation in PEG gels on human mesenchymal stem cell viability. J. Tissue Eng. Regen. Med. 2, 296.
Schwarz, U.S., Bischofs, I.B., 2005. Physical determinants of cell organization in soft media. Med. Eng. Phys. 27, 763–772.
Shu, X.Z., Ghosh, K., Liu, Y., Palumbo, F.S., Luo, Y., Clark, R.A., Prestwich, G.D., 2004. Attachment and spreading of fibroblasts on an RGD peptide-modified injectable hyaluronan hydrogel. J. Biomed. Mater. Res. A 68, 365–375.
Verrier, S., Pallu, S., Bareille, R., Jonczyk, A., Meyer, J., Dard, M., Amédée, J., 2002. Function of linear and cyclic RGD-containing peptides in osteoprogenitor cells adhesion process. Biomaterials 23, 585–596.
Wang, X., Yan, C., Ye, K., He, Y., Li, Z., Ding, J., 2013. Effect of RGD nanospacing on differentiation of stem cells. Biomaterials 34, 2865–2874.
Wen, J.H., Vincent, L.G., Fuhrmann, A., Choi, Y.S., Hribar, K.C., Taylor-Weiner, H., Chen, S., Engler, A.J., 2014. Interplay of matrix stiffness and protein tethering in stem cell differentiation. Nat. Mater. 13, 979–987.
Wilson, M.J., Liliensiek, S.J., Murphy, C.J., Murphy, W.L., Nealey, P.F., 2012. Hydrogels with well-defined peptide-hydrogel spacing and concentration: impact on epithelial cell behavior( ). Soft Matter 8, 390–398.
Wolfenson, H., Iskratsch, T., Sheetz, Michael, P., 2014. Early events in cell spreading as a model for quantitative analysis of biomechanical events. Biophys. J. 107, 2508–2514.
Yang, F., Williams, C.G., Wang, D.A., Lee, H., Manson, P.N., Elisseeff, J., 2005. The effect of incorporating RGD adhesive peptide in polyethylene glycol diacrylate hydrogel on osteogenesis of bone marrow stromal cells. Biomaterials 26, 5991–5998.
Yim, E.K.F., Darling, E.M., Kulangara, K., Guilak, F., Leong, K.W., 2010. Nanotopography-induced changes in focal adhesions, cytoskeletal organization, and mechanical properties of human mesenchymal stem cells. Biomaterials 31, 1299.
Zhang, D., Sun, M.B., Lee, J., Abdeen, A.A., Kilian, K.A., 2016. Cell shape and the presentation of adhesion ligands guide smooth muscle myogenesis. J. Biomed. Mater. Res. A 104, 1212–1220.
Zustiak, S.P., Durbal, R., Leach, J.B., 2010. Influence of cell-adhesive peptide ligands on poly(ethylene glycol) hydrogel physical, mechanical and transport properties. Acta Biomater. 6, 3404–3414.

## Supplementary Information

Supplementary Figure 1

Nearest neighbour analysis was conducted using data extracted from confocal images. DAPI channel images were analysed using Cell Profiler Software to threshold and segment the images for the nuclei to be recognised as objects. Nearest neighbour (R-values) analysis was determined by calculating the ratio between the mean distance of the first neighbour for each nucleus (RA) and mean distance which would be expected in a randomly distributed population (R'E) (Clark and Evans, 1954). A lower R-value correlates to higher aggregation of samples, whereas higher values closer to 1 represent samples distributed at random.

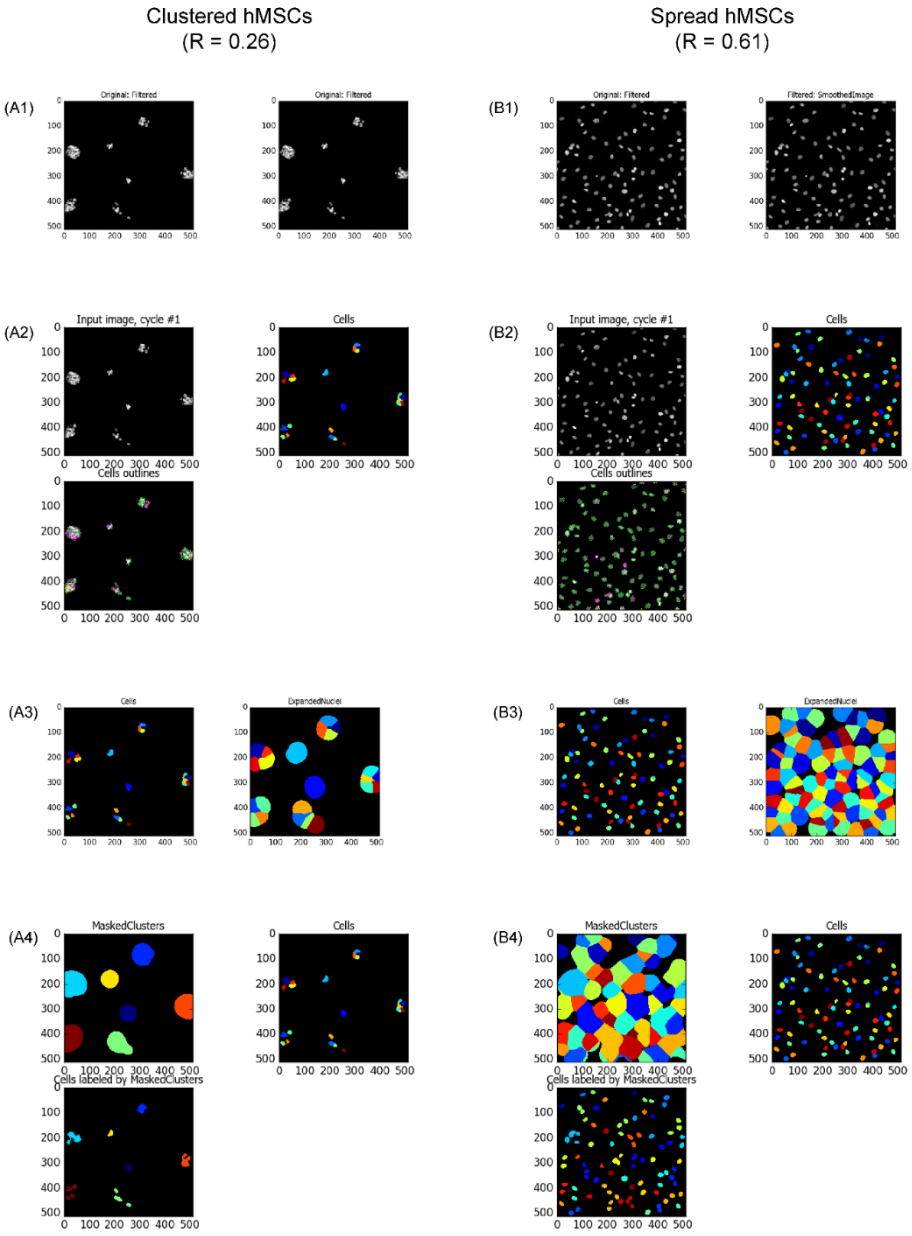


Fig. S1: Methodology to determine R-value. Images A1-A4 represent clustered hMSCs seeded on soft hydrogels functionalised with RGD and B1-B4 represent spread hMSCs seeded on stiff hydrogels. DAPI channel images were smoothened, thresholded and segmented to recognise nuclei as objects (A1 and B1). The distance to the first neighbour was measured for each nucleus and used for the nearest neighbour analysis as described by Clark and Evans. Nuclear outlines were expanded by 20 pixels (the average nucleus diameter) to count the number of neighbours within the expanded radius (A3 and B3). A4 shows a blurred and thresholded

image to allow a visual check on the segmentation and neighbour assignment in the nearest neighbour analysis

Supplementary Figure 2

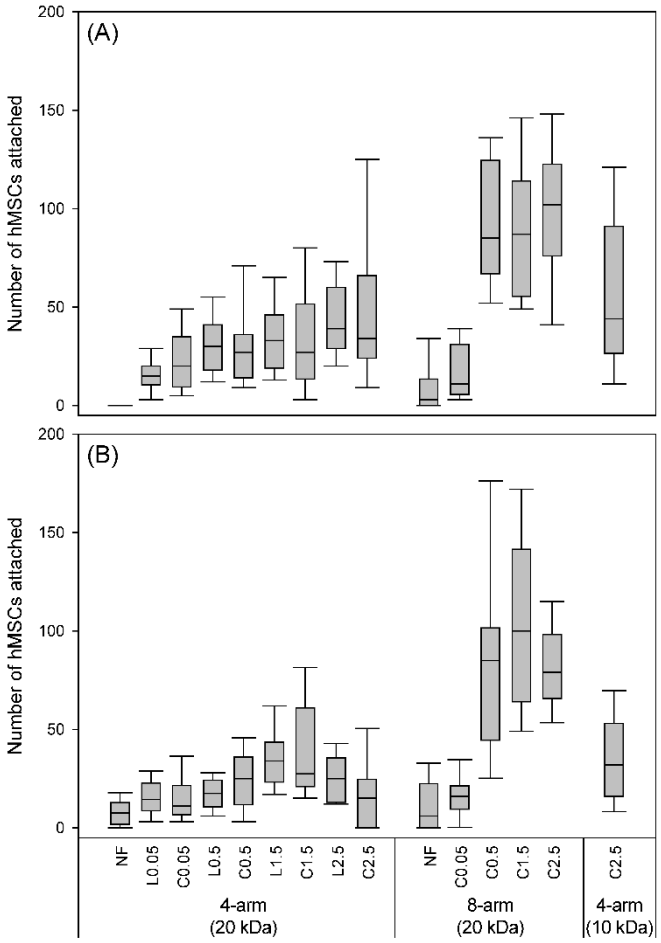


Fig. S2: Number of hMSCs observed per field of view via confocal microscopy (n=30). Each graph represents data obtained from independent experiments involving triplicates per gel group. Thirty images per gel group were obtained for data analysis. C: cyclic RGD, L: linear RGD, NF: non- functionalised.